Aus dem Institut für Molekulare Immunologie

des Helmholtz Zentrum München

Kommissarischer Direktor: Prof. Dr. Ralph Mocikat

und dem Comprehensive Pneumology Center Munich (CPC)

Institute for Experimental Pneumology

Direktor: Prof. Dr. med. Oliver Eickelberg

Immunobiological Functions of Matrix Metalloproteinase-13 in Bone Marrow-Derived Dendritic Cells and its Contribution to the Pathogenesis of Bronchiolitis Obliterans Syndrome

Dissertation

zum Erwerb des Doktorgrades der Naturwissenschaften

an der Medizinischen Fakultät der Ludwig-Maximilians-Universität München

vorgelegt von

Juliane Bartmann

aus München

2015

Gedruckt mit Genehmigung der Medizinischen Fakultät der Ludwig-Maximilians-Universität München

Betreuerin: Prof. Dr. rer. nat. Elfriede Nößner
Zweitgutachter: Prof. Dr. Peter Jon Nelson
Dekan: Prof. Dr. med. Dr.h.c. Maximilian Reiser, FACR, FRCR
Tag der mündlichen Prüfung: 02.09.2015

CONTENT

I ZUSAMMENFASSUNG

Trotz intensiver medizinischer und wissenschaftlicher Forschung sind Lungentransplantationen häufig immer noch die einzige therapeutische Möglichkeit zur Behandlung vieler Lungenerkrankungen im Endstadium. Das Langzeitüberleben vieler Organempfänger wird durch das Auftreten einer chronischen Dysfunktion der Lunge, der sogenannten „chronic lung allograft dysfunction“ (CLAD) stark limitiert, die zu einer Sterberate von 90% der Patienten innerhalb der ersten zehn Jahren führt. Unter CLAD werden verschiedene Arten von Lungendysfunktionen zusammengefasst, wobei das Bronchiolits obliterans Syndrom (BOS) die häufigste Form darstellt. BOS ist charakterisiert durch einen Verschluss der kleinen Atemwege, verursacht durch luminale Fibrose, begleitet von großflächiger Zerstörung der Bronchialepithelzellen und einem massiven Einwandern von Leukozyten. Dendritische Zellen (DCs) gehören zu den antigenpräsentierenden Leukozyten, die durch Aktivierung des adaptiven Immunsystems eine entscheidende Rolle bei der BOS-Pathogenese spielen. Des Weiteren wurde bei dieser Erkrankung eine Beteiligung von spezifischen Enzymen, den sogenannten Matrix Metalloproteinasen (MMPs) nachgewiesen, die an der Regulierung der Migration, der Zytokinspiegel sowie diverser weiterer Zellfunktionen beteiligt sind. Murine pulmonale DCs exprimieren im Vergleich zu anderen Leukozyten unter Ruhebedingungen vor allem MMP-12 und -13. Über ihre Funktion in DCs, ihre Rolle in Entzündungsprozessen und ihre Beteiligung bei der Pathogenese von BOS ist jedoch wenig bekannt.

Ziel dieser Dissertation war es spezifische immunbiologische Funktionen von ausgewählten MMPs, vornehmlich MMP-12 und -13, in DCs zu identifizieren und deren Einfluss auf die Pathogenese des experimentellen BOS zu analysieren.

Für die funktionalen *in vitro* Analysen wurden DCs aus dem Knochenmark von Mäusen generiert (“bone marrow-derived DCs“ (BMDCs)). Die Expression von MMP-12 und -13 konnte in den generierten BMDCs auf mRNA- und Proteinebene bestätigt sowie deren Aktivität in Zellüberständen quantifiziert werden. Die Behandlung der BMDCs mit Lipopolysaccharid (LPS) erhöhte die Expression von MMP-13 sowie dessen Aktivität. Funktionale Analysen mit einem spezifischen Inhibitor für MMP-13 zeigten eine verringerte Kapazität der BMDCs zur Endozytose von löslichem Ovalbumin (OVA), wohingegen Reifung und Migration der Inhibitor behandelten Zellen nicht beeinflusst wurden. Weiterhin konnte gezeigt werden, dass eine MMP-13-Inhibition die Oberflächenexpression des Haupthistokompatibilitätskomplex der Klasse I (MHC-I) auf BMDCs und in Folge die Aktivierung von T-Zellen verringerte. Ein verändertes Zytokin- und Chemokin-Profil der BMDCs nach Inhibition von MMP-13 unterstrich weiterhin den regulierenden Einfluss den MMP-13 auf die DC-Funktion besitzt. Besonders Zytokine wie Interleukin (IL) -12, IL-23 und IL-6, welche vor allem eine Rolle bei der Regulierung und Polarisierung von T-Zellen spielen, waren signifikant reduziert (*Manuskript in revision*).

Des Weiteren wurde die Rolle von MMP-13 für die Pathogenese von BOS *in vivo* untersucht. Hierfür wurde das Tiermodell der subkutanen Tracheatransplantation, das sogenannte "heterotopic trachea transplant (HTT) model", etabliert und verwendet. Die Transplantate allogen transplantierter Tiere zeigten den typischen BOS-Phänotyp mit luminalem Tracheenverschluss, epithelialen Veränderungen sowie massivem Leukozyteneinstrom. Im Vergleich zu den syngen transplantierten Tieren zeigten die Tracheen der allogen transplantierten Tiere einen Anstieg an MMP-13 mRNA. Zudem konnte MMP-13 in Gewebeschnitten der Tracheen mit Hilfe der Immunfluoreszenzfärbung (IF) lokalisiert werden. In einer Pilotstudie, in welcher der MMP-13 Inhibitor allogen transplantierten Mäusen verabreicht wurde, konnte ein milderer BOS-Phänotyp festgestellt werden.

Die vorliegende Studie beschreibt somit, dass MMP-13 über die Beeinflussung wichtiger DC-Funktionen, z.B. der Antigenpräsentation und der Sekretion von Zytokinen und Chemokinen, einen regulierenden Einfluss auf die T-Zellaktivierung hat. Weiterhin deuten die Ergebnisse darauf hin, dass MMP-13-Inhibition ein möglicher Therapieansatz bei immunbiologischen Prozessen im Allgemeinen und bei BOS im Besondern sein könnte.

II SUMMARY

Despite intensive medical and scientific research, lung transplantation is often the only therapeutic option for end-stage pulmonary diseases. Long-term survival after lung transplantation is dramatically limited due to the occurrence of chronic lung allograft dysfunction (CLAD), which leads to death in 90% of the patients within the first ten years. Bronchiolitis obliterans syndrome (BOS) is the most frequent subgroup of CLAD. BOS is characterized by occlusion of the airways caused by luminal fibrosis, epithelial damage, and influx of leukocytes. Dendritic cells (DCs) are antigen-presenting cells among the leukocytes which can activate the adaptive immune system and, thereby, participate in the pathogenesis of BOS. Matrix metalloproteinases (MMPs) are enzymes that are important for the regulation of diverse cellular functions and are reported to participate in the development of experimental BOS. It is published that murine pulmonary DCs express specific MMPs, such as MMP-12 and -13, but little is known about their functions in DCs and their role in inflammatory conditions.

The objective of the thesis was to identify specific functions of selected MMPs, mainly MMP-12 and -13, in DC immunobiology and to determine the contribution to the pathogenesis of experimental BOS.

For the functional cell assays, bone marrow-derived DCs (BMDCs) were generated. MMP-12 and -13 expression was quantified in BMDCs at mRNA and protein level and, furthermore, their activities were investigated. It was observed that treatment with the pro-inflammatory stimulus lipopolysaccharide (LPS) strongly enhanced MMP-13 mRNA expression and activity, indicating an important role of MMP-13 in inflammatory processes. Functional cell-based assays revealed that the capacity of BMDCs to endocytose soluble ovalbumin (OVA) was significantly decreased by inhibition of MMP-13, while BMDC migration and maturation remained unchanged. Furthermore, inhibition of MMP-13 reduced the surface expression of the Major Histocompatibility Complex class I (MHC-I) and lowered the capability of murine BMDCs to activate $CD8^+$ T cells. Alterations in the BMDC cytokine/chemokine profile after inhibition of MMP-13, in particular the reduction of T cell targeting cytokines such as interleukin (IL) -12, IL-23, and IL-6, further emphasized the role of MMP-13 in the regulation of BMDC immunobiology (*manuscript in revision*).

To study the relevance of MMP-13 *in vivo,* a murine heterotopic trachea transplant (HTT) model was established. Allogeneic transplanted animals revealed the typical BOS-phenotype showing luminal occlusion, epithelial damage, and leukocyte influx. Increased MMP-13 mRNA expression was detected in allografts compared to syngrafts suggesting a role of MMP-13 in the pathogenesis. Furthermore, MMP-13 was localized in transplanted tracheas by the use of immunofluorescence (IF) staining. Finally, a pilot treatment study using the specific MMP-13 inhibitor revealed an attenuated BOS-phenotype in allografts.

In summary, the present study describes a novel role of MMP-13 in regulating DC functions including antigen presentation, cytokine/chemokine secretion, and T cell activation by BMDCs and indicates that inhibition of MMP-13 might be a promising therapeutic approach to moderate inflammatory processes in general and to alleviate the pathogenesis of BOS in particular.

1 INTRODUCTION

1.1 Dendritic cells (DCs) and their role in the immune system

The host defense by the mammalian immune system is based on the interplay of the innate nonspecific immune response and the specific adaptive immune response[1-3]. Dendritic cells (DCs), natural killer (NK) cells, macrophages, and granulocytes belong to the innate immunity and permit, together with complement and interferons, a rapid protection against pathogens. Furthermore, they are able to communicate the danger of pathogen invasion to the adaptive immune system and, thereby, provoke a cascade of defense mechanisms[4]. The adaptive immune system consists of T and B cells. The generation of a large diversity of highly antigen-specific clones and the development of an immunological memory are the characteristics of the adaptive immune system. The cells which orchestrate and regulate this highly sophisticated and potent system are the antigen-presenting cells (APC). B cells, macrophages, and DCs are professional APCs constitutively expressing the major histocompatibility complex (MHC) class II proteins, while other cell types such as fibroblasts, epithelial cells, glia cells, and vascular endothelial cells are classified as non-professional APCs[5]. Among APCs, DCs are unique, as they can initiate primary immune responses[6-9].

1.1.1 The immunobiology of DCs

The life cycle of a DC starts in the bone marrow. DC progenitors leave the bone morrow and circulate as precursors through blood and the lymphatic system. They are resident in peripheral tissues as immature DCs and build up a defense line serving as guards against pathogens[10,11]. Attracted by cytokines and chemokines, they follow signals of tissue damage, take up foreign and self antigens, and migrate to the lymphoid organs where they meet and activate naïve T cells through antigen presentation[12]. Beside antigen presentation, another important ability of DCs is the release of specific cytokines and chemokines to direct the T cell response towards a specific type, such as T helper cells type (Th)1/Th2 cells, or to attract other immune cells (schematized in Figure 1.1).

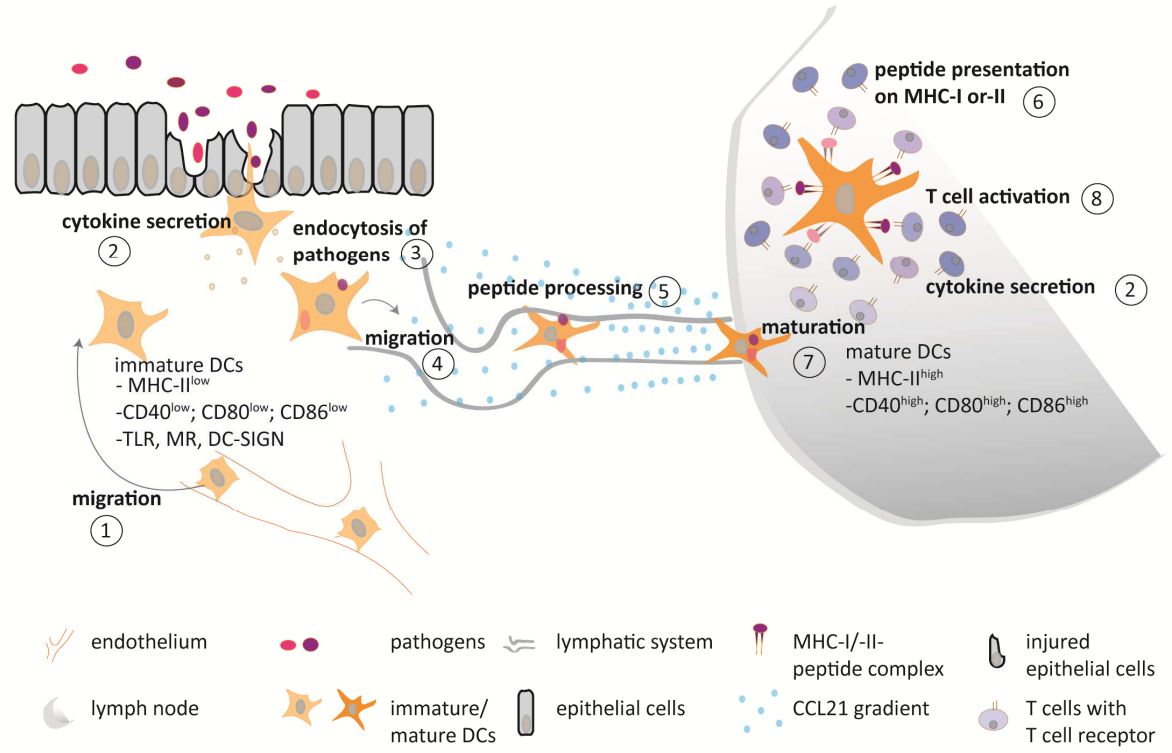

Figure 1.1: Schematic overview of DC function.
[1] DCs migrate as precursors from the blood system to the area of infection, baited by danger signals, which are recognized by a panel of Toll-like receptors (TLR). These signals include typical microbial signals, such as lipopolysaccharide (LPS), viral dsRNA, as well as endogenous danger signals, such as heat-shock proteins, tumor necrosis factor (TNF)-α, and interleukin-1β (IL-1β), released by stressed and necrotic cells of damaged tissue. [2] In addition, DCs themselves secret cytokines and chemokines to bait other immune cells. At the area of pathogen invasion [3], DCs take up antigens, for instance by endocytosis (e.g. via mannose receptor (MR)), phagocytosis, or pinocytosis. At this functional stage, DCs express a variety of different endocytic receptors, including fragment crystallizable (Fc)-receptors, lectin-like receptors, and receptors for complement binding. While immature DCs express endocytic receptors strongly, they are poor in MHC-II surface expression. This phenotype changes after antigen uptake. [4] DCs migrate with the trapped antigen to the lymph nodes, [5] process the antigen, and [6] present it on MHC-I or -II to cytotoxic or helper T cells. Following the chemokine (C-C motif) ligand (CCL)21 gradient, they migrate through the lymphatic system to the lymph nodes. [7] At this stage, DCs express a variety of co-receptors, like cluster of differentiation (CD)40, CD80, CD86, and increase the MHC-II surface expression dramatically to interact optimally with T lymphocytes. [8] Binding of a MHC/peptide-complex on the surface of DCs to the specific T cell receptor on T lymphocytes initiates the adaptive immune response. (Figure adapted and modified from Vermaelen and Pauwels, 2004)[13].

1.1.1.1 Migration, antigen uptake, and maturation of DCs

DCs do not reside at one place. They migrate through the endothelium to the infected area and further to the lymphoid organs to activate the adaptive immune system. At the area of pathogen invasion, DCs take up antigens, for instance by endocytosis[14], phagocytosis[15,16], or pinocytosis[14]. DCs undergo dramatically morphological and functional changes, defined as maturation, which enable them to operate optimal at the different stages during their life cycle[17-19]. As immature cells, DCs express receptors which are required to capture antigens[14,20], whereas mature DCs downregulate these receptors and upregulate co-stimulatory molecules, such as cluster of differentiation (CD)40, CD58, CD80, and CD86[21]. Furthermore, mature DCs show an increased surface expression of MHC-II molecules[22] as well as a shift in lysosomal compartments with an

increase in DC lysosome-associated membrane protein (DC-LAMP)[6,17,23] (Figure 1.1). Altogether, these phenotypic and functional changes facilitate the optimal processing and presentation of antigens. DC maturation can be induced by various pathogen-derived molecules, such as lipopolysaccharides (LPS)[24], bacterial DNA[25-29], as well as double-stranded RNA[29]. Additionally, T cell-derived signals and the balance between pro-inflammatory and anti-inflammatory cytokines in the DC microenvironment contribute to the regulation of the DC maturation process.

1.1.1.2 Antigen processing and presentation by DCs

DCs present the antigen-derived peptides to T cells in one of the following three pathways[17]. Endogenous proteins are routinely degraded in the cytosol by the proteasome and loaded on MHC-I in the endoplasmic reticulum (ER) for the final presentation to $CD8^+$ cytotoxic T lymphocytes[30-32] (Figure 1.2 left, MHC-I pathway).

Exogenous proteins, internalized for example by endocytosis, are degraded in endosomal compartments and loaded on MHC-II to activate $CD4^+$ T cells[20-22,33-40] (Figure 1.2 right, MHC-II pathway).

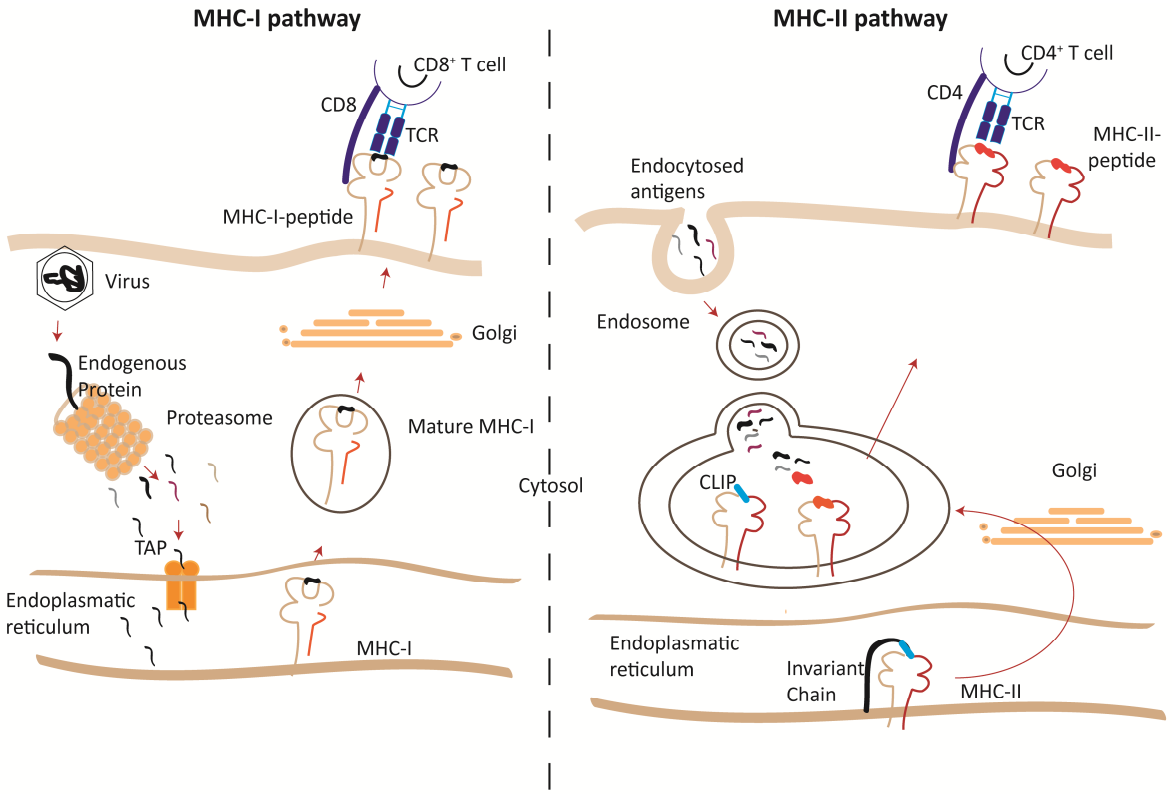

Figure 1.2: Antigen processing and presentation on MHC-I or MHC-II.
(Left) MHC-I pathway: Endogenous proteins, like those of viruses, are degraded in the cytosol by the proteasome. The degraded antigens enter the ER as peptides through the transporter associated with the antigen processing (TAP). Peptides of 8-10 amino acids in length (depicted in black) find a place in the binding groove of the MHC-I molecule. Once the peptide is loaded onto the MHC class I molecule, the complex leaves the ER through a secretory pathway to reach the cell surface. The surface peptide-MHC-I complex can now be recognized by the T cell receptor (TCR) on $CD8^+$ T cells in combination with the CD8 co-receptor.
(Right) MHC-II pathway: Exogenous proteins are internalized by endocytosis and degraded in the endosome. The MHC-II complex is synthesized in the ER. In the ER the invariant chain (depicted in black and light blue) binds to the MHC-II molecule to stabilize the MHC-II complex and to avoid unspecific peptide biding. After passing from the ER to the Golgi, the MHC-II molecule enters the late endosome that contains the degraded proteins. The invariant chain is broken down by a protease called cathepsin leaving a small fragment named CLIP (depicted in blue) in the MHC-II binding groove until it is replaced by the exogenous peptide (depicted in red). Typically, peptides of 15-24 amino acids in length are presented by the MHC-II molecule. On the surface, the MHC-II-peptide complex can be recognized by $CD4^+$ T cells with the help of the CD4 co-receptor (Figure adapted and modified from Villadangos and Schnorrer, 2007)[41].

In 1976, Michael J. Bevan first described a third mechanism named cross-presentation, where exogenous proteins could also be presented on MHC-I and stimulate $CD8^+$ T cells[32]. The "cytosolic" and the "vacuolar" pathway have been reported as the two main pathways in cross-presentation[42]. In case of the "cytosolic" pathway, internalized proteins access the cytosol, are degraded by the proteasome, and loaded on MHC-I molecules[43-48]. In contrast, in the "vacuolar" pathway, antigens are processed within the phagosome by endocytic proteases and loaded on MHC-I directly in the phagosome[49,50]. Cross-presentation is thought to be crucial for the defense against viruses that do not directly infected APCs and against tumor cells[51,52].

1.1.1.3 Interaction of DCs with T and B cells

DC-T cell interaction is based on an antigen-specific T cell receptor (TCR) on T cells that recognizes its corresponding peptide bound on MHC-I or -II on DCs. *In vivo*, this interaction takes place in lymphoid organs where immunity is primed[53,54]. The TCR-MHC recognition is known as ”signal one” and is supported by multiple adhesion molecules, such as integrin β1 and β2 as well as members of the immunoglobulin superfamily (lymphocyte function-associated antigen (LFA)-2, intercellular adhesion molecules (ICAM)-3, ICAM-1, and LFA-3)[7,8,55]. If a TCR interacts with its cognate peptide-MHC complex, the adhesion between the two cells becomes tightened, thereby enabling the interaction of co-stimulatory molecules on the DC with the corresponding ligands expressed on the T cell[55,56]. The recognition of the co-stimulatory molecules is known as ”signal two” and facilitates T cell activation. For instance, the interaction of the co-stimulatory molecule CD40 on DCs with its ligand (CD40-L) on T cells activates DCs, increases the expression of further co-stimulatory molecules, such as CD80 and CD86, and promotes specific cytokine release[20,57-60]. The interface between the DC and the T cell is known as immunological synapse[61].

Beside T cell activation, DCs are also able to activate naïve and memory B cells. The secretion of interleukin (IL)-12 in combination with IL-6 by DCs supports the differentiation of B cells into plasma cells[62,63]. Furthermore, DCs can regulate effectors of the innate immunity, such as NK cells and NK T cells, either via direct cell contact or by modulating cytokines. IL-12, IL-15, and IL-18 are typical cytokines that promote NK or NK T cell activation[64,65].

Depending of the maturation state and the surrounding microenvironment, DCs play not only a role in the induction but also in the suppression of immunity. DCs induce peripheral T cell tolerance by continuously presenting self- or harmless antigens to T cells in the absence of co-stimulatory molecules and/or activating cytokines[66]. As part of their tolerogenic function, DCs were further reported to induce regulatory T cells *in vitro*[67]. However, how important DCs are for the process of regulatory T cells induction *in vivo* remains to be fully elucidated.

1.1.1.4 Release of specific cytokines by DCs

As mentioned before, DCs release a variety of cytokines and chemokines depending on their maturation state and the local microenvironment. These cytokines can either activate or dampen the immune response or direct immune cells to differentiate into a specific cell type.

IL-12, IL-23, and IL-6 are typical pro-inflammatory cytokines. IL-12, beside interferon (IFN)-γ, is known to be the main cytokine regulating Th1 differentiation[68] and, thereby, serves as a critical mediator of $CD8^+$ T cell activation by driving the necessary $CD4^+$ T cell help towards a Th1 phenotype[69-72]. Furthermore, IL-12 is reported to induce T and NK cells to secrete cytokines, such as IFN-γ, tumor necrosis factor (TNF)-α, macrophage colony-stimulating factor (M-CSF), granulocyte macrophage colony-stimulating factor (GM-CSF), IL-2, IL-3, IL-8, and IL-23[69,73-76] and to increase expansion and survival of effector/memory T cell populations by reducing apoptosis in $CD4^+$ and $CD8^+$ T cells[68,76]. IL-12 comprises of two subunits, p35 and p40 and shares

the same p40 subunit with IL-23. IL-23 is another related heterodimeric cytokine that consists of a different second subunit (p19)[77].

IL-23 also induces proliferation and IFN-γ production but preferentially stimulates naïve $CD4^+$ T cells and Th17 memory T cell populations[78]. The two subunits, p19 and p35, show homology with IL-6, another cytokine that baits T cells, regulates T cell apoptosis, and is known as a downstream factor of IL-23[78]. Beside the release of these three described cytokines, DCs further secret typically anti-inflammatory cytokines, such as IL-10 and transforming growth factor (TGF)-β and, moreover, cytokines that promote Th2 differentiation, for instance, IL-4 and IL-5[79].

In addition to cytokines, DCs express a variety of chemokines, such as chemokine (C-C motif) ligand (CCL)3, CCL4, CCL5, chemokine (C-X-C motif) ligand (CXCL)1, CXCL2, and lipopolysaccharide-induced CXC chemokine (LIX), which function as chemoattractants for various cells, such as neutrophils and basophils[80,81]. In general, DC-derived cytokines and chemokines promote leukocyte differentiation and attraction.

1.1.2 DC subsets in human and mice

In general and as outlined above, DCs are a heterogeneous group of cells whose several subpopulations differ in phenotype and function. Furthermore, they vary between species, such as between human and mice[82].

Four different DC subsets have been identified in human blood: the $CD123^+$ plasmacytoid DC (pDC) subset, which produces large quantities of type I interferons[83] and three myeloid DC (mDC) types encompassing the $CD1c^+$, $CD16^+$, and $CD141^+$ DC subsets[84]. In human tissue, five DC types have been described so far which are grouped in $CD1c^+$ conventional DCs (cDCs) type 1, $CD141^+$ cDCs type 2[85] (formerly termed mDCs type 1 and 2), $CD209^+$ monocyte-derived DCs[86], $CD303/304^+$ pDCs, and Langerhans cells[87-89].

In mice, DCs are classified into similar subtypes as in humans encompassing the myeloid-derived $CD11b^+$ cDCs type 1 and $CD8\alpha^+$ cDCs type 2 as well as $mPDCA1^+$ pDCs, monocyte-derived DCs, and Langerhans cells[88,90]. These five subsets show differences in phenotype, localization, and function and display comparable functions to those in humans. Murine cDCs express high levels of CD11c and in mature state high levels of MHC-II and co-stimulatory molecules, such as CD80, CD86, and CD40, similar to the human system[91-94]. $CD8\alpha^+$ cDCs are specialized in cross-presentation of exogenous antigens on MHC-I molecules to $CD8^+$ T cells[95], whereas pDCs express high levels of IFN-α in response to IL-12 and are reported to prime allogeneic T cells less efficiently than $CD8\alpha^+$ cDCs[96].

Murine classical DCs can be generated *in vitro* by culturing bone marrow-derived precursor cells with GM-CSF[97-100]. This method is widely used to gain large numbers of naïve DCs for *in vitro* analyses. DCs can also be derived from blood monocytes by culturing them in GM-CSF and IL-4[101,102]. This is the main method to generate DCs in the human setting where bone marrow cells are difficult to obtain.

1.1.3 The role of DCs in disease settings

Taking their central role as regulator of immunity, DCs are intensively studied in various human disease settings, such as autoimmune disease[103,104], tumor development[105,106], transplant dysfunctions[107], virus infections[108], and allergy[109] as well as in different lung diseases, such as chronic obstructive pulmonary disease (COPD)[110], asthma[111,112], and bronchiolitis obliterans syndrome (BOS)[113,114]. As DCs play a role in the induction of both, immunity and tolerance, they are clinically used to manipulate the immune response in the intended direction. For instance, *ex vivo* tumor antigen-loaded DCs are used to stimulate tumor-reactive T cells *in vivo* to control cancer[106]. In addition, the induction of tolerance by *in vitro* expansion of DCs that induce antigen-specific regulatory T cells (Tregs) is an approach to treat autoimmune disease or asthma[115].

Besides cancer and autoimmune diseases, DCs are reported to play a role in the development of various lung diseases, such as COPD and BOS. Here, progression of the disease is often interrelated with extensive remodeling and repair processes of the lung. In these pathological pulmonary remodeling processes, specific enzymes, so-called matrix metalloproteinases (MMPs), are reported to be involved. Therefore, interplay between DCs and MMPs may contribute to the pathogenesis of inflammatory lung diseases.

1.2 Matrix metalloproteinases (MMPs)

1.2.1 Function of MMPs

MMPs belong to the family of zinc-dependent endopeptidases. The first MMP was discovered by Gross and Lapiere in 1962 in the regressing tadpole tail[116]. Since then, more and more MMPs have been described. The MMP family currently includes 25 secreted as well as cell-anchored enzymes[117]. By degrading different structural matrix and non-matrix proteins, MMPs are involved in diverse biological and pathological processes, such as embryogenesis and differentiation, wound healing, tissue repair and remodeling, as well as cancer development and inflammatory diseases[118-120]. As such, these enzymes are mainly known to degrade extra cellular matrix proteins. Recent studies, however, indicate an involvement of MMPs in various other cellular processes. Based on the new discovered ability of MMPs to modify cytokines/chemokines and their receptors, they play important roles in innate immunity and in inflammatory processes[121].

1.2.2 Structure of MMPs

MMPs usually consist of a pro-domain, a catalytic domain, and a C-terminal hemopexin-like domain (Figure 1.3). The highly conserved pro-domain, with a length of around 80 amino acids, typically contains the consensus sequence PRCXXPD. The catalytic domain (170 amino acids) contains a zinc ion in the active site, linked to three histidine residues. Furthermore, MMPs have a proline-rich hinge region that connects the catalytic domain with a carboxy-terminal hemopexin-like domain (200 amino acids), which is important for substrate recognition (Figure

1.3). The majority of MMPs are secreted, with the exception of MMP-14, -15, -16, -17, -25, and -24, which are membrane-anchored[121-123].

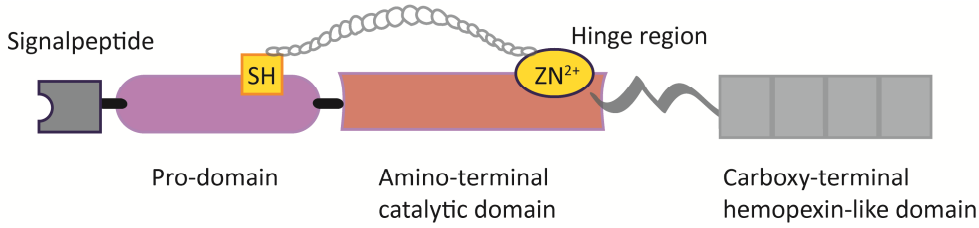

Figure 1.3: Basic structure of MMPs.
The basic structure of MMPs consists of a N-terminal signal peptide (depicted in dark grey), a pro-domain (depicted in magenta) that is linked to a zinc ion of the catalytic domain (depicted in red) via a thiol group, and a carboxy-terminal hemopexin-like domain (depicted in grey). The bonding between the thiol group and the zinc ion (both depicted in yellow) ensures the inactive state of the pro-peptide. (Figure adapted and modified from Song *et al.*)[124]

1.2.3 Regulation of MMPs

MMPs can be regulated on transcriptional level as well as through the activation of the pro-enzyme and the inactivation of the active MMP. MMPs are generated as pro-peptides that are kept in a catalytically inactive state. This inactivity is sustained by the bonding between the thiol group of a cysteine residue of the pro-domain and the zinc ion of the catalytic domain (Figure 1.3). A process known as cysteine-switch mechanism activates the pro-enzyme by proteolysis of the pro-domain or by rearrangement of the cysteine thiol group[122,125,126]. MMPs can be activated by plasmin and urokinase type plasminogen activator (uPA) and tissue-type plasminogen activator (tPA)[127] as well as by other MMPs, oxidants[128,129], and chemicals, such as 4-aminophenylmercuric acetate (APMA)[130]. Activated MMPs are tightly regulated to prevent host damage by their protease activities. Active forms of MMPs are inhibited by their natural inhibitors, named tissue inhibitors of metalloproteinases 1-4 (TIMPs) and by the general proteinase inhibitor α2-macroglobulin[131]. The overall shape of the TIMP molecule is “wedge-like”. The N-terminal residues of TIMPs bind into the entire length of the active site cleft of their cognate MMPs and form a 1:1 complex that leads to inhibition[132,133]. Beside the general proteinase inhibitor α2-macroglobulin and TIMPs, small inhibitors of metalloproteinase (IMPs) and large inhibitors of metalloproteinase (LIMPs) are two additional groups of MMP inhibitors[134]. However, TIMPs are the major natural inhibitors and are, therefore, often studied in association with MMPs. Besides these natural occurring MMP inhibitors, more than 50 pharmaceutical produced specific or broad spectrum inhibitors are described to inhibit MMP functions[135].

1.2.4 MMP-12 and -13

MMP-12, also named macrophage metalloelastase as it is mainly produced by macrophages, is expressed as a 53 kDa pro-enzyme. For activation, it is processed into a 45 kDa form, followed by modification into the final active form of 22 kDa. Mouse and human MMP-12 share 64%

homology and are rarely expressed in healthy adult tissue[136]. MMP-12 is strongly induced in developing and remodeling processes which occur in the placenta as well as in inflammatory processes[137]. Targets of MMP-12 are various proteins like elastin[136], gelatin, myelin basic proteins, pro-TNF-α[138], type IV collagen, fibronectin, vitronectin, entactin, laminin, aggrecan[139], proteoglycan, α1-proteinase inhibitor[140], α2-macroglobulin[141], fibrinogen, factor XII[142], and urokinase-type plasminogen activator receptor (uPAR)[143].

MMP-13 (collagenase-3) belongs together with MMP-1 and MMP-8 to the subgroup of collagenases. It is expressed as a pro-peptide of 60-65 kDa that is further processed into an intermediate 50-55 kDa form and finally into the 48 kDa active form[144,145].

The catalytic domain of human MMP-13 has 97% homology to mouse MMP-13[146,147]. As known so far, active MMP-13 cleaves collagen I-III[148], IV, IX, X, XIV, fibronectin, tenascin, osteonectin[149], gelatin[150], collagen telopeptides, casein[151], aggrecan[152], α2-macroglobulin[153], complement factor Clq[154], fibrinogen, and factor XII[142]. Furthermore, active MMP-13 can also cleave other MMPs, such as pro-MMP-2 and -9[155] or cytokines and chemokines, such as MCP-3, pro-TGF-β, pro-TNF-α, SDF-1[156], and CXCL12[122]. MMP-13 can further be activated by other MMPs, such as MMP-2, -3, and membrane-type1 (MT1) -MMP[155]. It plays a major role in skeletal development, tissue remodeling, wound healing, and angiogenesis[157-160]. MMP-13 was first cloned from human breast tumor[145] but is expressed also during remodeling processes by plasma cells[161], fibroblasts[162,163], chondrocytes[164-166] osteoblasts, vascular smooth muscle cells[167], neurons[168], endothelial cells[157], and also in a variety of neoplastic cells[155,158,169].

Interestingly, recent studies have shown that MMP-12 and -13 are also expressed in murine bone marrow-derived dendritic cells (BMDCs)[170] as well as in murine pulmonary DCs[171].

For both MMPs, knock-out (ko) mice are available which exhibit a normal lifespan with no prominent phenotypic abnormalities indicating that theses enzymes do not serve vital functions in development or homeostasis[117]. However, MMP-12 ko mice reveal reduced elastolytic capacity of macrophages and a diminished ability of macrophages to migrate[172]. MMP-13 ko mice reveal defects in the growth plate cartilage with a marked increase in the hypertrophic chondrocyte zone. Furthermore, two MMP-13 ko lines, described in the literature, display a delay in primary ossification[160,173,174].

1.2.5 MMP-12 and -13 in normal immune responses and in diseases

When invading organisms attack the host immune system, MMPs participate in the immune response by degradation of extracellular matrix (ECM) components and by modulation of cytokines and chemokines. They play important roles in leukocyte recruitment by proteolysis of the basement membrane[175,176] and by modulating the cytokine/chemokine gradient[177,178] as well as by the destruction of bacteria by defensin activation[179]. While controlled MMP activity is required for the normal immune response, uncontrolled activity can harm the host intensively resulting in tissue damage and chronic inflammation. Given their important role in tissue homeostasis and

remodeling, MMPs are reported to participate in a wide range of diseases. Dysregulation of MMP-12 has been shown to be associated with inflammatory skin diseases[180,181], atherosclerosis[182], aneurysms[183], and cancers[184,185] as well as in inflammatory pulmonary diseases, such as COPD[186,187]. The influence of MMP-12 in COPD was demonstrated by MMP-12 ko mice which appeared to be protected against smoking-induced emphysema[188].

Apparently due to its ability to degrade a wide range of ECM components, dysregulation of MMP-13 leads to extensive degradation of the collagenous ECM, detected in osteoarthritis and rheumatoid arthritis[173,189], periodontitis[190], as well as in malignant tumors, such as breast carcinomas[145,191,192], various squamous cell carcinomas[193-195], cutaneous basal cell carcinomas[194], and chondrosarcomas[196].

1.2.6 MMPs in the lung

Various studies explicitly reported the participation of different MMPs in the development and remodeling process of the lung from the very beginning of lung bud formation throughout the alveolarization processes. In contrast, very little is known about the involvement of MMPs in the regeneration of the lung after injury and tissue destruction. In animal models of inflammatory lung diseases, a clear correlation between the onset of inflammation and increased MMP levels was reported[197]. Therefore, a large effort has been devoted to determine the exact role of MMPs in different inflammatory lung diseases. Involvement of MMPs was reported in most human lung diseases, such as idiopathic pulmonary fibrosis[198], COPD[199,200], asthma[199], cystic fibrosis[201], and especially in BOS[202-204]. In humans, increased MMP-9 levels are reported to correlate with progression of BOS[202,203,205] whereas in murine studies various MMPs, such as MMP-2, -8, -9, and MT1-MMP are reported in the development of experimental BOS[206-208]. These reports support the notion that MMPs might be potential targets for therapeutic treatment. However, the participation of specific MMPs and their exact function in BOS is poorly understood.

1.3 Bronchiolitis obliterans syndrome (BOS)

Lung transplantation is the only therapeutic option for end-stage pulmonary disorders. Whereas short-term survival after lung transplantation could be improved due to surgical techniques and immunosuppressive therapy[209], long-term survival is still limited by the occurrence of chronic lung allograft dysfunction (CLAD). The two main subgroups of CLAD are BOS and the restrictive allograft syndrome (RAS)[210,211]. Five years after transplantation, the survival rate of the patients is approximately 50%, whereas the 10-year-survival rate is only 26%[212]. Furthermore, the median survival after the diagnosis of BOS is only three years as most patients response poorly to immunosuppression[213]. A progressive decline in the forced expiratory volume 1 (FEV1), progressive dyspnea, and cough are the clinical features that lead to the diagnosis of BOS[214,215]. Histopathologically, BOS is characterized by fibroproliferative lesions of bronchioles. It is accompanied by luminal fibrosis, epithelial damage, and influx of lymphocytes, histiocytes, and

plasma cells, which finally leads to luminal occlusion of the airways[216-221]. In some patients vascular sclerosis of the pulmonary arteries and veins is although observed[221]. The pathogenesis of BOS is very complex and heterogenic. Acute rejection, lymphocytic bronchitis, and infections are reported as strong risk factors for BOS[222-224]. Different studies suggest that excessive fibroproliferation due to abnormal tissue remodeling and defects in the regeneration of the epithelium are the result of epithelial and subepithelial airway injury. It is reported that this airway injury may occur due to alloimmune-dependent and -independent mechanisms[225]. Therefore, a pivotal role of the adaptive immune system in the pathogenesis of BOS seems to be indicated. However, the exact mechanisms and the underlying molecular pathways leading to BOS remain elusive.

1.3.1 Participation of DCs in BOS

BOS is reported to result mainly from chronic presentation of donor-derived antigens to recipient T cells via a self-MHC-donor peptide complex[226-228]. Antigen presentation by DCs, which are the most potent APCs of the innate immune system, is considered to be important in the developmental process of BOS. In the early phase after transplantation, donor-derived DCs migrate to the lymph nodes of the recipient and induce the alloimmune response (direct pathway) that can lead to acute rejection[229]. Solari and co-workers could demonstrate in human kidney transplant patients that a depletion of DCs significantly reduced acute rejection[230]. In later stage after transplantation, recipient DCs take up and process damaged donor cells and present the foreign peptides on self-MHC to T cells (indirect pathway)[231]. While the direct pathway dominates the early posttransplant period, the indirect pathway remains active during the whole life of transplant and is, therefore, considered to drive BOS. As DCs are thought to substantially contribute to the pathogenesis of BOS, different groups investigated the role of DCs in CLAD. In 1990 the group of Yousem found an increase in DC numbers in lung allografts that were chronically rejected[114]. In contrast, eight years later, Milnes and colleagues reported a decline in the amount of $CD1a^+$ DCs in lung allografts[232]. In 2000, Leonard and co-workers suggested that the importance of DC numbers in BOS is underestimated due to the usage of inappropriate DC markers. Using the typical dendritic morphology and MHC-II instead of CD1a expression for DC detection, they confirmed an increase in DCs in patients with worsening BOS compared to stable patients[113]. In general, due to the lack of a unique marker for pulmonary DCs, contradicting reports exist in the literature on the correlation of DC number and the pathogenesis of BOS. However, in a BOS animal model, increased numbers of DCs were reported by Kleinjan *et al.*[233]. They showed that blocking of critical co-stimulatory molecules expressed on DCs prevents the development of the BOS phenotype. This report indicates that DCs are key players in the pathogenesis of murine experimental BOS. However, further research effort is necessary to identify the precise role of DCs in this disease.

1.3.2 The role of MMPs in BOS

The development of BOS is associated with extracellular matrix remodeling and inflammatory activity. In both of these processes, MMPs are known to play a pivotal role as outlined in section 1.2. Therefore, efforts were made to determine the role of MMPs in the pathogenesis of BOS and, furthermore, to verify MMPs as sensitive markers for BOS. Different groups reported an increase of MMP-9 relative to TIMP-1 in sputum[205] and bronchoalveolar lavage fluid[202,203]. Therefore, MMP-9 was assumed to serve as indicator of BOS. However, Smith and coworkers suggested that the increased levels of MMPs are due to ischemia reperfusion injury after transplantation or the result of an acute rejection[234].

Different animal models have been developed to study the pathogenesis of experimental BOS *in vivo*. The heterotopic trachea transplant (HTT) model is often used to explore the pathogenesis of BOS as it mimics the development of BOS quickly and robustly. This model is less technically demanding in comparison to whole lung transplant models and, therefore, reduces variability within experimental studies[235]. Furthermore, it better reflects the chronic changes, whereas models of orthotopic lung transplantation lead to acute rejection phenotypes. Different reports suggest an involvement of specific MMPs, such as MMP-2, -8, -9, and MT1-MMP in the development of experimental BOS in the HTT model[206-208].

Specific MMPs, such as MMP-9 mentioned above, have been already intensively studied in BOS and its inhibition ameliorated the progression of experimental BOS. However, the disadvantage of pharmaceutical MMP-9 inhibition is the broad expression of MMP-9 in a variety of cells, e.g. neutrophils, and, thereby, the occurrence of severe side effects in the host. Therefore, there is significant interest to find other proteases of the MMP family that would serve as more specific pharmacological targets. To consider the utilization of specific MMP inhibitors as therapeutic option in patients, detailed knowledge of MMP function is essential. Nowadays, MMPs are no longer just considered as enzymes that only degrade extracellular matrix components, but instead, are also important in inflammatory processes, e.g. in the regulation of cytokines/chemokines[177,178], in migration[175,176], and likely other functions of immune cells. In DC biology, MMP-12 and -13 are reported to be highly expressed in murine pulmonary DCs compared to macrophages and monocytes[171] and thus, may contribute to the function of pulmonary DCs, possibly influencing the progression of BOS.

1.4 Objectives of this thesis

DCs and MMPs are both reported to participate in the pathogenesis of BOS. Current evidence suggests that the activity of MMPs is no longer limited to a role in the degradation of EMC products but extends beyond that to including regulatory activities in various other cell functions and inflammatory processes. Murine pulmonary DCs have been shown to express specific MMPs, such as MMP-12 and -13[171], but little is known about their functions in DCs and their role in inflammatory conditions.

The first aim of the thesis was to establish various functional assays to identify the role of selected MMPs (mainly MMP-12 and -13) in the immunobiology of DCs. The second aim was to correlate these specific MMPs to the pathogenesis of BOS *in vivo*.

To achieve these aims, murine DCs were generated from bone marrow cells and analyzed for their MMP expression profile under inflammatory condition. BMDCs were further used to study the involvement of identified MMPs in DC migration, OVA-endocytosis, antigen presentation, T cell activation, and cytokine profile by using specific MMP-12 and -13 inhibitors.

For the *in vivo* studies, the HTT model was established and used to localize the identified MMPs (MMP-12 and -13) in the grafts and to analyze alterations of these MMPs between syngrafts and allografts. The HTT model was further used to analyze the effect of MMP-13 inhibition on the progression of experimental BOS *in vivo.* Therefore, MMP-13 inhibitor was administered intraperitoneal (i.p.) every second day and changes in the BOS phenotype were analyzed.

2 MATERIAL AND METHODS

2.1 Material

2.1.1 Antibodies

Table 2.1: Antibodies for flow cytometry analysis

Target name	Host/Clonality	Supplier	Fluorochrome	Catalog No.
H-2K^b MHC-I	Mouse/ monoclonal (mc)	BioLegend; Fell, Germany	PE	#116507
MHC-II	Rat/mc	BioLegend; Fell, Germany	PerCP/Cy5.5	#107626
CD80	Hamster/mc	BioLegend; Fell, Germany	Pacific blue (PB)	#104723
CD86	Rat/mc	BioLegend; Fell, Germany	PE	#105007
CD40	Rat/mc	BioLegend; Fell, Germany	PE/Cy7	#124621
CD11c	Hamster/mc	BioLegend; Fell, Germany	APC	#117310
H-2K^b bound to SIINFEKL	Mouse/mc	BioLegend; Fell, Germany	PerCP/Cy5.5	#141610
CD11b	Rat/mc	BD Bioscience; Heidelberg, Germany	PE	#553311
CD45	Rat/mc	BD Bioscience; Heidelberg, Germany	FITC	#553080
Ly-6G/Ly-6C	Rat/mc	BD Bioscience; Heidelberg, Germany	V450	#560453
F4/80	Rat/mc	BioLegend; Fell, Germany	APC/Cy7	#123118
CD3	Rat/mc	BioLegend; Fell, Germany	PB	#100213
CD19	Rat/mc	BioLegend; Fell, Germany	PE	#115508
CD4	Rat/mc	BioLegend; Fell, Germany	PerCP/Cy5.5	#100539
CD8α	Rat/mc	BioLegend; Fell, Germany	APC/Cy7	#100713
NK1.1	Mouse/mc	BioLegend; Fell, Germany	APC	#108710

Table 2.2: Isotypes for flow cytometry analysis

Isotype name	Host/Clonality	Supplier	Fluorochrome	Catalog No.
IgG2a, κ	Mouse/mc	BioLegend; Fell, Germany	PE	#400211
IgG2b, κ	Rat/mc	BioLegend; Fell, Germany	PerCP/Cy5.5	#400631
IgG	Hamster/mc	BioLegend; Fell, Germany	PB	#400925
IgG2a, κ	Rat/mc	BioLegend; Fell, Germany	PE	#400507
IgG2a, κ	Rat/mc	BioLegend; Fell, Germany	PE/Cy7	#400521
IgG	Hamster/mc	BioLegend; Fell, Germany	APC	#400911
IgG2b, κ	Mouse/mc	BioLegend; Fell, Germany	PerCP/Cy5.5	#400112
IgG2b, κ	Rat/mc	BD Bioscience; Heidelberg, Germany	PE	#555848
IgG2b, κ	Rat/mc	BD Bioscience; Heidelberg, Germany	V450	#560457
IgG2a, κ	Rat/mc	BioLegend; Fell, Germany	APC/Cy7	#400523

Table 2.3: Primary antibodies for immunofluorescence staining

Target name	Host/Clonality	Supplier	Fluorochrome	Catalog No.
CD45	Rat/polyclonal (pc)	Abcam; Cambridge, UK	-	#ab25386
CD45	Rabbit/pc	Abcam; Cambridge, UK	-	#ab10558
CD3	Rabbit/pc	Abcam; Cambridge, UK	-	#ab16669
MMP-12	Rabbit/mc	Abcam; Cambridge, UK	-	#ab52897
MMP-13	Mouse/mc	Merck Millipore; Schwalbach, Germany	-	#IM78
MMP-13	Rabbit/pc	Abcam; Cambridge, UK	-	#ab75606
CD11c	Hamster/mc	Angio-Proteomie; Boston, USA	-	#mAP-0047
CD11c	Hamster/mc	BioLegend; Fell, Germany	-	#117301
CD11c	Rabbit/pc	Santa Cruz; Heidelberg, Germany	-	#sc-28671
MHC-II	Mouse/mc	Bio-Rad AbD Serotec; Puchheim, Germany	-	#MCA46GA
MHC-II	Rat/mc	Abcam; Cambridge, UK	-	#ab 64528
MHC-II	Rat/mc	eBioscience; Frankf. am Main, Germany	-	#14-5321
α-SMA	Mouse/mc	Sigma-Aldrich; Taufkirchen, Germany	-	#A5228
CD31	Rabbit/pc	Santa Cruz; Heidelberg, Germany	-	#sc-28188
E-cadherin	Mouse/mc	BD Bioscience; Heidelberg, Germany	-	#610181
Galectin3	Rabbit/pc	Santa Cruz; Heidelberg, Germany	-	#sc-20157
Collagen I	Rabbit/pc	Rockland-inc.; Hamburg, Germany	-	#600-401-103

Table 2.4: Isotypes for immunofluorescence staining

Target name	Host	Supplier	Fluorochrome	Catalog No.
IgG	Hamster	BioLegend; Fell, Germany	-	#400901
IgG1	Mouse	Merck Millipore; Schwalbach, Germany	-	#MABC002F

Table 2.5: Secondary antibodies for immunofluorescence staining

Target name	Host	Supplier	Fluorochrome	Catalog No.
anti-hamster IgG	Goat	BioLegend; Fell, Germany	DyLight 594	#405504
anti-mouse IgG	Goat	Invitrogen, Life Technologies; Carlsbad, USA	Alexa Fluor 488	#A11001
anti-rat IgG (H+L)	Goat	Invitrogen, Life Technologies; Carlsbad, USA	Alexa Fluor 488	#A11006
anti-mouse IgG (H+L)	Goat	Invitrogen, Life Technologies; Carlsbad, USA	Alexa Fluor 568	#A11004
anti-rabbit IgG (H+L)	Goat	Invitrogen, Life Technologies; Carlsbad, USA	Alexa Fluor 568	#A11011

2.1.2 Buffers and solutions

DNA loading buffer (6x) (Fermentas, Thermo Fisher Scientific)

Substance	Concentration
Tris/HCl, pH 7.6	10 mM
Bromophenol blue	0.03%
Xylene cyanol FF	0.03%
Glycerol	60%
EDTA	60 mM

HEPES (N-2-hydroxyethylpiperazine-N-2-ethane sulfonic acid) (Sigma-Aldrich):

Substance	Concentration
HEPES	1 M

Lämmli loading buffer (6x):

Substance	Concentration
SDS	12% (w/v)
Glycerol (87%)	60% (v/v)
Bromophenol blue	0.06% (w/v)
Tris/HCl, pH 6.8	375 mM
Dithiothreitol (DTT)	600 mM

PBS (Phosphatate buffered saline) pH 7.4 (10x):

Substance	Concentration
NaCl	1.37 M
KCl	27 mM
Na_2HPO_4	100 mM
KH_2PO_4	20 mM
NaCl	1.37 M

RIPA (radio-immunoprecipitation assay) buffer:

Substance	Concentration
Tris-Cl pH 7.4	50 mM
NaCl	150 mM
NP40	1% (v/v)
Na-deoxycholate	0.25% (v/v)

SDS (sodium dodecyl sulphate) solution (20%) (w/v):

Substance	Volume/Weight
SDS	200 g
Millipore-H_2O	1 L

SDS-PAGE (sodium dodecyl sulfate polyacrylamide gel electrophoresis) running buffer:

Substance	Concentration
Tris/HCl, pH 7.4	250 mM
Glycine	1.92 M
SDS	1% (w/v)

SDS-PAGE separation gels (12%):

Substance	Volume
Millipore-H_2O	3.1 ml
1.5 M Tris/HCl pH 8.8	2.25 ml
SDS 20%	45 µl
Acrylamide	3.6 ml
APS 10%	30 µl
TEMED	6 µl

SDS-PAGE stacking gel (4%):

Substance	Volume
Millipore-H_2O	1.8 ml
0.5 M Tris/HCl pH 6.8	750 µl
SDS 20%	15 µl
Acrylamide	400 µl
APS 10%	15 µl
TEMED	3 µl

TBS (Tris-buffered saline) (10x):

Substance	Concentration
Tris/HCl pH 7.4	10 mM
NaCl	150 mM

TBS-T (TBS with TWEEN®20) (1x):

Substance	Concentration
TBS (10x)	10% (v/v)
Tween®20	0.1% (v/v)
Millipore-H_2O	89.99% (v/v)

Transfer buffer (10x):

Substance	Concentration
Tris/HCl	250 mM
Glycine	1.92 M

Transfer buffer (1x):

Substance	Concentration
Transfer Buffer (10x)	10% (v/v)
Methanol	10% (v/v)
Millipore-H_2O	80% (v/v)

2.1.3 Cell lines

Table 2.6: Murine cell lines

Name	Description	Supplier
B3Z	$CD8^+$ T cell hybridoma cell line specific for $OVA_{257-264}$-peptide (SIINFEKL), expresses β-galactosidase under control of the IL-2 promoter	Nilabh Shastri (Department of Molecular and Cell Biology, University of California)
DOBW	$CD4^+$ T cell line specific for $OVA_{323-339}$-peptide	Cliff Harding (Washington University School of Medicine, Department of Pathology)

2.1.4 Laboratory equipment and software

Table 2.7: Laboratory equipment

Product	Manufacturer
-80°C freezer U570 HEF	New Brunswick; Hamburg, Germany
-20°C freezer MediLine LGex 410	Liebherr; Biberach, Germany
Agarose gel running chamber	Biorad; Hercules, USA
Analytical scale XS20S Dual Range	Mettler Toledo; Gießen, Germany
Autoclave DX-45	Systec; Wettenberg, Germany
Autoclave VX-120	Systec; Wettenberg, Germany
Cell culture work bench Herasafe KS180	Thermo Fisher Scientific; Darmstadt, Germany
Centrifuge MiniSpin plus	Eppendorf; Hamburg, Germany
Centrifuge Rotina 420R	Hettich; Tuttlingen, Germany
Centrifuge with cooling, Micro200R	Hettich; Tuttlingen, Germany
CO_2 cell incubator BBD6620	Thermo Fisher Scientific; Darmstadt, Germany
Demineralized water	Thermo Fisher Scientific; Darmstadt, Germany
Deparaffination machine microm HMS740	Thermo Fisher Scientific; Darmstadt, Germany
Dispenser, Ceramus 2-10ml	Hirschmann Laborgeräte; Eberstadt, Germany
Dry ice container Forma 8600 Series, 8701	Thermo Fisher Scientific; Darmstadt, Germany
Electronic pipet filler	Eppendorf; Hamburg, Germany
Embedding machine, Microm EC350	Zeiss; Oberkochen, Germany
Film developer Curix 60	AGFA; Morsel, Belgium
Fridge MediLine LKv 3912	Liebherr; Biberach, Germany
Gel electrophoresis chamber MINIeasy	Carl Roth; Karlsruhe, Germany
Gel imaging system ChemiDoc XRS+	Biorad; Hercules, USA
Ice machine ZBE 110-35	Ziegra; Hannover, Germany
Intelli-Mixer RM-2	Schubert & Weiss Omnilab; Munich, Germany
Light Cycler LC480II	Roche Diagnostics; Mannheim, Germany
Liquid nitrogen cell tank BioSafe 420SC	Cryotherm; Kirchen/Sieg, Germany
Liquid nitrogen tank Apollo 200	Cryotherm; Kirchen/Sieg, Germany
LSR II (flow cytometer)	BD Bioscience; Heidelberg, Germany
Magnetic stirrer KMO 2 basic	IKA; Staufen, Germany
Mastercycler gradient	Eppendorf; Hamburg, Germany
Mastercycler Nexus	Eppendorf; Hamburg, Germany
Micro-Dismembrator Sartorius	Thermo Fisher Scientific; Darmstadt, Germany
Microscope Axio Imager M2 (fluorescence)	Zeiss; Jena, Germany
Microscope Axiovert 40	Zeiss; Jena, Germany
Microscope LSM 710 (confocal)	Zeiss; Jena, Germany
Microtom, Hyrax M55	Zeiss; Jena, Germany
Multipette stream	Eppendorf; Hamburg, Germany
Nalgene® Freezing Container (Mr. Frosty)	Omnilab; Munich, Germany
NanoDrop 1000	PeqLab; Erlangen, Germany
pH meter InoLab pH 720	WTW; Weilheim, Germany
Pipettes Research Plus	Eppendorf; Hamburg, Germany
Plate centrifuge 5430	Eppendorf; Hamburg, Germany
Plate reader Tri-Star LB941	Berthold Technologies; Bad Wildbach, Germany
Plate reader Sunrise	Tecan; Crailsheim, Germany
Roll mixer	VWR International; Darmstadt, Germany
Power Supply Power Pac HC Power Supply	Biorad; Hercules, USA
Scale XS400 2S	Mettler Toledo; Gießen, Germany

Shaker Duomax 1030	Heidolph; Schwabach, Germany
Tissue processor Microm STP420D	Thermo Fischer Scientific; Waltham, USA
Thermomixer compact	Eppendorf; Hamburg, Germany
Ultrapure water supply MilliQ Advantage A10	Merck Millipore; Darmstadt, Germany
LSM Top table centrifuge MCF-2360	Schubert & Weiss Omnilab; Munich, Germany
Vortex Mixer	IKA; Staufen, Germany
Vacuum pump NO22AN.18 with switch 2410	KNF; Freiburg, Germany
Water bath Aqua Line AL 12	Lauda; Lauda-Königshofen, Germany

Table 2.8: Software

Software	Producer
Axio Imager Software	Zeiss; Jena, Germany
Endnote X6	Thomson Reuters; San Francisco, USA
GraphPad Prism 5	GraphPad Software; La Jolla, USA
FlowJo	Tree Star; Ashland, USA
Image Lab Version	Biorad; Hercules, USA
LightCycler® 480 SW 1.5	Roche Diagnostics; Mannheim, Germany
Magellan Software	Tecan; Crailsheim, Germany
Tri-Star MicroWin 2000	Berthold Technologies; Bad Wildbach, Germany

2.1.5 Chemicals and consumables

Table 2.9: Chemicals

Product	Manufacturer
Ammonium peroxodisulfate (APS)	AppliChem; Darmstadt, Germany
Bovine serum albumin (BSA)	Sigma-Aldrich; Taufkirchen, Germany
Bromphenolblue-Sodiumsalt	AppliChem; Darmstadt, Germany
CCL19	PeproTech; Hamburg, Germany
Chloroform	AppliChem; Darmstadt, Germany
Collagen G	Biochrom; Berlin, Germany
Complete® Mini without EDTA (Protease-inhibitor)	Roche Diagnostics; Mannheim, Germany
Coomassie Brilliant Blue R-250 staining solution	BioRad; Hercules, USA
CountBright™ counting beads	Invitrogen, Life Technologies; Carlsbad, USA
Chlorophenol red-β-D-galactopyranoside (CPRG)	Roche Diagnostics; Mannheim, Germany
Cultrex Collagen IV	R&D systems; Wiesbaden-Nordenstadt, Germany
Cutasept	Bode science center; Heidenheim, Germany
DAPI (4',6-diamidino-2-phenylindole)	Sigma-Aldrich; Taufkirchen, Germany
Desoxyribonucleotide mix (dNTPs)	Thermo Fisher Scientific; Darmstadt, Germany
Dimethyl sulfoxide (DMSO)	Carl Roth; Karlsruhe, Germany
Dithiothreitol (DTT)	AppliChem; Darmstadt, Germany
ECL Plus Western Blotting Substrate	Pierce, Thermo Fisher Scientific; Schwerte, Germany
Eisenhämatosylin, Weigert's, Reagent A	Carl Roth; Karlsruhe, Germany
Eisenhämatosylin, Weigert's, Reagent B	Carl Roth; Karlsruhe, Germany
Eosin Alcoholics	Carl Roth; Karlsruhe, Germany
Eosin G 0.5%	Carl Roth; Karlsruhe, Germany
Acetic acid	AppliChem; Darmstadt, Germany
Ethanol (p.a.)	AppliChem; Darmstadt, Germany

Fetal bovine serum (FBS) "GOLD", heat inactivated	PAA, GE Healthcare; Cölbe, Germany
Fluorescence mounting medium	Dako; Hamburg, Germany
Gamunex® (10%)	Grifolds; Barcelona, Spain
Glycine, molecular biology grade	AppliChem; Darmstadt, Germany
GM-CSF (murine)	PreproTech; Hamburg, Germany
Haemalaun solution Mayers	Carl Roth; Karlsruhe, Germany
Haematoxylin solution Gill	Carl Roth; Karlsruhe, Germany
HANKs' Balanced Salt Solution Modified	Sigma-Aldrich; Taufkirchen, Germany
Heparin	AppliChem; Darmstadt, Germany
HEPES, 1 M	AppliChem; Darmstadt, Germany
Isopropanol, (p.a.)	AppliChem; Darmstadt, Germany
Light Cycler 480 SybrGreen I Master Mix	Roche Diagnostics; Mannheim, Germany
LPS (Lipopolysaccharides, Escherichia coli K-235)	Sigma-Aldrich; Taufkirchen, Germany
Magnesiumchlorid-Hexahydrat MB	AppliChem; Darmstadt, Germany
Magnetic Lumines Screening Assay	R&D systems; Wiesbaden-Nordenstadt, Germany
Methanol, (p.a.)	AppliChem; Darmstadt, Germany
MMP-12 inhibitor 408	Merck; Grafing, Germany
MMP-12 protein, recombinant mouse	R&D systems; Wiesbaden-Nordenstadt, Germany
MMP-13 protein, recombinant mouse	MyBioSourceMerck; Grafing, Germany
MMP-13 inhibitor (CL82198)	Tocris Bioscience, Biozol, Eching, Germany
Non-fat dried milk powder	AppliChem; Darmstadt, Germany
Nonidet P-40	AppliChem; Darmstadt, Germany
$OVA_{323-339}$-peptide	AnaSpec; Seraing, Belgium
$OVA_{Alexa\ 488}$	Invitrogen, Life Technologies; Carlsbad, USA
Ovalbumin grade VI	Sigma-Aldrich; Taufkirchen, Germany
Paraformaldehyde	Sigma-Aldrich; Taufkirchen, Germany
Penicillin-Streptomycin (10000 U/ml)	Gibco, Life Technologies; Carlsbad, USA
Poly-L-Lysine (0.01% solution)	Sigma-Aldrich; Taufkirchen, Germany
Protein marker V	Peqlab; Erlangen, Germany
Random hexamers	Life Technologies; Carlsbad, USA
Rotiphorese Gel 30 (37,5:1) 500ml	Carl Roth; Darmstadt, Germany
SIINFEKL-peptide	Sigma-Aldrich; Taufkirchen, Germany
Sodium chloride	AppliChem; Darmstadt, Germany
Sodium Deoxycholate	VWR; Ismaning, Germany
Sodium dodecyl sulphate (SDS) pellets	Carl Roth; Darmstadt, Germany
SuperSignal West Dura Duration Substrate	Pierce, Thermo Fisher Scientific; Schwerte, Germany
SuperSignal West Femto Substrate	Pierce, Thermo Fisher Scientific; Schwerte Germany
SuperSignal West Pico Substrate	Pierce, Thermo Fisher Scientific; Schwerte, Germany
SybrSafe (10000x in DMSO)	Invitrogen Life Technologies; Carlsbad, USA
Tetramethylethylenediamine (TEMED)	AppliChem; Darmstadt, Germany
Tris base, buffer grade	AppliChem; Darmstadt, Germany
Triton X-100	AppliChem; Darmstadt, Germany
Trypan blue	Sigma-Aldrich; Taufkirchen, Germany
Tween 20	AppliChem; Darmstadt, Germany
UltraPure DNase/RNase-Free Distilled Water	Invitrogen, Life Technologies; Carlsbad, USA
Water soluble tetrazolium (WST) -1	Roche Diagnostics; Mannheim, Germany
Xylol (Isomere)	Carl Roth; Darmstadt, Germany
β-Mercaptoethanol	AppliChem; Darmstadt, Germany

Table 2.10: Consumables

Product	Manufacturer
96 well MaxiSorp ELISA plate	Nunc; Wiesbaden, Germany
96 well plates, white, for luciferase assay	Berthold Technologies; Bad Wildbad, Germany
Whatman blotting paper 3 mm	GE Healthcare; Freiburg, Germany
Cell culture dishes	Corning, Thermo Fisher Scientific; Schwerte, Germany
Cell culture flasks	Nunc; Wiesbaden, Germany
Cell culture multi well plates	TPP Techno Plastic Products; Switzerland
Cell scraper/lifter	Corning, Thermo Fisher Scientific; Schwerte, Germany
Counting chamber	Brand GmbH; Wertheim, Germany
Cryo vials 1.5 ml	Greiner Bio-One; Frickenhausen, Germany
Cryo vials for microdismembrator 1.2 ml	Nalgene, Thermo Fisher Scientific; Schwerte, Germany
Falcon tubes (5 ml, 50 ml)	BD Bioscience; Heidelberg, Germany
Filter tips	Biozym Scientific; Hessisch Oldendorf, Germany
Glas Pasteur pipettes	VWR International; Darmstadt, Germany
Hyperfilm® ECL™ Film	Amersham, GE Healthcare; Freiburg, Germany
Measuring pipettes sterile, single use (2 ml, 5 ml, 10 ml, 25 ml, 50 ml)	VWR International; Darmstadt, Germany
Nylon filters, pore size 70 µm, 40 µm	BD Bioscience; Heidelberg, Germany
Microscope slides, superfrost plus	Thermo Fisher Scientific; Darmstadt, Germany
Menzler-Gläser	Thermo Fisher Scientific; Darmstadt, Germany
PCR plates	Kisker Biotech; Steinfurt, Germany
Reaction tubes (0.5 ml, 1.5 ml)	Eppendorf; Hamburg, Germany
Stainless steel grinding balls (9 mm)	Neolab; Heidelberg, Germany
Sealing foil for PCR plates	Kisker Biotech; Steinfurt, Germany
Shaver, Med comfort	Sanismart; Waltropp, Germany
Tips	Eppendorf; Hamburg, Germany
Transwell, PC membrane, 5.0 µm pore size, 0.33 cm^2 surface area	Corning, Thermo Fisher Scientific; Schwerte, Germany

2.1.6 Kits

Table 2.11: Kits

Product	Manufacturer	Catalog number
BCA Protein Assay kit	Biochrom; Berlin, Germany	#23221
IL-2 ELISA Duo Set	R&D systems; Wiesbaden, Germany	#DY202
PeqGold RNA kit	Peqlab; Erlangen, Germany	#12-3398
RNase-Free DNase set	Qiagen; Hilden, Germany	#79254
Sensolyte 520 MMP-13 Assay kit	Ana Spec; Fremont, USA	#71156
Sensolyte 520 MMP-12 Assay kit	Ana Spec; Fremont, USA	#71157
Sensolyte Plus 520 MMP-13 Assay kit	Ana Spec; Fremont, USA	#72019

2.1.7 Enzymes

Table 2.12: Enzymes

Product	Manufacturer
Collagenase I	Biochrom; Berlin, Germany
DNase I	AppliChem; Darmstadt, Germany
RNase inhibitor 20 U/µl	Invitrogen, Life Technologies; Carlsbad, USA

2.1.8 Quantitative real-time polymerase chain reaction (RT-PCR)

Primers for quantitative polymerase chain reaction (qPCR) were purchased from Eurofins MWG Operon; Ebersberg, Germany as desalted oligonucleotide lyophilisates and dissolved in DNase/RNase-free water to a concentration of 15 µM.

Table 2.13: Mouse primer

Gen		Sequence 5' – 3'
MMP-2	fw	TGATGCTTTTGCTCGGGCCTTA
	rev	TTTACGCGGACCACTTGTCCTT
MMP-9	fw	CGTCGTGATCCCCACTTACT
	rev	AACACACAGGGTTTGCCTTC
MMP-12	fw	TGATGCAGCTGTCTTTGACC
	rev	GTGGAAATCAGCTTGGGGTA
MMP-13	fw	ATCCCTTGATGCCATTACCA
	rev	AAGAGCTCAGCCTCAACCTG
TIMP-1	fw	GGCATCCTCTTGTTGCTATCACTG
	rev	GTCATCTTGATCTCATAACGCTGG
TIMP-2	fw	GGCGTTTTGCAATGCAGACGTA
	rev	ATCTTGCACTCACAGCCCATCT
TIMP-3	fw	TTCTGCAACTCCGACATCGTGA
	rev	CAGGCGTAGTGTTTGGACTGAT
α-enolase	fw	TTGCTTTGCAGGGATCCTACT
	rev	GATCATCAGCTTGTCAATCTT

2.2 Methods

2.2.1 Generation of BMDCs

Femur and tibia of female C57BL/6 mice were harvested and sterilized for 30 seconds in 4 ml of 80% ethanol (AppliChem). Bones were transferred in a 15 ml Falcon tubes (BD Bioscience) and washed with 10 ml phosphatate buffered saline (PBS). Bone marrow cells were sterilely collected by cutting the edges of the bones with a scalpel blade and flushing out the cells with 2 ml DC medium. Cells were centrifuged for ten minutes at 1200 rpm at 4°C, followed by depletion of erythrocytes using 3 ml of lysis buffer. After washing with 10 ml of DC medium, cell pellets were resuspended in 10 ml DC medium and filtrated through a 40 µm nylon cell strainer (BD Bioscience). Afterwards, cells were centrifuged using the same conditions and counted with a Neubauer cell counting chamber. Cell viability was determined by trypan blue (Sigma-Aldrich) staining as described in section 2.2.4. Subsequently, 0.75 x 10^6 cells/ml were cultured in 24-well plates in DC medium supplemented with 1 µg/ml GM-CSF (PreproTech) at 37°C in a humidified cell incubator with 5% CO_2. On day six, loosely and non-adherent cells were collected by carefully rinsing the wells with DC medium. Afterwards, cells were cultured in new 24-well plates and supplemented with fresh GM-CSF. On day seven, loosely- and non-adherent cells were harvested and re-suspended in DC medium for further experiments. To control the purity of BMDCs and their

maturation state, cells were analyzed on day seven for the surface expression of MHC-I, MHC-II, CD80, CD86, CD40, and CD11c (abs all from BioLegend) as described in section 2.2.9.9.1. The purity of $CD11c^+$ BMDCs, which were used subsequently for experiments, was more than 70% with a similar maturation state. Beside the usage of wild-type (wt) C57BL/6 mice, MMP-12 ko mice were additionally used to generate MMP-12 ko BMDCs. Femur and tibia of female MMP-12 ko mice[172], kindly provided by the group of Marcus Mall (Department of Pneumology, University Hospital Heidelberg), were shipped on ice within 24 hours. BMDCs were generated as described above.

Table 2.14: DC medium

Reagent	Concentration
L-Glutamine, Penicillin-Streptomycin	500 µg/ml, 100 U/ml
Inactive FBS	10%
Na-Pyruvate	1 mM
Non-essential amino acids	1x
2-Mercaptoethanol	50 µM
HEPES	10 mM
Add 500 ml RPMI medium	

2.2.2 Cell culture of cell lines

The $CD8^+$ T cell hybridoma cell line B3Z was used, kindly provided by the group of Nilabh Shastri (Department of Molecular and Cell Biology, University of California), which is specific for $OVA_{257-264}$-peptide (SIINFEKL) and expresses β-galactosidase under control of the IL-2 promoter[236]. Additionally, the $CD4^+$ T cell line DOBW was used which is specific for $OVA_{323-339}$-peptide[237], kindly provided by the group of Cliff Harding (Washington University School of Medicine, Department of Pathology).

1 x 10^6/ml B3Z cells or 0.5 x 10^6/ml DOBW cells were cultured in T cell medium (cell culture flasks) at 37°C in a cell incubator with 5% CO_2. Cells were split 1:10 every second day. Therefore, non-adherent and loosely adherent cells were collected in 50 ml tubes, centrifuged at 400 g for four minutes at room temperature (RT), counted (see section 2.2.4), and cultured in culture flasks.

Table 2.15: T cell medium

Reagent	Concentration
L-Glutamine, Penicillin-Streptomycin	500 µg/ml, 100 U/ml
Inactive FCS	10%
Add 500 ml IMDM medium	

2.2.3 Preservation and defrosting of cells

For freezing, 1 x 10^7 DOBW or B3Z cells were resuspended in 1 ml FBS supplemented with 10% dimethyl sulfoxide (DMSO) (Carl Roth) in a specific cryo tube and stored overnight in a Mister Frosty (Omnilab) at -80°C. For long-time storage, tubes were transferred to liquid nitrogen.

To defrost cells, cryo tubes were briefly warmed in a 37°C water bath and quickly diluted in 5 ml T cell medium. Cells were centrifuged at 400 g for four minutes. Finally, cell pellets were resuspended in T cell medium and cultured as described in section 2.2.2.

2.2.4 Cell counting and detection of dead cells

To detect the amount of live and dead cells, the cell suspension was diluted and mixed 1:10 with trypan blue. This dye does not cross the cell membrane of living cells and, therefore, stains only dead cells. Four big squares of a Neubauer counting chamber were counted and living cells were calculated using the following formula.

$$\text{Concentration (c) [cells/ml]} = \text{counted cells/4} \times \text{dilution factor} \times 10^4$$

2.2.5 Cell treatment

As inflammatory stimulus and to mature BMDCs, cells were treated with LPS (Escherichia coli K-235, Sigma-Aldrich) on day seven. In addition, the protein OVA (Ovalbumin grade VI, Sigma-Aldrich) was used to study the process of antigen uptake and processing. If not stated otherwise, 10 µg/ml LPS or 1 mg/ml OVA was administered to BMDCs. For the functional analysis, MMP-13 inhibitor N-[4-(4-morpholinyl)butyl]-2-benzofurancarboxamide hydrochloride (CL82198) (Tocris Bioscience) or MMP-12 inhibitor (S)-2-(8-(Methoxycarbonylamino)dibenzo[b,d]furan-3-sulfonamido)-3-methylbutanoic acid (MMP408) (Merck) was used with following concentrations: MMP-12 inhibitor: 10 µM, 20 µM, 50 µM and MMP-13 inhibitor: 50 µM, 100 µM, 200 µM, and 500 µM.

2.2.6 Detection of cell viability by WST-1 assay

BMDCs were treated with the indicated inhibitor concentrations overnight and water soluble tetrazolium-1 (WST) assay was performed according to the manufacture`s protocol. This colorimetric assay is based on the cleavage of a tetrazolium salt, MTS, by mitochondrial dehydrogenases forming formazan in viable cells. Cells that are viable and metabolically active produce greater amount of formazan resulting in an accumulation of WST-1. Overnight was chosen as timeframe for the toxicity test as this was the longest period of co-incubation with the inhibitors during the functional assays.

2.2.7 Functional analysis

If not stated differently, all cells used in the below described functional analysis were centrifuged at 400 g.

2.2.7.1 Migration assay through collagen I

Collagen I gel was prepared on ice as follows: 0.7 M NaOH and 1 M HEPES buffer were mixed 1:1 and transferred in a new tube. An equal amount of 10x PBS plus 20% FBS was added to the tube and mixed with collagen in the relation 1:5. Each transwell (PC membrane, 5.0 µm pore size, Corning) was filled with 50 µl of gel and allowed to polymerize for two hours at 37°C. Transwells were placed in 12-well plates filled with 600 µl RPMI plus 0.5% BSA supplemented with CCL19 (10 µg/ml) (PeproTech) or with PBS as control. BMDCs were centrifuged at RT for 6 minutes and resuspended in RPMI plus 0.5% BSA. Subsequently, BMDCs were pre-treated with different concentrations of MMP-12 or MMP-13 inhibitor for one hour. Afterwards, 2 x 10^5 BMDCs in 100 µl were seeded on top of each collagen-filled transwell and either treated with LPS (10 µg/ml) or left untreated. 24 hours later, 500 µl of the cell suspension was harvested from each bottom chamber and stained without washing step for CD11c and MHC-II. 25 µl CountBright™ absolute counting beads (Life Technologies) were added and the $CD11c^+$ BMDCs that had migrated through the gel and reached the bottom chamber were counted using an LSR II flow cytometer (BD Bioscience) and FlowJo software (Tree Star).

2.2.7.2 Migration assay through collagen IV

Collagen IV (R&D) was diluted 1:5 with distilled Millipore-H_2O. 100 µl of collagen IV gel was filled in each transwell and polymerized overnight at 37°C. Afterwards, the remaining liquid on top of the collagen-coated transwells was carefully aspirated and transwells were placed in 12-well plates filled with 600 µl RPMI plus 0.5% BSA supplemented with 10 µg/ml CCL19 or with PBS as control. BMDCs were placed on top of the transwells. Cells were further cultured as described in section 2.2.7.1 with minor differences. As collagen IV is a target substrate of MMP-12 but not of MMP-13, only MMP-12 dependent migration was analyzed here. Due to the lower thickness of collagen IV, the migration time was four hours until the cells were collected from the bottom chamber. In addition, to control that collagen IV was completely covering the transwells, BMDCs were seeded on top of transwells without collagen.

2.2.7.3 Endocytosis assay

2 x 10^5 BMDCs in 100 µl DC medium were transferred to specific polypropylene round-bottom tubes (FACS-tubes) (BD Bioscience) and pre-treated with indicated amounts of MMP-12 or MMP-13 inhibitor for one hour at 37°C, cooled down on ice for ten minutes, and incubated with $OVA_{Alexa\ 488}$ (10 µg/ml) (Life Technologies) at 4°C (control) or 37°C (endocytosis). One hour later, the process of endocytosis was stopped with 2 ml of ice-cold PBS supplemented with 0.5% BSA. Cells were additionally washed three times with PBS-BSA buffer. Therefore, tubes were filled with 1 ml PBS-BSA buffer, centrifuged at 4°C for ten minutes, and supernatant was discarded. Finally, cell pellets were resuspended in 70 µl PBS-BSA buffer, blocked with 10 µl Gamunex (Grifolds), and stained with 20 µl of ab-mix for DCs (Table 2.16). The intensity of OVA-uptake was analyzed

by flow cytometry. For detailed analysis, BMDCs were divided in different analysis groups based on their expression intensity of MHC-II.

Table 2.16: Ab-mix for DCs

Anti-mouse Ab	Dilution	Supplier	Fluorochrome	Isotype
MHC-II	1:100	BioLegend	PerCP/Cy5.5	Rat IgG2b, κ
CD11c	1:50	BioLegend	APC	Hamster IgG

2.2.7.4 T cell activation assay

OVA cross-presentation and T cell activation was detected using the $CD8^+$ T cell hybridoma cell line B3Z. 2 x 10^5 BMDCs in 200 µl DC medium was seeded in 96 well-plates. Cells were either not treated (group one) or pre-treated with indicated amounts of MMP-13 inhibitor for one hour at 37°C (group two). Subsequently, cells were pulsed with 1 mg/ml soluble OVA grade VI or 1 µg/ml SIINFEKL-peptide as positive control, or PBS as negative control for three hours. Finally, BMDCs were centrifuged for 8 minutes at 540 g at 4°C and washed with 200 µl of ice-cold PBS. Afterwards, BMDCs were cultured with indicated amounts of inhibitor overnight in the presence of 1 x 10^5 B3Z cells in 200 µl T cell medium without phenol red indicator to avoid erroneous results during the colorimetric LacZ assay. Cells were centrifuged and supernatant was harvested. The remaining cells on the 96-well plates were washed with 200 µl cold PBS and incubated for three hours with LacZ buffer at 37°C. Activation of B3Z cells was monitored by measuring IL-2 accumulation in the cells by a colorimetric LacZ assay (absorbance 570/620 nm) and in the supernatant by an IL-2 enzyme-linked immunosorbent assay (ELISA) (R&D). Note that group one was subjected to the inhibitor only after the OVA-uptake was already completed, whereas group two was exposed to the inhibitor before the pulsing with OVA protein and once more after the pulsing, during the co-incubation with the T cells. To exclude direct influences of the inhibitor on B3Z cells, non-inhibitor-treated BMDCs were pulsed with SIINFEKL-peptide for two hours. Afterwards, they were washed with cold PBS and fixed in 1% paraformaldehyde (PFA) (Sigma-Aldrich) for 30 minutes on ice. Finally, after a further washing step, BMDCs were co-incubated with B3Z cells in T cell medium together with indicated amounts of inhibitor.

Peptide presentation via the classical MHC-II pathway and activation of $CD4^+$ T cells was detected by using the $CD4^+$ T cell hybridoma cell line DOBW instead of B3Z cells. Experiments were performed as described for B3Z cells with slight variations. 1 x 10^5 BMDCs were co-incubated with 2 x 10^5 DOBW cells in 200 µl T cell medium. To detect the influence of MMP-13 inhibition on DOBW cells, untreated DCs were pulsed with $OVA_{323-339}$-peptide (AnaSpec) for two hours, subsequently fixed, washed, and co-incubated with indicated amounts of inhibitor and DOBW cells in 200 µl T cell medium. Activation of DOBW cells was monitored by measuring IL-2 secretion using an ELISA.

Table 2.17: LacZ buffer

Reagent	Concentration/Volume
β-Mercaptoethanol	225 µl
$MgCl_2$	4.5 mM
NP40	0.07%
CPRG	0.046 mg/ml
PBS	add to 50 ml

2.2.8 Molecular biology

2.2.8.1 mRNA isolation

Total RNA was isolated from cells or trachea tissue using pepGold total RNA kit (Peqlab) according to the manufacture`s protocol. Unless described differently, isolation was performed at RT. Briefly, cells were lysed and DNA was removed using a DNA removing column. Subsequently, RNA was precipitated by 70% ethanol and isolated by a PerfectBind RNA column. DNase digestion was made within 15 minutes with 73.5 µl DNase I Digestion Buffer and 1.5 µl RNase-free DNase I (20 units/µl) directly on the column and after diverse washing steps, mRNA was eluted with 40 µl of sterile RNase-free dH_2O by centrifugation. Subsequently, reverse transcription was performed.

For mRNA isolated from trachea tissue, mRNA elution was performed similarly, but with one additionally homogenization step. For tissue homogenization, frozen trachea tissue was grinded with a stainless steel ball in a cryo tube applying 3000 rpm for 30 seconds in the microdismembrator. In order to avoid thawing of the tissue, the homogenized material was snap frozen in liquid nitrogen before shaking another 30 seconds with 3000 rpm in the microdismembrator. The frozen powder was dissolved in 1 ml Roti-Quick 1 Solution and incubated for 20 minutes on ice before it was jolted for ten seconds with 3000 rpm in the microdismembrator. The lysate was transferred to another fresh tube and 1 ml of Roti-Quick-Solution 2, based on a Phenol-Chloroform solution, was added and mixed intensively. After ten minutes of incubation on ice, the mixture was centrifuged 15 minutes at 13000 rpm at 4°C and the upper aqueous layer was separated and transferred to a new tube. After this lysis procedure, samples were supplemented with 70% ethanol and further processed as described above.

2.2.8.2 cDNA synthesis and qRT-PCR

Reverse transcription was performed using the GeneAMP PCR kit (Applied Biosystems) together with random hexamers and 1 µg of isolated mRNA per reaction. Denaturation was performed in an Eppendorf Mastercycler (lid = 90°C, 70°C for 10 minutes, and 4°C for 5 minutes), followed by reverse transcription (Eppendorf Mastercycler: lid = 105°C, 20°C for 10 minutes, 42°C for 60 minutes, and 99°C for 5 minutes).

Table 2.18: Mastermix for reverse transcription

Reagent	Stock concentration	Volume [µl]
$MgCl_2$	5 mM	8
10x Buffer	10 mM	4
dNTPs	1 mM	4
Random Hexamers	2.5 µM	2
RNase Inhibitor	1 U/µl	2
Reverse Transcriptase	2.5 U/µl	2
Denat. RNA	1 µg	18
Total		40

cDNA was used subsequently for qRT-PCR or stored at -20°C. qRT-PCR reactions were performed in duplicates with SYBR Green I Master in a LightCycler® 480 II (Roche) with standard conditions: 95°C for five minutes followed by 45 cycles of 95°C for five seconds (denaturation), 59°C for five seconds (annealing), and 72°C for 20 seconds (elongation).

Table 2.19: Mastermix for qRT-PCR

Reagent	Stock concentration	Volume [µl]
SybrGreen I Master Mix	2x	5
Primer Mix	15 µM each	0.5
cDNA	8.33 ng/µl	3
H_2O		1.5
Total		10

For standardization of relative mRNA expression, target genes were normalized to α-enolase expression. Relative transcript abundance of a gene is expressed in ΔCT values ($\Delta CT = CT_{reference} - CT_{target}$). Relative changes of mRNA levels are presented as ΔΔCT values ($\Delta\Delta CT = \Delta CT_{treated} - \Delta CT_{control}$). Mouse primer sequences were as detailed in Table 2.13.

All primers for quantitative PCR were designed with NCBI's PrimerBLAST (http://www.ncbi.nlm.nih.gov/tools/primer-blast/) and tested for primer hybridization, primer-dimer, and hairpin formation by oligoanalyzer tool from Integrated DNA Technologies (http://eu.idtdna.com/analyzer/applications/oligoanalyzer/#Structure%201). If possible, the following primer criteria were adhered to: amplicon size ≤ 500 bp, GC content ≈ 50%, T_M (primer) ≈ 60°C, and size of primer 18 - 24 bp.

For determination of the RNA and DNA concentration, absorbance at 260 nm was measured using the NanoDropTM 1000 spectrophotometer. As blank, control H_2O was measured.

2.2.9 Protein biochemistry

2.2.9.1 Protein isolation and concentration determination

Cells were centrifuged at 400 g for 8 minutes and frozen at -80°C for later analysis. For protein isolation, cells were denaturated on ice for 30 minutes in 70 µl RIPA lysis buffer containing

protease/phosphatase inhibitors. Protein extracts were separated by centrifugation at 14000 g for 15 minutes at 4°C. Protein concentrations were determined using BCA assay from 1:5 diluted samples according to the manufacture's protocol.

2.2.9.2 Protein analysis by Western blot

Cell lysates were mixed with 6x Lämmli buffer and PBS to gain equal amounts of total proteins, denaturated for five minutes at 95°C, separated in 10% SDS-polyacrylamide gels, and blotted onto a nitrocellulose membrane. After blocking with 5% milk in TBST (0.1% Tween 20/TBS) for 30 minutes, membranes were incubated with the respected primary antibody overnight at 4°C while shaking. After washing three times for ten minutes with TBST, membranes were incubated with HRP-conjugated secondary antibodies for one hour at RT. After washing three times with TBST, the membranes were incubated for five minutes with Dura Duration Substrate and bands were visualized by enhanced chemiluminescence. Signals were detected using x-ray films and automatically developed with the film developer Curix 60.

2.2.9.3 Protein analysis by immunofluorescence (IF) staining

Tracheas were fixed in 4% PFA and incubated overnight at 4°C. The next day tracheas were embedded in paraffin blocks using an embedding machine. After discarding 20 µm of the upper end of the embedded trachea, 2 µm thick pieces were cut in series with a microtome and collected on object slides. After drying the slides for 30 minutes at 60°C, the tissue was deparaffinated and cooked with Citrate buffer (pH 6.0) in a decloaking chamber for 30 seconds at 125°C and for ten seconds at 90°C. This step is important to get access to antibody binding sites that are covered due to the fixation and embedding process. Afterwards, slides were slowly cooled down and washed three times with Tris buffer. To block the endogen peroxidase, slides were put in 2% H_2O_2 for 15 minutes. The washing step with Tris buffer was repeated three times and 100 µl of primary antibody in appropriated dilution was put on the tissue for one hour at RT. Slices were washed again three times with Tris buffer and 100 µl of the secondary antibody (1:250) was added for 30 minutes at RT. To detect another protein on the same slice, the process was repeated with the corresponding primary and secondary antibody. Finally, slides were counterstained with DAPI (1:2500) for one minute in the dark and washed three times with Tris buffer. The slides were covered with fluorescence mounting medium, dried, and stored at 4°C in the dark or were directly taken for immunofluorescence images. Antibodies are listed in Table 2.3 - Table 2.5.

2.2.9.4 Immunohistochemical analysis by H&E and Masson Trichrome staining

Hematoxylin and eosin (H&E) staining

Fixed tracheas were embedded, cut, and deparaffinated as described in section 2.2.9.3. The slides were incubated in Meyers` Hämalaun solution for 6 minutes, washed in distilled water, washed for 15 minutes in running tap water, and finally washed two minutes in distilled water. Slides were immersed for ten minutes in 100 ml Eosin Y solution (0.5%), supplemented with one drop of acetic

acid, washed in running tap water for five minutes, and incubated in 80% ethanol for another five minutes. The tissues on the slides were dehydrated by incubating two times in 100% ethanol followed by two times in Xylene for five minutes. Finally, the slices were prepared for long-time storage by embedding in mounting medium (Entellan). Dried slices were stored at 4°C.

Masson Trichrome staining

Fixed tracheas were embedded, cut, and deparaffinated like described in section 2.2.9.3. Slides were incubated in equal amounts of Weigerts` iron hematoxylin A and B solution for ten minutes and afterwards put in Picric acid alcoholic stable solution for four minutes. After washing three seconds in distilled water, slides were immersed in acid solution E and incubated for ten minutes. Afterwards, slides were immediately incubated in light green solution F for five minutes and washed in distilled water. The tissue was dehydrated rapidly through ascending concentrations of ethanol by immersing the slides one minute at 90%, one minute at 95%, and one minute at 100% ethanol. Finally, the slides were cleared in Xylen for 20 minutes, embedded in mounting medium (Entellan), and stored at 4°C.

2.2.9.5 MMP-12 activity assay

To measure active MMP-12 in response to an inflammatory stimulus, BMDCs were cultured in the absence or presence of LPS (10 µg/ml). Active MMP-12 in the supernatant of BMDCs was measured three hours after LPS treatment using SensoLyte® 520 MMP-12 assay according to manufactures instructions (extinction = 490 nm; emission = 520 nm). The SensoLyte® 520 MMP-12 assay is based on the same method as described in section 2.2.9.6 for SensoLyte® Plus 520 specific MMP-13 assay but without the usage of the specific anti-MMP antibody. In contrast to MMP-13 there exists no commercially available specific MMP-12 activity assay.

To quantify the efficacy of the MMP-12 inhibitor to inhibit murine MMP-12, recombinant murine MMP-12 protein (R&D Systems) was activated by the organomercurial derivate APMA for 120 minutes at 37°C, incubated with MMP-12 inhibitor at different concentrations, and quantified by the same activity assay. In case of the recombinant MMP-12 protein, the SensoLyte® 520 MMP-12 assay without specific antibody was sufficient.

2.2.9.6 MMP-13 activity assay

To detect active MMP-13, BMDCs were cultured in the absence or presence of LPS (10 µg/ml) or OVA (1 mg/ml). Active MMP-13 in the supernatant of BMDCs was measured three hours after LPS or OVA treatment using SensoLyte® Plus 520 specific MMP-13 assay according to manufactures instructions. Briefly, a specific anti-MMP-13 monoclonal antibody was used in combination with a MMP fluorogenic substrate (5-FAM/QXL®520 FRET peptide). The fluorescence signal was monitored (extinction = 490 nm; emission = 520 nm) upon MMP-13 induced cleavage of the fluorescence resonance energy transfer (FRET) substrate.

To quantify the efficacy of the MMP-13 inhibitor to inhibit murine MMP-13, recombinant murine MMP-13 protein (Emelca Bioscience) was activated by APMA for 40 minutes at 37°C, incubated with MMP-13 inhibitor at different concentrations, and quantified by SensoLyte® 520 MMP-13 assay (extinction = 490 nm; emission = 520 nm).

2.2.9.7 IL-2 enzyme-linked immunosorbant assay (ELISA)

Mouse IL-2 protein concentration in cell supernatants of B3Z cells or DOBW cells were analyzed with the IL-2 DuoSet ELISA from R&D Systems according to the manufacture's protocol using Nunc MaxiSorp® flat-bottom 96-well plates. Supernatants were obtained by centrifugation of cells in 96-well plates at 540 g for 7 minutes at 4°C. Supernatant was stored at -80°C for later analysis.

2.2.9.8 Cytokine screening by Luminex assay

200 µl of 2 x 10^5 BMDCs in DC medium were cultured with 10-500 µM MMP-13 inhibitor for 24 hours, followed by treatment with LPS (10 µg/ml). Supernatant of BMDCs was harvested three hours after LPS treatment. Cytokine and chemokine profile were analyzed using Luminex bead-based multiplex screening assay (R&D) according to manufactures instructions. The customer based assay detected the following chemokines and cytokines: CCL2/JE/MCP-1, CCL3/MIP-1α, CCL4/MIP-1β, CCL5/RANTES, CCL20/MIP-3α, CXCL1/KC, CXCL2/MIP-2, CXCL10/IP-10/CRG-2, IFN-γ, IL-1β, IL-6, IL-10, IL-12p70, IL-13, IL-23p19, LIX, TNF-α, and CXCL12/SDF-1α.

2.2.9.9 Flow cytometry analysis

For all flow cytometry experiments the basic gating strategy was as follows: After separating the cell population of interest according to their size and granulation by forward (FSC) and side (SSC) scatter, dead cells were separated by Propidium iodide (PI) staining. PI is a fluorescent molecule that can only bind to DNA of dead cells whereas it is discharged in living cells. Afterwards, doublet cells were excluded by FSC-A/FSC-W gating, followed by gating on the different cell types by specific antibodies.

2.2.9.9.1 Surface expression of DCs

To determine the surface expression of MHC-I, MHC-II, CD80, CD86, CD40, and CD11c, (Table **2.20** and Table 2.21) cells were treated with 10, 50, 100, 200, and 500 µM MMP-13 inhibitor overnight together with LPS (10 µg/ml) or OVA (1 mg/ml). Data were collected on LSR II and analyzed with FlowJo software.

Table 2.20: Ab-mix for maturation markers

Anti-mouse ab	Dilution	Supplier	Fluorochrome	Isotype
MHC-II	1:100	BioLegend	PerCP/Cy5.5	Rat IgG2b, κ
CD80	1:50	BioLegend	PB	Hamster IgG
CD86	1:100	BioLegend	PE	Rat IgG2a, κ
CD40	1:50	BioLegend	PE/Cy7	Rat IgG2a, κ
CD11c	1:50	BioLegend	APC	Hamster IgG
in 20 µl PBS + 2% FBS				

Table 2.21: Ab-mix for MHC-I presentation

Anti-mouse ab	Dilution	Supplier	Fluorochrome	Isotype
CD11c	1:50	BioLegend	APC	Hamster IgG
H-2K^b MHC-I	1:50	BioLegend	PE	Mouse IgG2a, κ
in 20 µl PBS + 2% FBS				

2.2.9.9.2 SIINFEKL-peptide presentation on MHC-I

To determine the presentation of the specific SIINFEKL-peptide on MHC-I (Table 2.22), BMDCs were pre-treated with indicated amounts of MMP-13 inhibitor for one hour. Afterwards, BMDCs were pulsed with 1 mg/ml soluble OVA grade VI (Sigma) for three hours, followed by washing and further cultivation overnight in DC medium supplemented with inhibitor. SIINFEKL-peptide (1 µg/ml) (Sigma) was used as positive control. Finally, BMDCs were washed and stained for H-2K^b combined SIINFEKL. Data were collected on LSR II and analyzed with FlowJo software.

Table 2.22: Ab-mix for quantification of SIINFEKL-peptide presentation

Anti-mouse ab	Dilution	Supplier	Fluorochrome	Isotype
CD11c	1:50	BioLegend	APC	Hamster IgG
H-2K^b bound to SIINFEKL	1:50	BioLegend	PerCP/Cy5.5	Mouse IgG2b, κ
in 20 µl PBS + 2% FBS				

2.2.9.9.3 Detection of apoptotic and dead cells

To detect apoptotic and dead cells by flow cytometry, PI/Annexin staining was performed according to the manufacture`s protocol. In the early phase of apoptosis the membrane phospholipid phosphatidylserine (PS) is translocated from the inner side of the plasma membrane to the outer side, thereby exposing PS to Annexin V, a calcium-dependent phospholipid-binding protein. Cells that are positive for Annexin V (FITC) and negative for PI are undergoing apoptosis. Cells that stain positive for both Annexin V and PI are either in the end stage of apoptosis, are undergoing necrosis, or are dead.

2.2.9.9.4 Surface expression of leukocyte populations in blood and lymph nodes of transplanted mice

Blood, lymph nodes, and tracheas were collected from mice as will be described in 2.2.10.

Tracheas

Tracheas, collected in RPMI medium with 0.7 mg/ml Collagenase A plus 25 µg/ml DNase I were grinded with the punch of a syringe and incubated for 60 minutes at 37°C. Afterwards, the tissue was homogenized using a syringe and subsequently filtrated through a 70 µm cell strainer by adding 10 ml RPMI plus 10% FBS. After two times of washing, cells were resuspended in buffer and counted by trypan blue staining. (Ab-mixes listed in Table 2.23 -Table 2.24).

Lymph nodes

Four lymph nodes per animal (two brachial, two axillary) were collected in RPMI and centrifuged at 300 g for ten minutes at 4°C, followed by homogenization with the punch of a syringe and filtration through a 40 µm cell strainer by adding 500 µl RPMI. After centrifugation, cells were counted by trypan blue staining and stained for flow cytometry analysis. To characterize the murine HTT model in detail, the different distribution of myeloid and lymphocytic populations in the lymph nodes of syngen and allogen transplanted animals were analyzed on the day of sacrification.

Blood

Whole-blood staining was performed after depletion of erythrocytes using the automatic lysis program of coulters immunology workstation. To characterize the murine HTT model in detail, the same staining strategy was performed as described above for lymph nodes.

Table 2.23: Ab-mix for myeloid cells

Anti-mouse ab	Dilution	Fluorochrome	Isotype
CD11b	1:100	PE	Rat IgG2b, κ
MHC-II	1:200	PerCP/Cy5.5	Rat IgG2b, κ
CD45	1:20	FITC	-
Ly-6G/Ly-6C	1:20	V450	Rat IgG2b, κ
F4/80	1:13	APC/Cy7	Rat IgG2a, κ
CD11c	1:13	APC	Hamster IgG
in 20 µl PBS + 2% FBS			

Table 2.24: Ab-mix for lymphocytes

Anti-mouse ab	Dilution	Fluorochrome	Isotype
CD3	1:20	PB	-
CD19	1:200	PE	-
CD45	1:40	FITC	-
CD4	1:100	PerCP/Cy5.5	-
CD8α	1:100	APC/Cy7	-
NK1.1	1:40	APC	-
in 20 µl PBS + 2% FBS			

2.2.10 Murine HTT model (mouse model)

Female C57BL/6 mice and female BALB/c mice were obtained from Jackson Immuno-Research Laboratories and used at the age of 8-10 weeks. All experiments were conducted according to the guidelines of the Ethics Committee of the Helmholtz-Center Munich and approved by the Regierungspräsidium Oberbayern, Germany.

Syngrafts and allografts were obtained by transplanting either C57BL/6 tracheas into C57BL/6 recipient (syngraft) or BALB/c tracheas into C57BL/6 recipient (allograft).

Donor mice were deeply narcotized with intraperitoneal (i.p.) administration of a mixture of 60% ketamine, 20% rompun, and 20% NaCl according to their body weight (around 0.6 ml) and sacrificed by cervical fracture. Skin of mice was sterilized with 70% ethanol and mice were fixed on a polystyrene plate. First, donor heart and lung were exposed via a midline incision through the skin and peritoneum extending through the rib cage and sternal notch. Second, thymus tissue was dissected away. Afterwards, the esophagus was separated from the trachea by blunt dissection and the trachea was then excised cephalad near the larynx and close to the hilu above the lung. Finally, the trachea was placed in PBS. Recipient mice were narcotized with i.p. administration of 0.2 mg/ml medetomidin (Orion Pharma, Hamburg), 2.0 mg/ml midazolam (Roche Pharma, Mannheim), and 0.02 mg/ml fentanyl (Janssen-Cliag, Neuss) according to their body weight. Skin of mice was sterilized with Cutasept. After shaving of a 1 cm × 1 cm large area behind the head on the back, a 3 mm transverse incision was made through the dermis and a 1.5 cm × 1.5 cm large subcutaneous pouch was created via blunt dissection. One trachea was placed into each animal and the skin pocket was closed with size 5.0 degradable suture, sterilized with Cutasept, and covered with iodine. After the instillation procedure, the narcosis was antagonized subcutaneously with 0.29 mg/ml atipamezol (Orion Pharma, Hamburg), 0.059 mg/ml flumazenil (Hexal, Holzkirchen), and 0.14 mg/ml naloxon (Actavis, Munich) according to the mouse body weight. Narcosis and antagonist was obtained through the Tierärztliche Hausapotheke of the Helmholtz Zentrum München. Mice which got the inhibitor were treated i.p. every second day with 25 µg (74 µM) (two animals per group) or with 100 µg (296 µM) (four animals per group) MMP-13 inhibitor (100 µl) or 100 µl NaCl as control. On day 14 and 21, syngrafts and allografts were harvested and collected either in 4% PFA for histology, or in RPMI (4°C) with 0.7 mg/ml collagenase A plus 25 µg/ml DNase I for flow cytometry, or were snap frozen in liquid nitrogen for RNA analysis. Additionally, blood and lymph nodes (axillary and branchial) were collected from each mouse on the day of sacrification and, subsequently, used for flow cytometry analyses. The blood (max. 0.8 ml) was collected from the abdominal aorta with a syringe wetted with heparin.

To quantify the BOS phenotype, luminal occlusion and epithelial loss were calculated on histological slices. Epithelial loss was calculated by measuring the distance of destroyed epithelium in relation to intact epithelium. Luminal occlusion was determined by following formula adapted from Grove *et al.*[238].

$$\text{Luminal occlusion} = \frac{\text{area within cartilage - area within residual lumen x 100}}{\text{area within cartilage}}$$

2.2.11 Statistical analysis

Statistical analysis was performed with GraphPad Prism 4 (GraphPad Software) using unpaired t-test, One-way Anova with Dunnett's multiple comparison test, Anova with Kruskal-Wallis Dunn's comparison test, or One-Sample t-test. Data are presented as mean ± S.D or median (25-75 percentile with minimum (min.) to maximum (max.).

3 RESULTS

DCs and MMPs are both considered to be important in the pathogenesis of BOS, as detailed in the introduction section. Whether the selected MMPs, MMP-12 and -13, are involved in BOS and whether they have specific immunobiological functions in DCs, which might promote the progression of BOS, have not been investigated so far. To elucidate possible immunobiological functions of MMP-12 and -13 in DC biology, experiments were performed with *in vitro* generated murine DCs. This knowledge should subsequently be applied to the *in vivo* mouse BOS model to gain insights how DC biology and MMPs might contribute to the pathogenesis of BOS *in vivo*.

3.1 *In vitro* analysis of MMP-12 and -13 in DC immunobiology

3.1.1 Analysis of generated bone marrow-derived DCs by flow cytometry

To obtain enough cells for the diverse functional assays, murine DCs derived from bone marrow (BMDCs) were chosen as source of DCs for the *in vitro* study. As shown in Figure 3.1 and detailed in section 2.2.1., cells were generated from bone marrow cells within one week by adding GM-CSF and harvesting non-adherent cells.

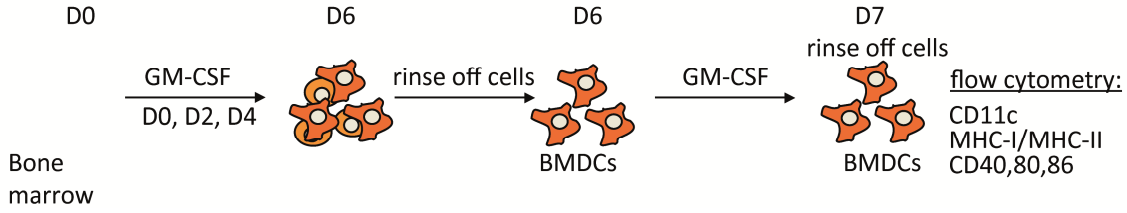

Figure 3.1: Generation of BMDCs *in vitro*.
BMDCs were generated within one week by adding GM-CSF and by separating them from the majority of remaining cells by cell adherence. On day seven, cells were harvested and analyzed for their expression profile.

To control the purity and the phenotype of generated BMDCs, cells were analyzed on day seven for the surface expression of CD11c, MHC-I, MHC-II, CD80, CD86, and CD40. First, cells were selected by forward and side scatter (Figure 3.2i), followed by exclusion of cell doublets (Figure 3.2ii) and separation of dead cells by live-dead staining with PI (Figure 3.2iii). Afterwards, remaining cells were gated on $CD11c^+$ cells (Figure 3.2iv-v) and either analyzed for MHC-I (Figure 3.2iv) or MHC-II expression (Figure 3.2v). The purity of $CD11c^+$ BMDCs, which were used subsequently for experiments, was at least 70% with a homogenous maturation state of the cell population (Figure 3.2vii-ix). For the later performed endocytosis assay (see section 3.1.3.2), $CD11c^+$ cells were further separated according to their MHC-II surface expression intensity (Figure 3.2vi). Additionally, to control their maturation state, cells were stimulated 24 hours with LPS or left unstimulated, subsequently gated for $CD11c^+$ BMDCs (Figure 3.2v), and further analyzed by three different maturation markers (CD40, CD80, and CD86). In line with previous reports[239],

BMDCs stimulated with LPS increased CD40, CD80, and CD86 compared to non-stimulated ones (Figure 3.2vii-ix).

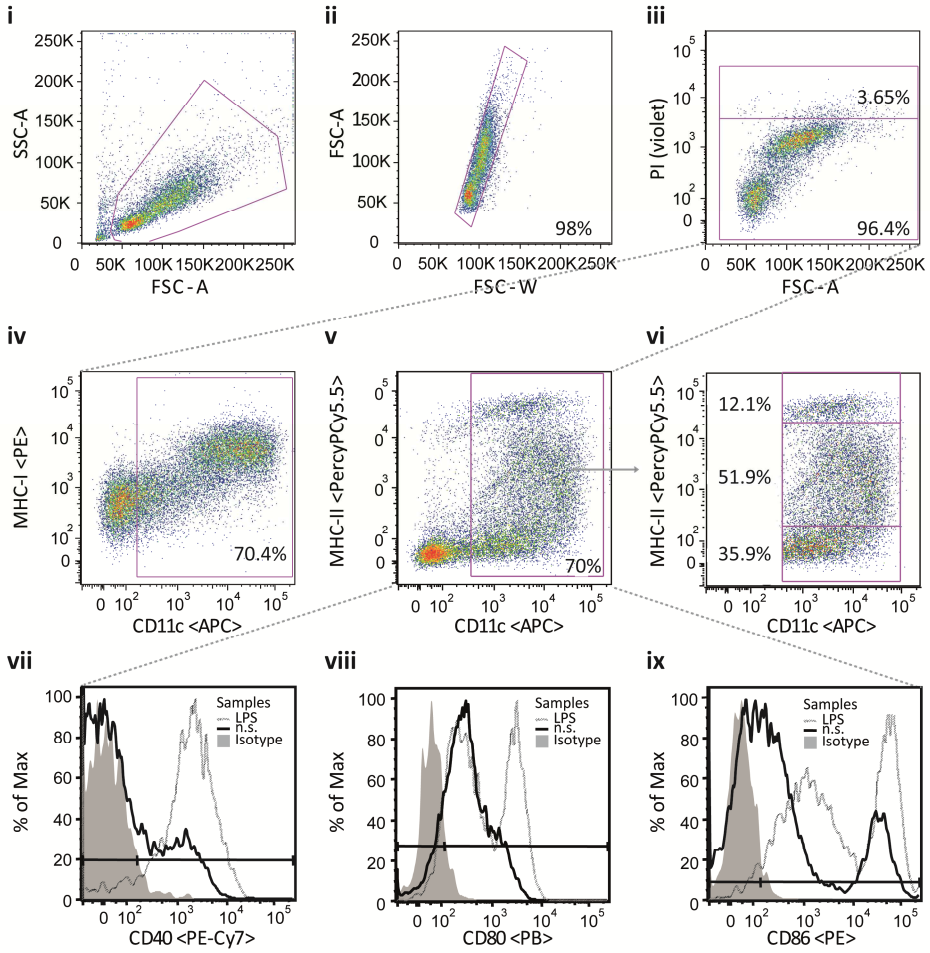

Figure 3.2: Gating strategy of generated BMDCs.
(i) Cells were gated according to their size and granulation followed by (ii) separation of doublets and (iii) dead cells. Afterwards, $CD11c^{+}$ cells were further analyzed for their (iv) MHC-I or (v) MHC-II expression. (vi) The intensity of MHC-II expression was further divided in $MHC\text{-}II^{low}$, $MHC\text{-}II^{dim}$, and $MHC\text{-}II^{high}$. The maturation state of BMDCs on day 7 was evaluated by the expression of the following markers: (vii) CD40, (viii) CD80, and (ix) CD86. To gain mature BMDCs, cells were stimulated on day seven with LPS for 24 h and analyzed subsequently for their maturation profile. Non-stimulated (n.s.).

3.1.2 Expression analysis of MMPs and TIMPs in DCs

To determine the importance of MMP-12 and -13 for the immunostimulatory function of DCs, expression of these MMPs was first verified in unstimulated immature BMDCs by qRT-PCR (Figure 3.3A). Expression of MMP-12 and -13 was detected with the following $\Delta CT_{(\alpha\text{-enolase-target})}$ values of 6 ± 1.2 and -2.2 ± 1.7 (mean ± SD), respectively. In addition, expression of the natural MMP inhibitors TIMP-1, -2, and -3, was also determined in these cells (ΔCT values of -4.3 ± 0.9, -3.4 ±1.5, and -5.1 ± 1.4, respectively). For comparison, BMDCs were also analyzed for the expression of two already very intensely studied MMPs, namely MMP-2 and -9 (ΔCT values of -3 ± 2.6 and 0.7 ± 1.1, respectively). In line with other studies[170], all MMPs were detected at low expression level under baseline conditions with MMP-12 showing the highest expression level.

To test for MMP-12 and -13 expression on protein level, Western blot analysis was performed. The presence of the zymogen (54 kDa) and the active form of MMP-12 (45 kDa) as well as the different forms of the MMP-13 protein, pro-enzyme (60 kDa), active form (54 kDa), and cleaved fragments (48/34 kDa) were detected in unstimulated BMDCs (Figure 3.3B).

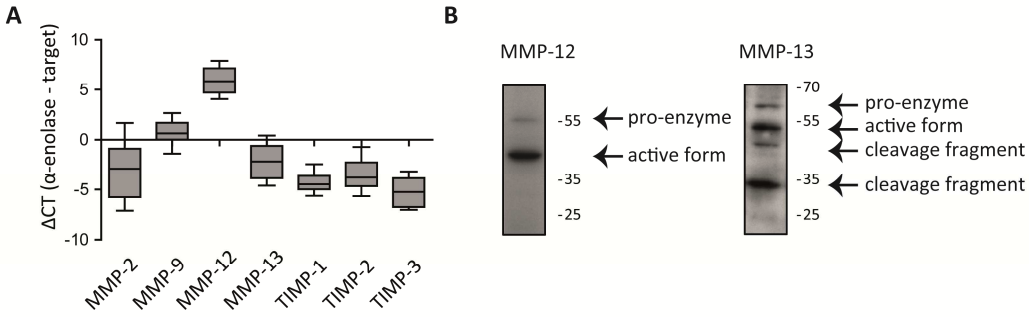

Figure 3.3: MMP-12 and -13 expression in unstimulated BMDCs on RNA and protein level.
(A) Total cell lysates of BMDCs were analyzed on day seven by qRT-PCR for the presence of MMP-12 and -13 as well as their TIMPs. Data are illustrated in a box plot (25 – 75 percentile with min. to max.) as ΔCT values (n = 13). (B) The zymogen (54 kDa) and the active form of MMP-12 (45 kDa) as well as the different forms of MMP-13, pro-enzyme (60 kDa), active form (54 kDa), and cleaved fragments (48/34 kDa) were validated by Western blot. Molecular weights of the protein marker are indicated (kDa). Results are representative of 5 independent experiments.

To determine the expression of MMP-12 and -13 in response to a pro-inflammatory stimulus, BMDCs were stimulated with 10 µg/ml LPS. Three different time points, 0.5, 3, and 24 hours of LPS-treatment were chosen for the expression kinetics. The highest induction of MMP-13 expression (7-fold) on mRNA level was found at three hours after LPS stimulation, which declined again over time within 24 hours (Figure 3.4). Regarding MMP-12 transcript levels no significant increase was detected.

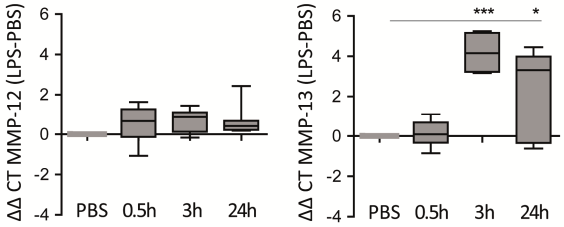

Figure 3.4: Expression kinetics of MMP-12 and -13 on RNA level.
Kinetic of BMDCs were performed to determine the appropriate duration for LPS stimulation. Therefore, BMDCs were cultured with LPS for 0.5, 3, and 24 h and alterations in the transcript levels of MMP-12 and -13 were analyzed by qRT-PCR. Data are shown as ΔΔCT values of LPS-stimulated BMDCs normalized to PBS-treated BMDCs for 11 independent experiments. Data are shown as box plot (25 – 75 percentile with min. to max.). Statistical analysis: Anova with Kruskal-Wallis Dunn's Comparison Test. *$p<0.05$ and ***$p<0.001$.

As LPS most effectively induced MMP-13 three hours after stimulation, this time point was chosen for further experiments. Beside the usage of the inflammatory stimulus LPS, the antigen OVA was included for further analysis. Using OVA, alterations in the expression profile of MMPs could be

analyzed while the antigen processing takes place. Alterations of specific MMPs during antigen uptake via the endocytotic pathway and during antigen processing and presentation can be analyzed in this way.

BMDCs treated either with LPS ($\Delta\Delta CT_{(LPS\text{-}n.t.)}$ = 2.5 ± 1.1 (mean ± SD)) or OVA ($\Delta\Delta CT_{(OVA\text{-}n.t.)}$ = 1.9 ± 0.3) displayed a significant increase of MMP-13 mRNA expression (Figure 3.5ii), whereas MMP-12 expression did not change significantly (Figure 3.5i). MMPs are controlled by their natural inhibitors. Therefore, TIMP-1, -2, and -3 were analyzed simultaneously for changes in their expression profile after LPS/OVA stimulation (Figure 3.5v-vii). TIMP-1 significantly increased only upon LPS stimulation (mean $\Delta\Delta CT_{(LPS\text{-}n.t.)}$ = 1.484 ± 1) whereas TIMP-2 significantly decreased in response to both stimuli ($\Delta\Delta CT_{(LPS\text{-}n.t.)}$ = -0.8 ± 0.6 and $\Delta\Delta CT_{(OVA\text{-}n.t.)}$ = -1.22 ± 0.7, respectively). The expression level of TIMP-3 did not display significant changes whereas MMP-2 and MMP-9 mRNA expression increased after both stimuli (Figure 3.5iii-iv).

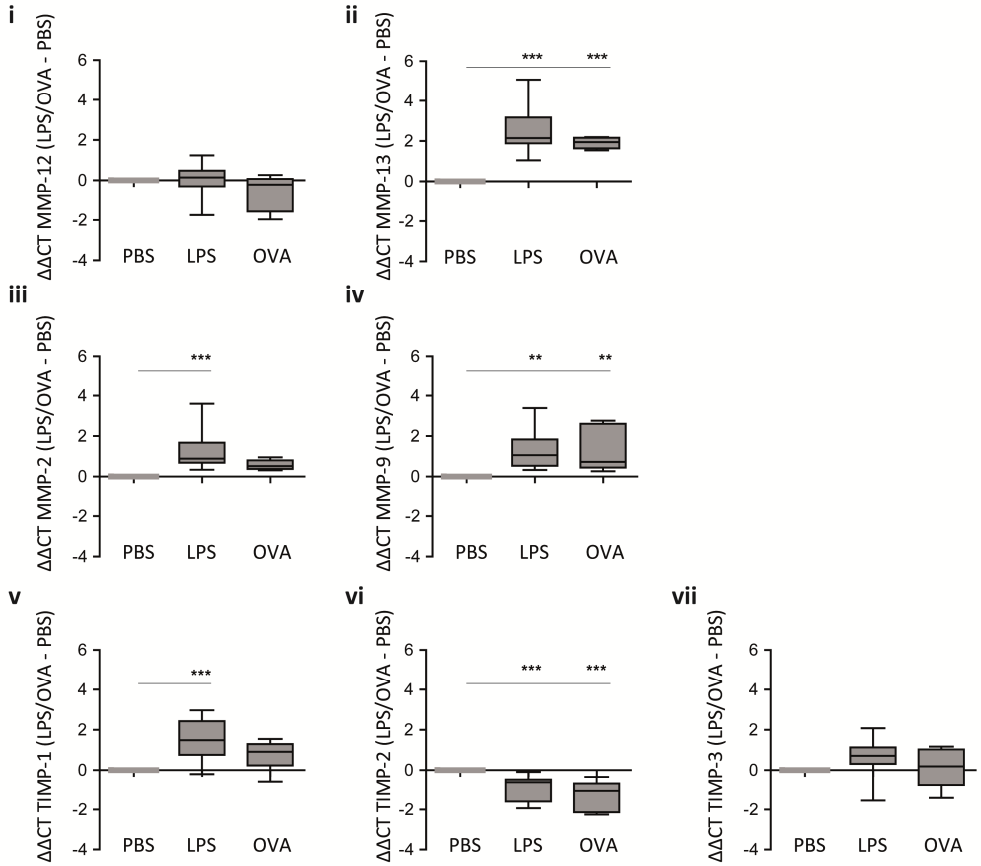

Figure 3.5: Increased MMP-13 expression after inflammatory stimulus.
BMDCs were stimulated with LPS (10 µg/ml) or OVA (1 mg/ml) for 3 h. Expression of different MMPs and TIMPs was analyzed by qRT-PCR. Data are shown as ΔΔCT values of LPS/OVA-stimulated BMDCs normalized to PBS-treated BMDCs for 11 (LPS) and 7 (OVA) independent experiments (box plot 25 – 75 percentile with min. to max.). Statistical analysis: Anova with Kruskal-Wallis Dunn's Comparison Test. **p<0.01 and ***p<0.001.

After confirming the expression of MMP-12 and -13 on RNA and protein level, specific MMP activity assays were performed to investigate whether the activity state of MMP-12 or -13 also

changed during inflammatory LPS stimulation. Indeed, active MMP-12 (factor = 1.14 ± 0.07) and MMP-13 (factor = 1.3 ± 0.2) increased after LPS stimulation (Figure 3.6).

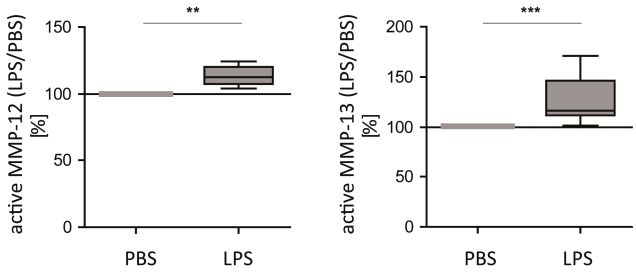

Figure 3.6: Increased active MMP-12 and -13 after LPS stimulation.
Active MMP-12 and -13 in the supernatant of BMDCs were determined 3 h after LPS stimulation by specific MMP assays. Data are displayed as box plot (25 – 75 percentile with min. to max.) with relative values of LPS-stimulated cells normalized to PBS-treated cells in percentages (n = 6). Statistical analysis: Unpaired t-test. **p<0.01 and ***p<0.001.

Taken together, these results confirmed the expression of MMP-12 and -13 in BMDCs under baseline conditions and revealed a significant upregulation, especially of MMP-13, in response to the inflammatory stimulus LPS.

3.1.3 Involvement of MMP-12 and -13 in BMDC functions

In order to determine a role of MMP-12 and -13 for the phenotype and function of BMDCs, in particular concerning migration, endocytosis, cytokine release, antigen presentation, and T cell activation, various functional assays were performed using two specific MMP inhibitors. The specific small molecule inhibitor MMP408 for MMP-12 inhibition and the specific small molecule inhibitor CL82198 for MMP-13 inhibition were used, respectively.

3.1.3.1 Efficacy and toxicity analysis of MMP-12 and -13 inhibitors

In order to rule out toxic side effects of the applied doses of the chosen inhibitors, toxicity tests were performed. Therefore, BMDCs were treated with the indicated amounts of inhibitors overnight, followed by the cell viability assay WST-1. MMP-12 inhibitor showed no toxic effect up to a concentration of 50 µM (Figure 3.7). Beyond that concentration, a clear increase in metabolically stressed or dead cells were detected as indicated by a decrease of WST turnover. In case of the MMP-13 inhibitor, no strong increase in cell death could be detected up to a concentration of 500 µM (Figure 3.8). A threshold of metabolic activity of 80% was selected. Accordingly, in further experiments, MMP-12 inhibitor was used in a concentration up to 50 µM and MMP-13 inhibitor up to 500 µM.

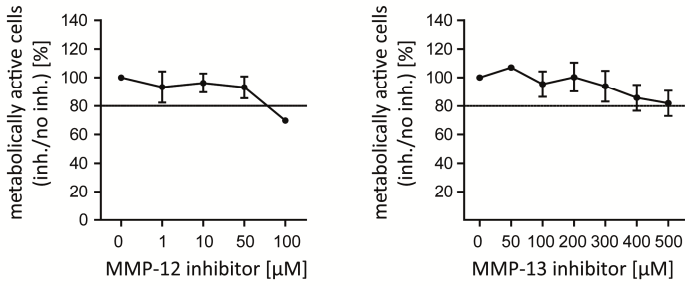

Figure 3.7: Toxicity measurements of MMP inhibitors using WST-1 assay.
WST-1 reagent was used to determine the toxic effect of MMP-12 and -13 inhibitors on BMDCs. Cells were treated with indicated amounts of inhibitors for 24 h followed by WST-1 assay. Data are shown as relative values of inhibitor-treated cells (inh.) normalized to non-treated (no inh.) cells in percentage (mean ± SD) (n = 8).

In a second step, the efficacy of murine MMP inhibition was verified with murine recombinant MMP-12 or MMP-13 as these inhibitors were originally designed for human MMPs. As demonstrated in Figure 3.8, both inhibitors decreased active recombinant murine MMP-12 or -13, respectively, in a dose-dependent manner, with a mean inhibition efficacy of up to 91% ± 7% at the highest MMP-12 inhibitor concentration of 50 µM and 67% ± 13% at the highest MMP-13 inhibitor concentration of 500 µM.

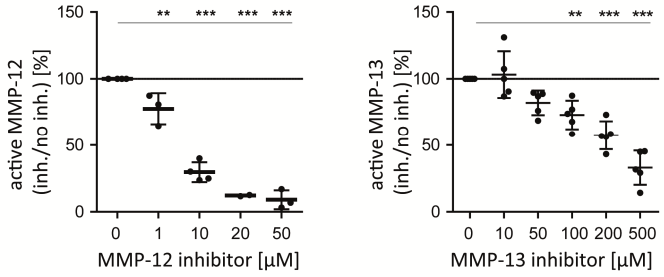

Figure 3.8: Efficacy of inhibitor for murine MMP-12 or -13 protein.
Recombinant murine MMP-12 or -13 protein was activated by 4-Aminophenylmercuric Acetate (APMA), incubated with the specific inhibitor at different concentrations, and quantified by specific MMP activity assays. Data are illustrated as relative values of active MMP-12 and -13 between inhibitor treated (inh.) and non-treated (no inh.) groups. (mean ± SD) (n = 4). Statistical analysis: Anova with Dunnett's Multiple Comparison Test. **p<0.01 and ***p<0.001.

Altogether, functionality of the two MMP inhibitors for the respective murine MMPs was validated and the concentrations with the highest inhibitory potential, that revealed no toxic side effects, were identified.

3.1.3.2 Involvement of MMP-12 and -13 in DC migration

In the process of host defense, DCs must leave the periphery to reach the area of infection and later move on to the lymph nodes where they finally activate T cells. Hence, the capability to migrate is one of the central functions of DCs. To investigate whether MMP-12 or -13 is involved in BMDC migration, a 3D collagen migration assay was performed with CCL19 as chemoattractant (Figure

3.9). Depending on the specific target-substrate, MMP-12 dependent migration was analyzed through collagen I and IV whereas MMP-13 dependent migration was performed through collagen I gel.

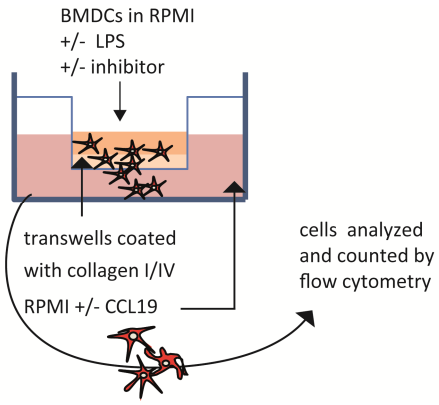

Figure 3.9: Design of the 3D migration assay.
Schematically overview of the 3D migration assay design.

First, the setup of the 3D migration assay was controlled without inhibitor application. As expected, no migration was detected through collagen I when the chemoattractant CCL19 was absent, independently of PBS/LPS treatment, validating CCL19 directed migration of BMDCs in the assay (Figure 3.10A). In case of collagen IV, 17% ± 8.5% (mean ± SD) of cells migrated even in the absence of CCL19 (Figure 3.10Bi).

To control for complete coverage of the transwells with collagen IV, a negative control without collagen IV coating was run in parallel. In case of non-coated transwells, an increase of 29% ± 8% (mean ± SD) of migrated cells was observed compared to transwells coated with collagen IV (Figure 3.10Bii), indicating that the collagen IV layer had built up a barrier for the cells. In the case of the thick collagen I layer, the integrity could be confirmed by eye with microscopy.

When comparing LPS stimulated and non-stimulated cells, LPS-stimulated BMDCs showed an increase of 36% ± 15% (mean ± SD) of migrated cells through collagen I compared to non-stimulated BMDCs (Figure 3.10A). In contrast, in case of collagen IV, 37% ± 17% (mean ± SD) fewer cells migrated after LPS stimulus (Figure 3.10Bi). The reason for this difference is unknown, but might be related to stronger cell adherence after LPS treatment. The adherence effect might lose its impact on the migration outcome during the elongated time frame of 24 hours in collagen I.

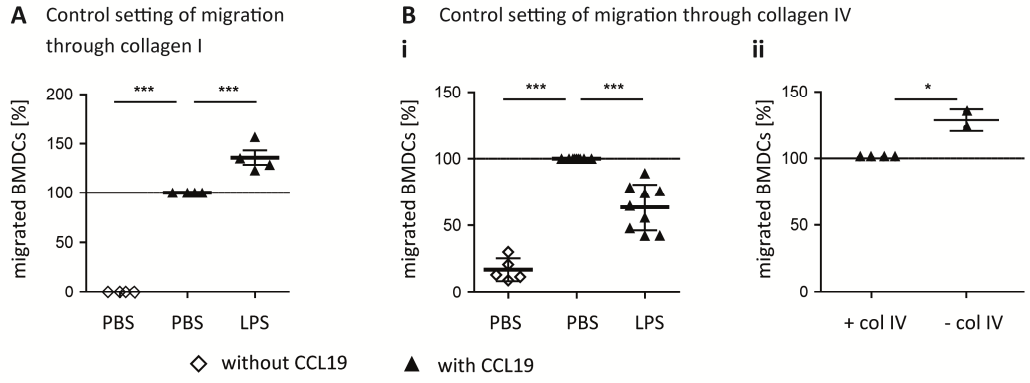

Figure 3.10: Control setting of the 3D migration assay.
(A and Bi) Comparison of BMDCs stimulated with LPS or PBS as control as well as with or without CCL19 as chemoattractant. (Bii) Analysis of collagen IV layer integrity by comparing DC migration through collagen coated or non-coated transwells. Statistical analysis: A and Bi: Anova with Dunnett's Multiple Comparison Test. ***p<0.001. Bii: Unpaired t-test. *p<0.05

Concerning the CCL19-directed BMDC migration capacity, neither the inhibition of MMP-12 nor inhibition of MMP-13 influenced migration of LPS-stimulated or unstimulated DCs (Figure 3.11A and B), independently of the target-substrate. In order to confirm that MMP-12 inhibition does not alter BMDC migration, BMDCs generated from MMP-12 ko cells were analyzed. Even MMP-12 ko BMDCs migrated similar compared to wt cells (Figure 3.11B right). The same analysis could not be performed for MMP-13 based migration as no MMP-13 ko animals were available.

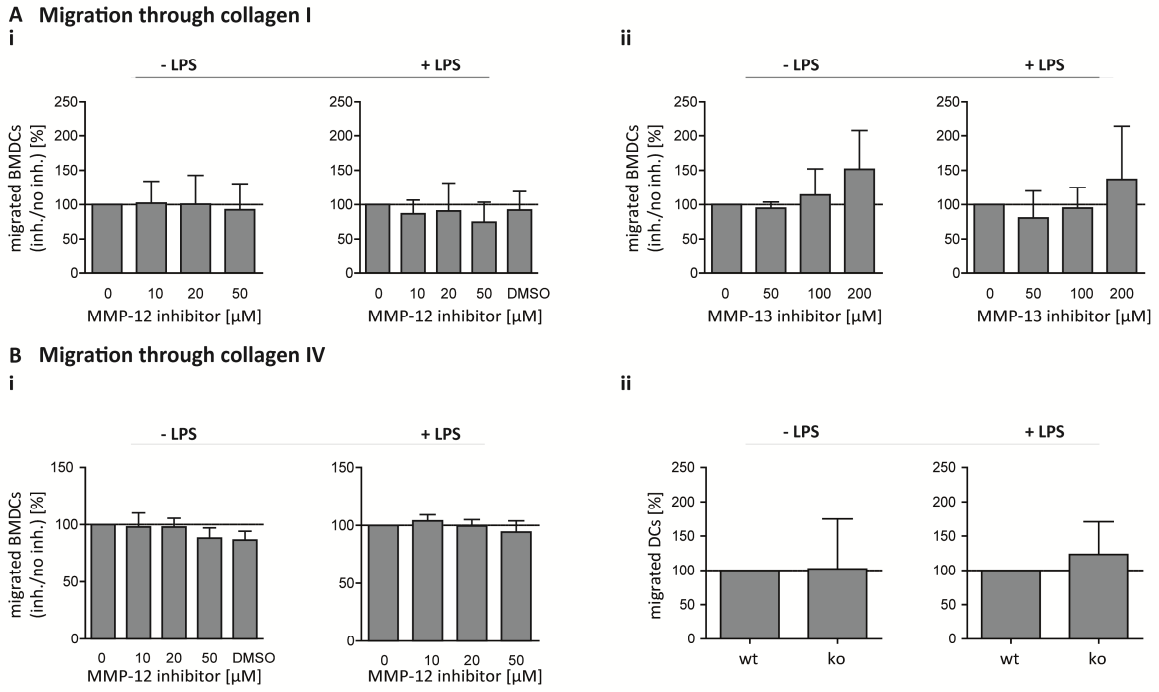

Figure 3.11: No influence of MMP-12 or -13 inhibition on BMDC migration.
Unstimulated or LPS-stimulated (-/+ LPS) BMDCs were incubated with MMP-12 or -13 inhibitor for 1 h or left untreated and seeded (A) overnight on collagen I, or (B) 4 h on collagen IV filled transwells. BMDCs which migrated towards the CCL19 into the bottom chamber were stained for CD11c and MHC-II, and counted with counting beads by flow cytometry. (A) Migration of DCs through collagen I after (i) MMP-12 or (ii) MMP-13 inhibition. Data are shown as relative values between inhibitor-treated (inh.) and non-inhibitor-treated (no inh.) groups (mean ± SD) (n = 4). (B) Migration of (i) BMDCs treated with MMP-12 inhibitor or (ii) MMP-12 ko cells through collagen IV. Data are shown as relative values between (i) inhibitor treated and non-treated groups or (ii) ko cells normalized to wt cells (mean ± SD) (n = 4). Statistical analysis: Anova with Dunnett's Multiple Comparison Test.

Taken together, these data suggest that MMP-12 and -13 do not have a strong role for BMDC migration.

3.1.3.3 Analysis of endocytic capacity of MMP-12 ko and wt DCs after MMP-13 inhibition

DCs take up foreign antigens to activate the antigen-specific T cell response. To determine whether MMP-12 or -13 influences the endocytic capability of BMDCs, MMP-12 ko cells and wt cells treated with the tested inhibitors were exposed to fluorochrome-labeled OVA. As shown in Figure 3.12i and Figure 3.13, soluble OVA was efficiently taken up by $CD11c^+$ BMDCs.

As shown in Figure 3.12ii, a significant lower number of MMP-12 ko cells endocytosed OVA (6% ± 2%). Concerning the amount of endocytosed OVA, as determined by the mean fluorescence intensity of OVA, a reduction of 38.5% ± 12% (mean ± SD) was detected in the MMP-12 ko group (Figure 3.12iii). In addition, the MHC-II surface expression profile of ko compared to wt BMDCs was analyzed. As documented in Figure 3.12iii, ko cells displayed higher MHC-II surface expression than WT cells.

Using the specific MMP-12 inhibitor, a decreased OVA-uptake was observed, however the same effect was seen in the DMSO vehicle control groups (data not shown), thus, indicating that the effect of the MMP-12 inhibitor was unspecific.

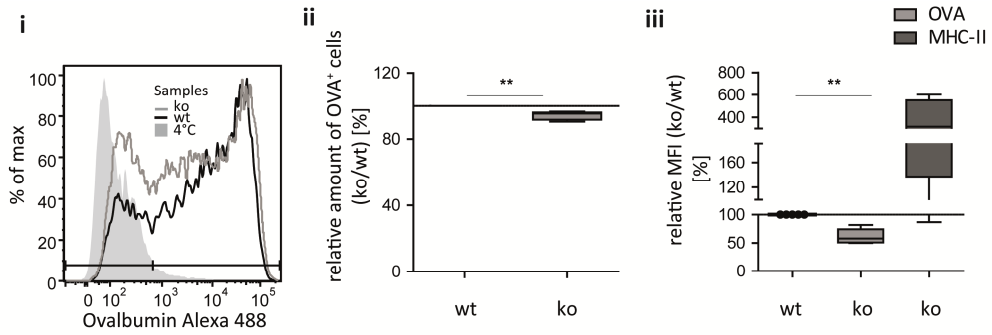

Figure 3.12: Decreased endocytosis of soluble OVA in MMP-12 ko BMDCs.
BMDCs were generated from MMP-12 ko mice or wt mice, cooled down on ice, then incubated with $OVA_{Alexa\ 488}$ for 1 h at 4°C (control) or 37°C, followed by staining for CD11c and MHC-II, and flow cytometry analysis. Data represent uptake of $OVA_{Alexa\ 488}$ by $CD11c^+$ DCs. (i) Representative result of 5 independent experiments. (■ = control at 4°C, ─ = wt at 37°C, ─ = MMP-12 ko at 37°C). (ii) Box plot (25 – 75 percentile with min. to max.) summary of 5 experiments illustrating the relative difference in number of cells that endocytosed OVA between MMP-12 ko and wt BMDCs. (iii) Quantification of the relative amount of internalized OVA and MHC-II between MMP-12 ko and wt BMDCs shown by MFI value. Statistical analysis: Anova with Dunnett's Multiple Comparison Test. **p<0.01.

Regarding inhibition of MMP-13, endocytic capability of BMDCs decreased in a dose-dependent manner (Figure 3.13). Using the highest inhibitor concentration, a significant lower number of DCs endocytosed OVA (17% ± 16% less) (Figure 3.13ii) and, furthermore, MMP-13 inhibitor-treatment reduced the OVA^+ cells of up to 16% ± 6% (mean ± SD) compared to the uninhibited DCs (Figure **3.13**iii).

To further determine whether the observed effect can be correlated to a specific BMDC phenotype, $CD11c^+$ BMDCs were grouped according to their MHC-II surface profile and subgroups were compared for their OVA-uptake. In line with other studies[33], immature BMDCs with low MHC-II surface expression showed stronger capability to capture OVA compared to MHC-II^{high} BMDCs. As demonstrated in Figure 3.13iv-vi, the reduction in endocytosis by MMP-13 inhibition was detected in all BMDCs subgroups independent of MHC-II expression level, even though the MHC-II^{high} subgroup showed very low overall OVA-uptake.

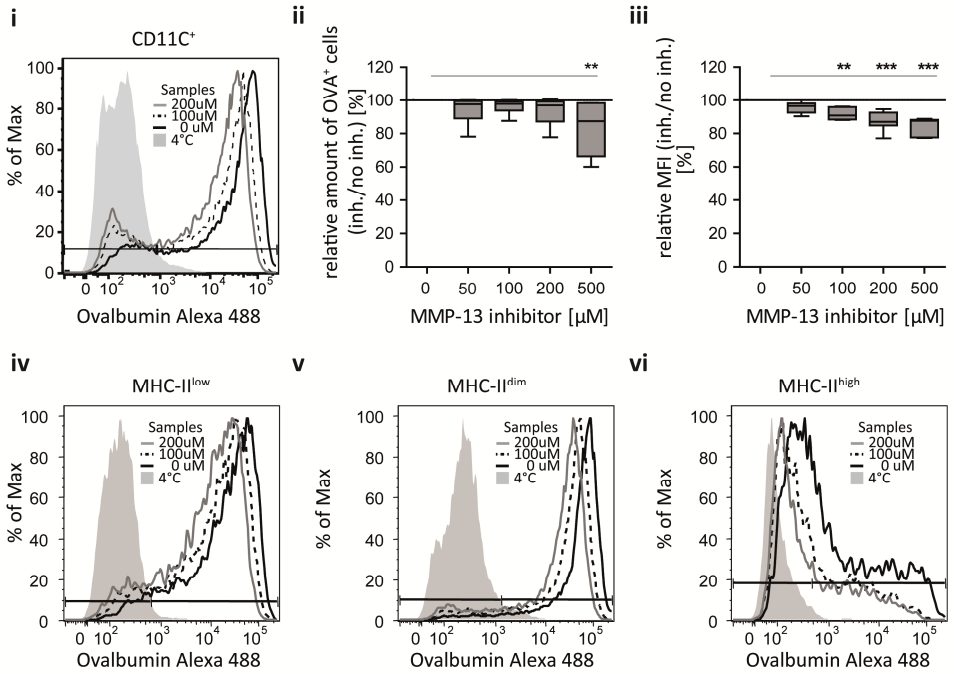

Figure 3.13: Involvement of MMP-13 in endocytosis of soluble OVA in BMDCs.
BMDCs were pre-treated with MMP-13 inhibitor for 1 h at 37°C or left untreated, cooled down on ice, then incubated with $OVA_{Alexa\ 488}$ for 1 h at 4°C (control) or 37°C, followed by staining for CD11c and MHC-II, and flow cytometry analysis. Data represent uptake of $OVA_{Alexa\ 488}$ by $CD11c^+$ BMDCs. (i) Representative result of 9 independent experiments, showing two inhibitor concentrations exemplarily. (■ = control at 4°C, ─ = non-treated at 37°C, ---- = 100 µM MMP-13 inhibitor at 37°C, and ─ = 200 µM MMP-13 inhibitor at 37°C). (ii) Box plot (25 – 75 percentile with min. to max.) summary of 9 experiments illustrating the relative difference in number of cells that endocytosed OVA between treated (inh.) and non-treated (no inh.) groups. (iii) Quantification of the relative amount of internalized OVA between treated and non-treated groups, shown by MFI values. Statistical analysis: Anova with Dunnett's Multiple Comparison Test. **p<0.01 and ***p<0.001. (iv-vi) Representative results of BMDCs that endocytosed OVA classified according to their MHC-II expression intensity.

These results indicate that MMP-13 participates in the regulation of soluble OVA endocytosis, resulting in reduction in the percentage of BMDCs that take up OVA as well as in the overall amount of endocytosed OVA when MMP-13 activity is inhibited. MMP-12 ko BMDCs revealed a decline in endocytosis but showed simultaneously a different MHC-II expression profile in comparison to wt BMDCs.

3.1.3.4 MMP-13 involvement in T cell activation

Another fundamental ability of DCs is the processing and presentation of antigens and, thereafter, the activation of the adaptive immune response. DCs treated with soluble OVA can either activate $CD4^+$ T cells via the classical MHC-II pathway or $CD8^+$ T cells by cross-presentation via the MHC-I pathway.

As the only commercially available MMP-12 inhibitor showed side effects due to the solvent (DMSO) and the MMP-12 ko cells had a different MHC-II surface profile and were therefore not comparable to wt cells, the focus of further investigations was set on MMP-13.

As the T cell activation assay includes besides BMDCs also the T cell line B3Z ($CD8^+$ T cell hybridoma cell line specific for $OVA_{257-264}$-peptide (SIINFEKL)), or the T cell line DOBW

($CD4^+$ T cell line specific for $OVA_{323-339}$-peptide), the effect of MMP-13 inhibition was tested on the T cells. To exclude potential toxicity of MMP-13 inhibitor on these types of cells, PI/Annexin staining of inhibitor-treated T cells was performed. Apoptotic and dead cells were analyzed by flow cytometry. Cells that are positive for Annexin V (FITC) and negative for PI are undergoing apoptosis. Cells that stained positive for both Annexin V and PI are either in the end stage of apoptosis, are undergoing necrosis, or are dead. Using this assay, only a moderate increase in apoptotic cells was detected in both T cell lines after MMP-13 inhibitor treatment (Figure 3.14). In addition, PI/Annexin staining detected no apoptotic effects of the MMP-13 inhibitor on BMDCs confirming the previous results observed with the WST assay (Figure 3.7).

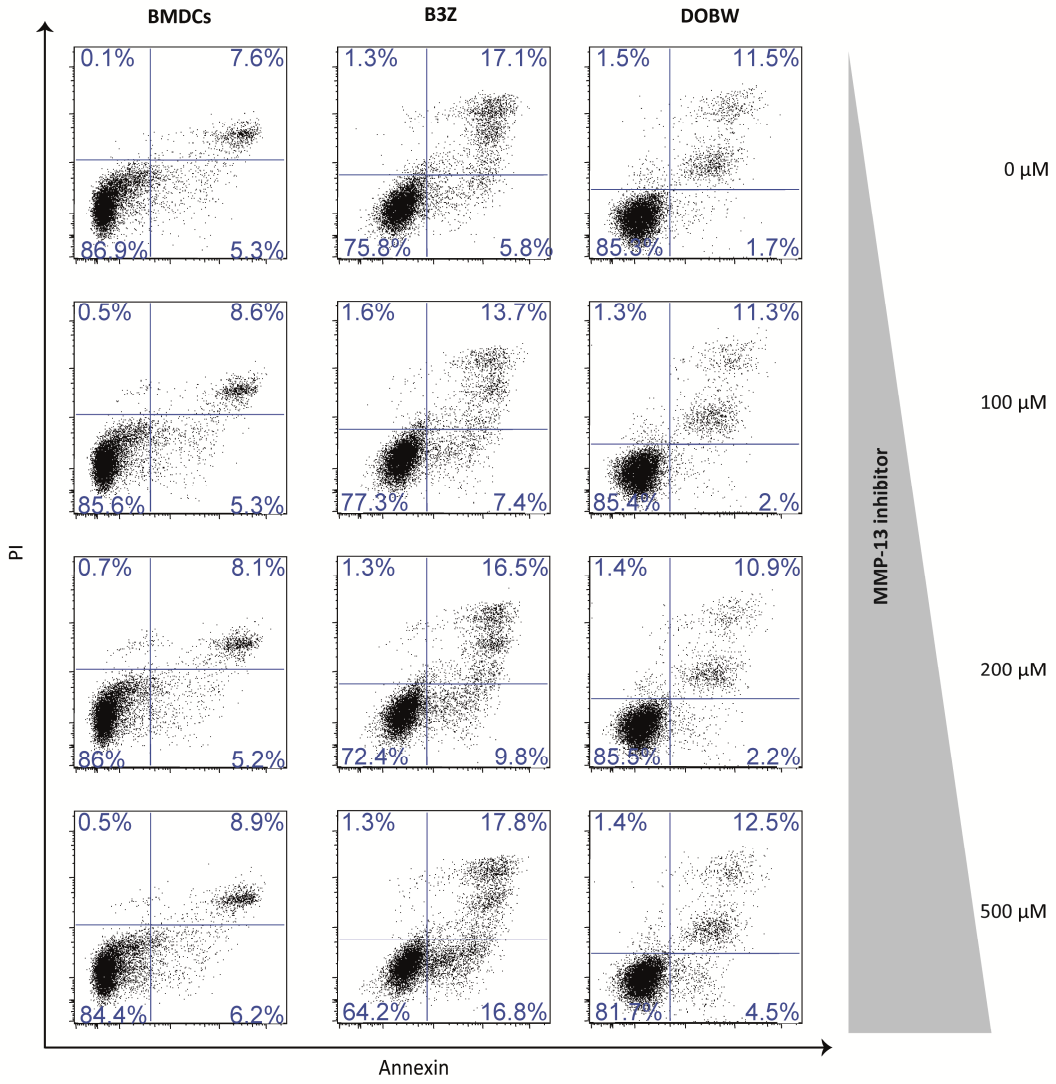

Figure 3.14: No toxic effect of MMP-13 inhibitor on BMDCs, B3Z, or DOBW cells.
PI/Annexin staining was used to determine the toxic effect of MMP-13 inhibitor on the different cell types. BMDCs, B3Z cells, or DOBW cells were treated with 10-500 µM MMP-13 inhibitor for 24 h. BMDCs (left), B3Z (center), and DOBW (right) cells were stained with Annexin V plus PI and analyzed by flow cytometry for percentages of dead and apoptotic cells. Results are representative of 3 independent experiments.

After excluding toxic side effects of the inhibitor on the two T cell lines, the T cell activation assays were performed. To elucidate a role of MMP-13 in the MHC-I pathway (cross-presentation) for T cell activation, OVA-treated BMDCs were co-cultivated with $CD8^+$ T cells (B3Z T cells), followed by measurement of IL-2 production by T cells as readout for T cell activation. In addition, a colorimetric LacZ assay was performed for the detection of T cell activation because B3Z T cells express β-galactosidase under the control of the IL-2 promoter. It was observed that the capability of BMDCs to activate $CD8^+$ T cells was significantly and strongly reduced in the presence of MMP-13 inhibitor in a dose dependent manner (Figure 3.15i-ii). To determine whether the observed effect is due to reduced endocytic capability of treated BMDCs (as shown in Figure 3.13), MMP-13 inhibitor was applied after the endocytosis phase. As depicted in Figure 3.15iii-iv, a similar reduction in T cell activation was detected, indicating that the reduction might be due to effects on processes subsequent to endocytosis.

As the inhibitor was present during DC and T cell co-culture, the inhibition could be due to effects on the DCs, the T cells, or both. To exclude a direct effect of the inhibitor on the $CD8^+$ T cells, BMDCs were pulsed with SIINFEKL-peptide in the absence of inhibitor, then fixed, and co-incubated with T cells in the presence of MMP-13 inhibitor. In this setting, where the inhibitor cannot alter DC function any longer, the previously observed reduction in IL-2 secretion was no longer detected (Figure 3.15v-vi), which excludes that MMP-13 inhibition manipulated the $CD8^+$ B3Z cells. Thus, it has to be concluded that MMP-13 inhibition not only alters OVA endocytosis (as shown in Figure 3.13) but has additional effects in the MHC-I cross-presentation pathway following the endocytosis process, which affect T cell activation.

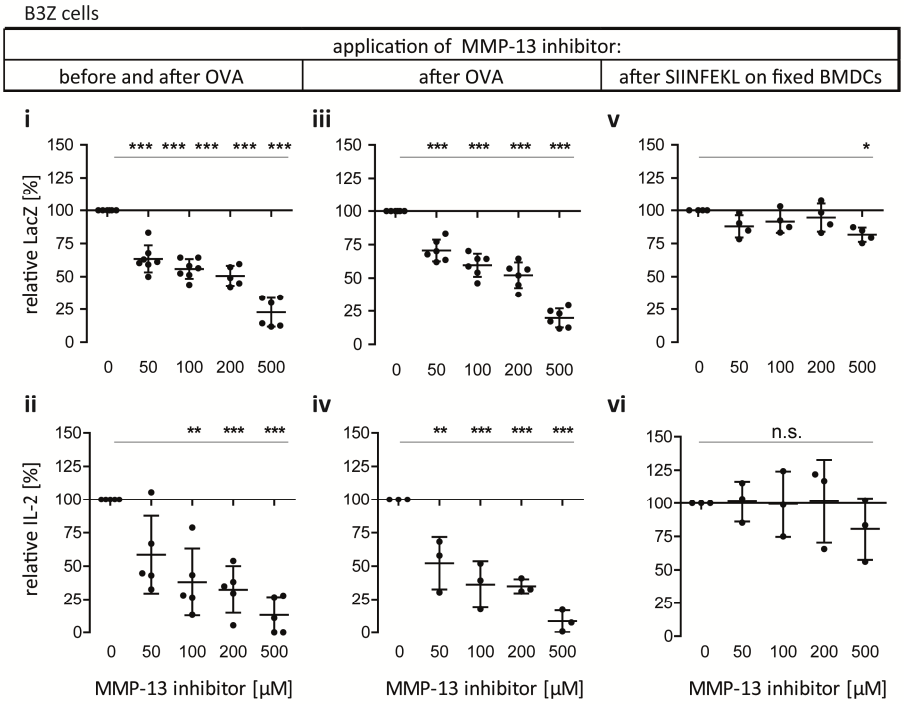

Figure 3.15: Decreased capacity of BMDCs to activate B3Z CD8$^+$ T cells by MMP-13 inhibition.
(i-ii) BMDCs were pre-treated with indicated amounts of MMP-13 inhibitor, followed by protein pulsing with OVA or PBS (3h), and cultured with indicated amounts of inhibitor overnight in the presence of CD8$^+$ T cell (B3Z). (Top) Activation of CD8$^+$ B3Z cells was monitored by measuring LacZ accumulation in a colorimetric assay (n =6) or (bottom) IL-2 secretion in the supernatant by ELISA (n = 5). (iii-iv) Experiments were performed as described above except that the inhibitor was added after pulsing with OVA (iii: n = 6, iv: n = 3). (v-vi) Untreated BMDCs were pulsed with SIINFEKL-peptide for 2 h, washed, fixed, and co-incubated with B3Z cells in the presence of indicated concentration of inhibitor overnight. (v: n = 4, vi: n = 3). Data are depicted as relative values between MMP-13 inhibitor treated (inh.) and non-treated (no inh.) groups (mean ± SD). Statistical analysis: Anova with Dunnett's Multiple Comparison Test. *p<0.05, **p<0.01, and ***p<0.001.

To further define whether MMP-13 also has a role in the classical MHC-II pathway, experiments were performed as described above using CD4$^+$ T cells. In the setting where the inhibitor was present during the whole experiment, a moderate reduction in CD4$^+$ T cell activation was observed (Figure 3.16i). In the setting where untreated SIINFEKL-pulsed and fixed DCs were used and the inhibitor was added during the DC-T cell co-culture, a comparable reduction in IL-2 secretion was measured (Figure 3.16ii). Thus, it has to be concluded that the MMP-13 inhibitor has a direct effect on the DOBW CD4$^+$ T cells and it cannot be discerned whether MMP-13 inhibition affects additional processes of the CD4$^+$ T cell activation.

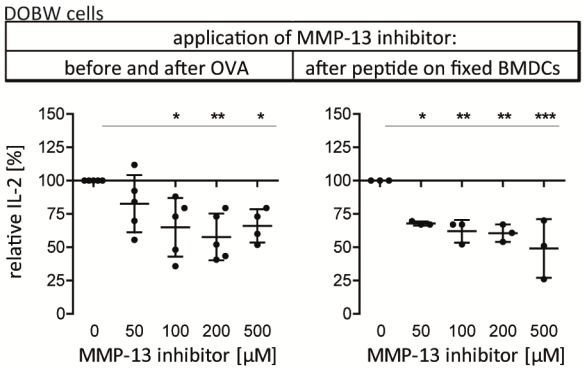

Figure 3.16: Inhibition does not affect BMDCs regarding activation of DOBW CD4$^+$ T lymphocytes.
Activation of DOBW CD4$^+$ T cells via MHC-II pathway was detected by performing similar experiments as described in Figure 3.15 with slight modification. (Left) DCs were pre-treated with indicated amounts of inhibitor for 1 h or left untreated, followed by protein pulsing with OVA or PBS (as control) for 3 h, washed, and cultured with indicated amounts of inhibitor overnight with CD4$^+$ T cells (DOBW cells). Activation of DOBW cells was monitored by measuring IL-2 secretion in the supernatant by ELISA (n = 5). (Right) Untreated BMDCs were pulsed with SIINFEKL-peptide for 2 h, washed, fixed, and then co-incubated with DOBW cells in the presence of indicated amounts of inhibitor (n = 3). Statistical analysis: Anova with Dunnett's Multiple Comparison Test. *p<0.05, **p<0.01, and ***p<0.001.

In summary, these results suggest that MMP-13 plays a crucial role in DCs, facilitating the activation process of CD8$^+$ T cells via the MHC-I pathway, whereas it seems to be less important or dispensable for the CD4$^+$ T cell activation via the MHC-II pathway.

3.1.3.5 Analysis of the MHC surface expression after inhibition of MMP-13

To induce protective CD8$^+$ T cell activation *in vivo*, sufficient peptide presentation by APCs is necessary. To determine the mechanism leading to reduced CD8$^+$ T cell activation in our system, alterations in the capability of BMDCs to present peptides after inhibition of MMP-13 was analyzed. Therefore, BMDCs were incubated with OVA protein in the absence or presence of MMP-13 inhibitor followed by flow cytometry staining of the complex of the OVA peptide (SIINFEKL) bound to H-2K^b of MHC-I. As depicted in Figure 3.17, SIINFEKL-presentation on MHC-I by BMDCs was reduced significantly at the highest inhibitor concentration.

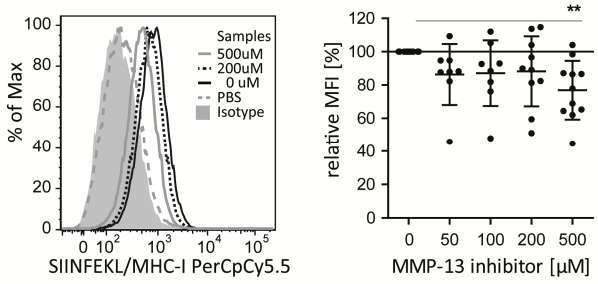

Figure 3.17: Involvement of MMP-13 in peptide presentation.
BMDCs were pre-treated with indicated amounts of MMP-13 inhibitor followed by treatment with OVA or PBS (control) for 3 h, washed, and cultured overnight in the presence of the MMP-13 inhibitor. Cells were washed and stained for CD11c and the complex of SIINFEKL bound to H-2K^b of MHC-I. (Left) Representative result of 11 independent experiments (■ = isotype, ---- =PBS, ─ = OVA without MMP-13 inhibitor, ... = OVA with 200 µM MMP-13 inhibitor, ─ = OVA with 500 µM MMP-13 inhibitor). (Right) Relative MFI values between inhibitor-treated (inh.) and non-treated (no inh.) CD11c$^+$ BMDCs (mean ± SD). Statistical analysis: Anova with Dunnett's Multiple Comparison Test. **p<0.01.

This result suggests that MMP-13 is involved in generating the peptide/MHC-I complex required for T cell activation by either regulating the loading of exogenous peptides onto MHC-I or participating in the MHC-I surface expression. To analyze whether inhibition of MMP-13 leads to a general reduction of the overall MHC-I surface expression, BMDCs were treated with MMP-13 inhibitor and OVA overnight, followed by flow cytometry analysis measuring total MHC-I surface molecules. In line with the reduced $CD8^+$ T cell activation shown in Figure 3.15, surface expression of MHC-I was significantly reduced on BMDCs treated with inhibitor, whereas MHC-II remained unchanged (Figure 3.18).

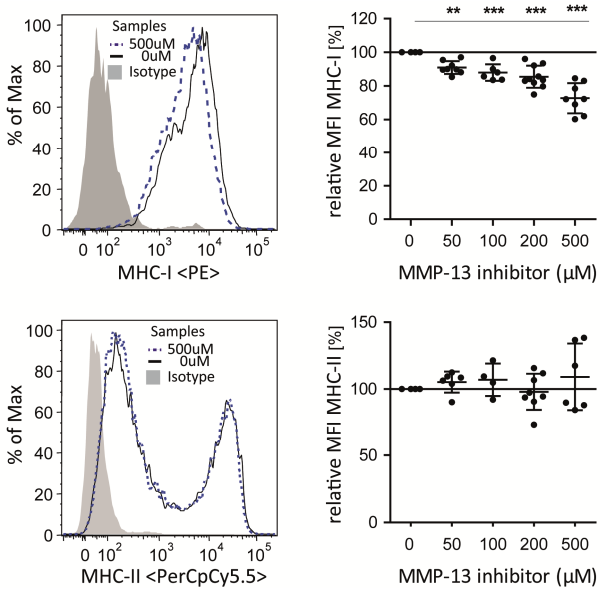

Figure 3.18: Decreased MHC-I surface expression on DCs after MMP-13 inhibition.
BMDCs were pre-treated with indicated amounts of MMP-13 inhibitor and cultivated with OVA overnight. Cells were washed and stained for CD11c and surface MHC-I or MHC-II, followed by flow cytometry analysis. Representative MHC-I or -II surface expression (■= isotype, ─ = without inhibitor, ... = 500 µM of MMP-13 inhibitor) and quantification of 6 experiments, respectively. Data are shown as relative MFI values between treated (inh.) and non-treated (no inh.) $CD11c^+$ BMDCs (mean ± SD). Statistical analysis: Anova with Dunnett's Multiple Comparison Test. **p<0.01 and ***p<0.001.

Taken together, a decline in total surface MHC-I, including the specific SIINFEKL-peptide on MHC-I, was determined after MMP-13 inhibition.

3.1.3.6 Analysis of the maturation profile and selectin expression after MMP-13 inhibition

T cells are activated by DCs through the recognition of specific peptides on MHCs together with the help of co-stimulatory molecules, such as CD40, CD80, and CD86, which are upregulated during maturation[21]. To determine whether MMP-13 participates in the maturation process of BMDCs, analysis of MMP-13 inhibitor-treated cells were performed. As expected, CD40, CD80, and CD86 were strongly upregulated after LPS stimulation compared to non-stimulated control (Figure 3.2vii-ix) and this pattern was identical when MMP-13 was inhibited (Figure 3.19).

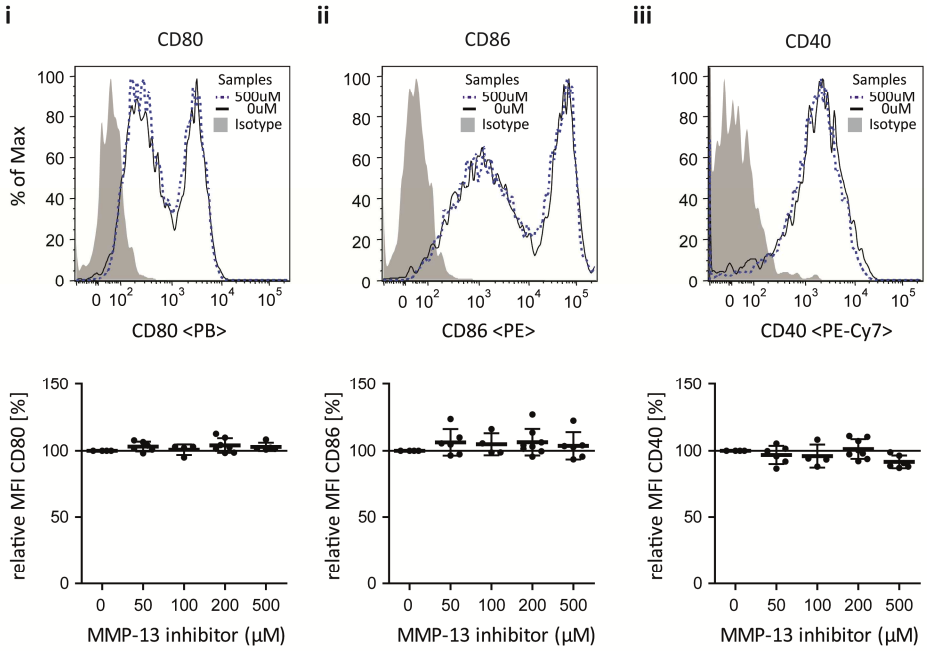

Figure 3.19: MMP-13 inhibition does not change the LPS-induced maturation profile of BMDCs.
BMDCs were pre-treated with indicated amounts of MMP-13 inhibitor, followed by stimulation with LPS, and cultivation overnight. Cells were washed and stained for CD11c, MHC-II, CD80, CD86, and CD40. (Top) Representative surface expression of BMDCs treated with LPS and inhibitor (■ = isotype, ─ = without inhibitor, ... = 500 µM of MMP-13 inhibitor). (Bottom) Quantification of 5 experiments illustrated as relative MFI values between inhibitor treated (inh.) and non-treated (no inh.) $CD11c^+$ BMDCs. Statistical analysis: Anova with Dunnett's Multiple Comparison Test (mean ± SD).

Next, alteration in the surface expression of the α-integrin CD11c after inhibition of MMP-13 was determined. Previous reports indicated that CD11c is involved in antigen presentation by DCs[240]. In the present study, inhibition of MMP-13 reduced the intensity of CD11c surface expression of BMDCs dose-dependently (Figure 3.20).

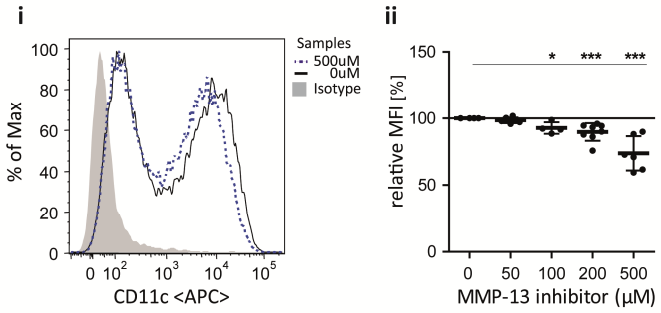

Figure 3.20: Decreased CD11c surface expression after inhibition of MMP-13.
Experiment was performed as described in Figure 3.19 and CD11c surface expression in response to inhibitor treatment was analyzed. (i) Representative surface expression of CD11c (■ = isotype, ─ = without inhibitor, ... = 500 µM of MMP-13 inhibitor). (ii) Quantification of 5 experiments illustrated as relative MFI values between inhibitor treated (inh.) and non-treated (no inh.) cells. Statistical analysis: Anova with Dunnett's Multiple Comparison Test (mean ± SD). *p<0.05 and ***p<0.001.

This observation indicated that MMP-13 does not participate in the maturation process of BMDCs but influences the CD11c surface expression.

3.1.3.7 Cytokine profile of BMDCs after inhibition of MMP-13

A fundamental characteristic of DCs is the capability to release cytokines that determine the polarization of the innate and adaptive immune response[81]. Therefore, the participation of MMP-13 in the cytokine profile of BMDCs was addressed. The release of 18 different cytokines and chemokines in response to LPS stimulation was analyzed by a Luminex cytokine/chemokine screening assay. Consistent with the literature[81], all detectable cytokines (Figure 3.21A) and chemokines (Figure 3.21A, B, and C) were increased upon inflammatory stimulus. IL-13, CCL20, CXCL12, IL-10, IL-1β, and IFN-γ were below the detection limit. Therefore, the effect of inhibition of MMP-13 on these factors could not be determined.

IL-12p70, IL-23p19, and IL-6, which are cytokines influencing T cell-mediated response, were significantly decreased by MMP-13 inhibition in a dose-dependent manner (Figure 3.21). Especially, IL-12p70 and IL-23p19 were strongly reduced at 500 µM MMP-13 inhibitor concentration with a reduction of 46% ± 12% (mean ± SD) (Figure 3.21A) and 49% ± 10% (Figure 3.21B), respectively. IL-6 showed moderate but significant reduction of 11% ± 6% (Figure 3.21C). On the contrary, CXCL10 and TNF-α were increased after MMP-13 inhibition (Figure 3.21D and E). CXCL10 was strongly elevated at the highest inhibitor concentration with an increase of 92% ± 49% (Figure 3.21D), whereas TNF-α increased moderately (6.1% ± 5.4%) (Figure 3.21E).

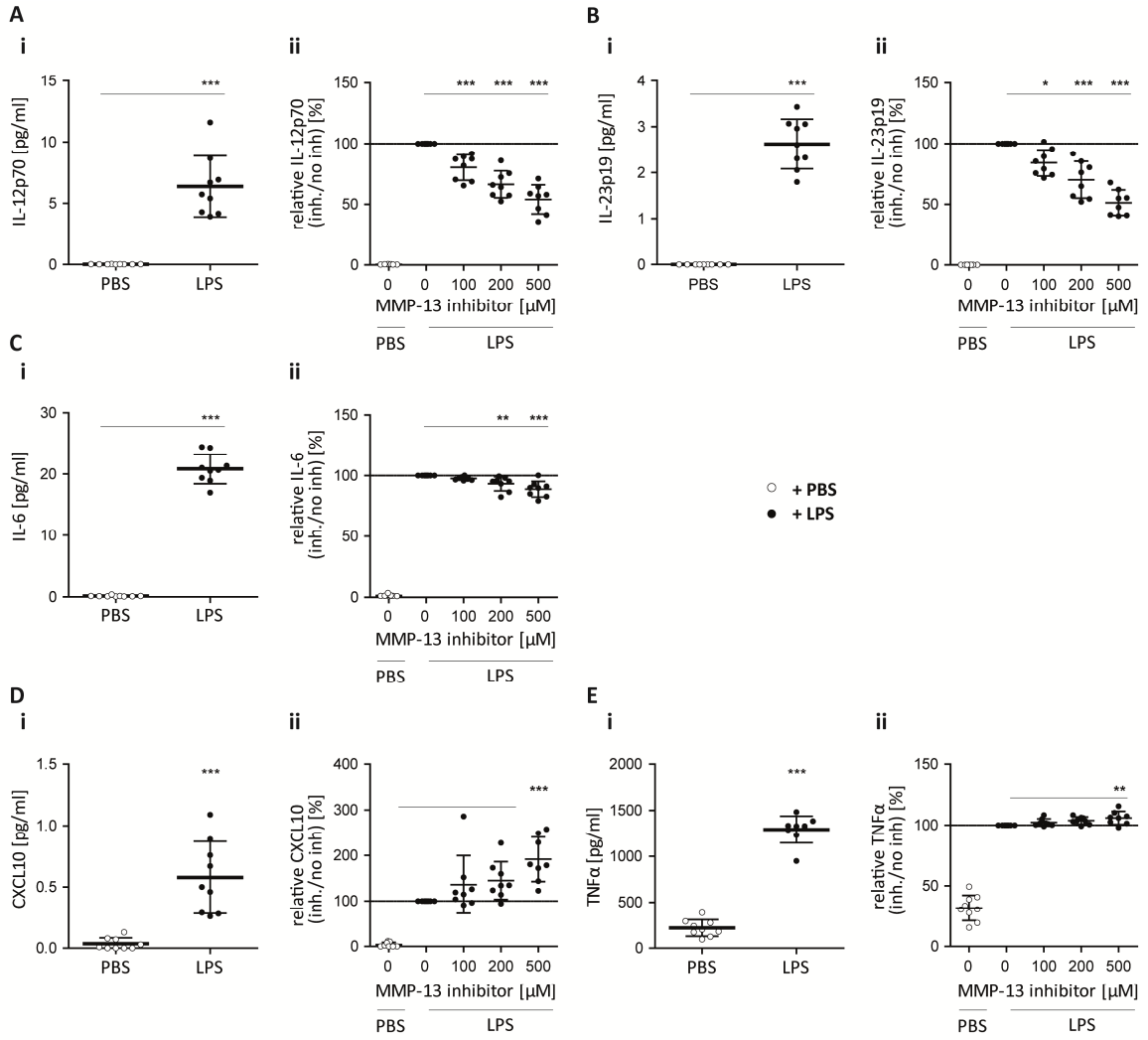

Figure 3.21: T cell-targeting cytokines/chemokines in response to LPS and after MMP-13 inhibition. BMDCs were cultured for 24 h followed by stimulation with LPS or PBS as control. Supernatant of BMDCs was harvested 3 h after stimulation. Cytokines and chemokines were analyzed using Luminex screening assay. Shown are: IL-12p70, IL-23p19, IL-6, CXCL10/IP-10/CRG-2, and TNF-α. Data are shown as (i) absolute cytokine/chemokine values (pg/ml) of PBS- or LPS-stimulated BMDCs and (ii) as relative values in percentage between LPS-stimulated BMDCs treated with (inh.) or without inhibitor (no inh.), or BMDCs stimulated with PBS instead of LPS (PBS) (n = 9). ○ = + PBS, ● = + LPS. PBS stimulated samples were not treated with inhibitor. Statistical analysis: i: unpaired t test. ii: Anova with Dunnett's Multiple Comparison Test (mean ± SD). *p<0.05, **p<0.01, and ***p<0.001.

In contrast, CCL5, a chemoattractant for basophils, eosinophils, and T cells as well as CXCL1 and LIX, activators of neutrophils, showed a moderate decline after inhibitor application (mean ± SD: 10% ± 7%, 6.2% ± 6.4%, and 7.9 ± 7.7%, respectively), (Figure 3.22A-C). Typical cytokines targeting neutrophils, CCL3, CCL4, and CXCL2 remained unchanged after inhibition of MMP-13 (Figure 3.22D-F).

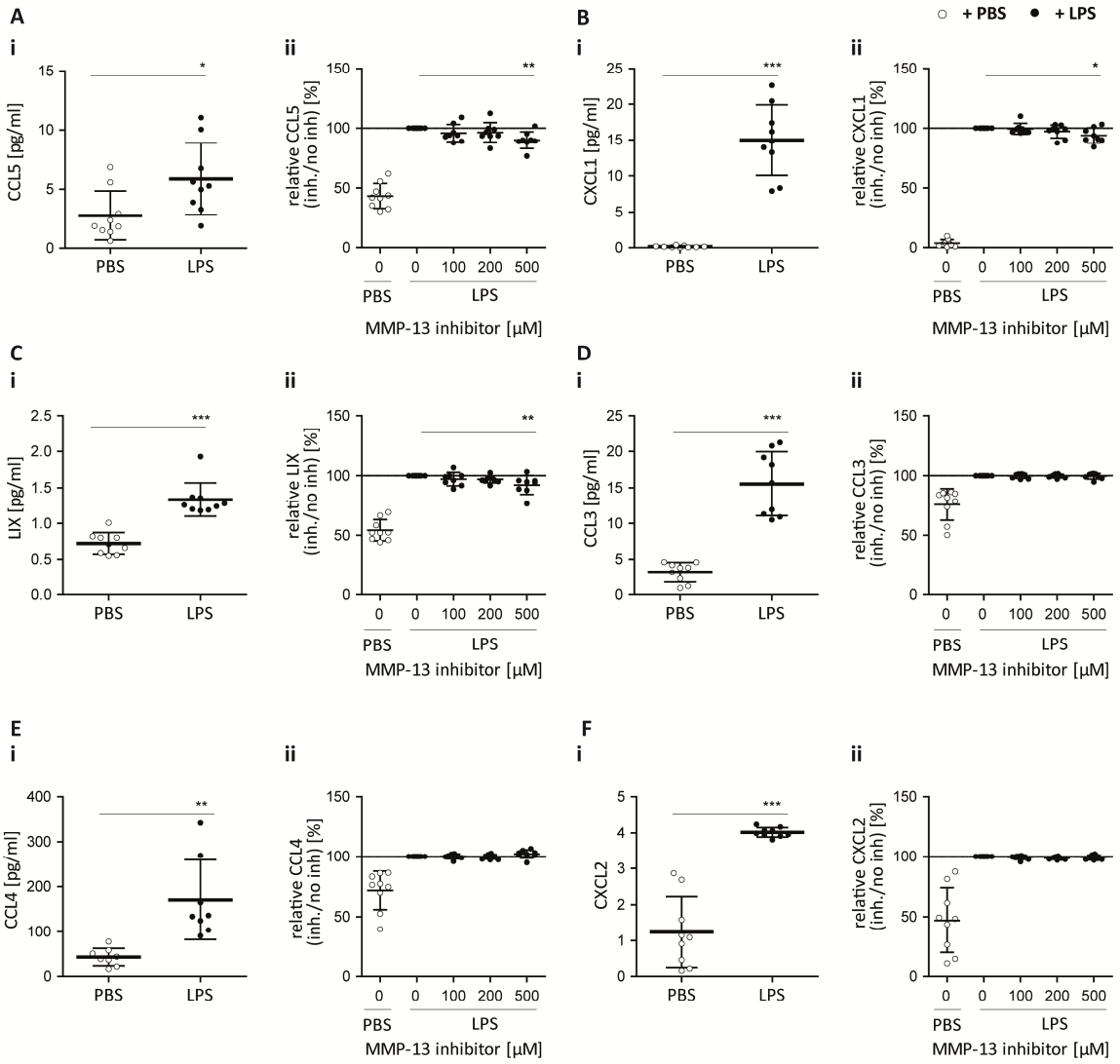

Figure 3.22: Granulocyte-attracting chemokines in response to LPS and after MMP-13 inhibition. Experiments were performed and analyzed as described in Figure 3.21. (A-C) CCL5, CXCL1, and LIX are typical chemokines that attract granulocytes. (D-F) CCL3, CCL4, and CXCL2 are typical chemokines that attract neutrophils. Data are shown as (i) absolute cytokine/chemokine values (pg/ml) of PBS- or LPS-stimulated BMDCs, and (ii) as relative values in percentage between LPS-stimulated BMDCs treated with (inh.) or without inhibitor (no inh.), or BMDCs stimulated with PBS instead of LPS (PBS) (n = 9). ○ = + PBS, ● = + LPS. PBS stimulated samples were not treated with inhibitor. Statistical analysis: i: unpaired t test. ii: Anova with Dunnett's Multiple Comparison Test (mean ± SD). *p<0.05 and **p<0.01.

Finally, CCL2, a chemokine that recruits monocytes, memory T cells, and DCs to the area of infection increased significantly at the highest inhibitor concentration (mean ± SD: 10.3% ± 9.2%) (Figure 3.23).

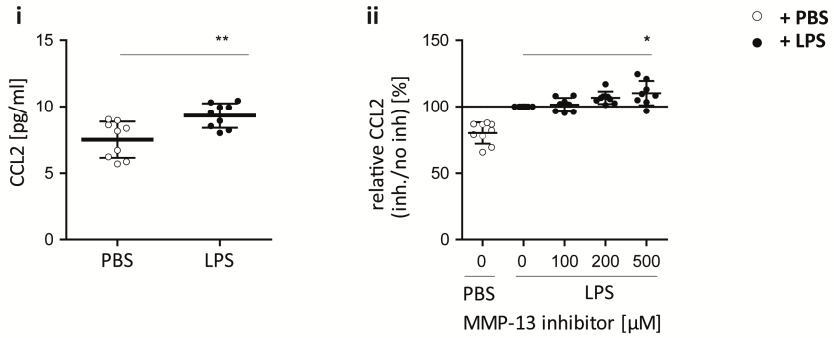

Figure 3.23: Monocyte- , memory T cell-, and DC-attracting chemokine in response to LPS and after MMP-13 inhibition.
Experiments were performed and analyzed as described in Figure 3.21. CCL2 recruits monocytes, memory T cells, and DCs. Data are shown as (i) absolute chemokine values (pg/ml) of PBS- or LPS-stimulated BMDCs, and (ii) as relative values in percentage between LPS-stimulated BMDCs treated with (inh.) or without inhibitor (no inh.), or BMDCs stimulated with PBS instead of LPS (PBS) (n = 9). ○ = + PBS, ● = + LPS. PBS stimulated samples were not treated with inhibitor. Statistical analysis: i: unpaired t test. ii: Anova with Dunnett's Multiple Comparison Test (mean ± SD). *p<0.05 and p**<0.01.

Together, these results suggest that MMP-13 plays a crucial role in maintaining or establishing the cytokine profile of BMDCs, whereby the inhibition of MMP-13 moderates mainly T cell-targeting cytokines.

The *in vitro* results taken together reveal an involvement of MMP-13 in BMDCs regarding the capacity of endocytosis, MHC-I presentation, and cytokine profile. The reduction in the MHC-I surface expression after MMP-13 inhibition further causes an attenuation of $CD8^+$ T cell activation.

3.2 *Ex vivo* analysis

After detecting MMP-13 as a regulator of DC function and thereby as a modulator of the innate and adaptive immune response *in vitro*, the aim was to determine whether these findings can be used for the treatment of inflammatory human diseases. Due to the broad impact of MMP-13 on the immune response, shown before in *in vitro* assays (section 3.1), it is conceivably that MMP-13 could be a potential target in various diseases where the immune response must be attenuated.

Other groups could already demonstrate an involvement of MMPs in the pathogenesis of BOS. These studies revealed the participation of MMP-2 and -9 in experimental BOS. However, little is known about the contribution of MMP-12 and -13 in BOS. Therefore, the aim was to address the potential role of MMP-12 and -13 in the development of experimental BOS and ask the question whether an inhibition of active MMP-13 could attenuate the disease. To answer this question, a mouse model was established.

3.2.1 Establishment of the HTT model

Different types of mouse models exist to study BOS. The heterotopic trachea transplant (HTT) model is very useful to determine the influence of the immune system in the outcome of BOS. In this model, the trachea of a donor mouse is transplanted under the skin on the back of a recipient mouse, schematized in Figure 3.24A and detailed in section 2.2.10. In case of syngeneic

transplantations, where the donor and recipient mice are of the same strains, no graft rejection occurs. On contrast, after organ transplantation of different strains (allograft), a graft rejection is visible that shows similar histologic features to that seen in human BOS (Figure 3.24B).

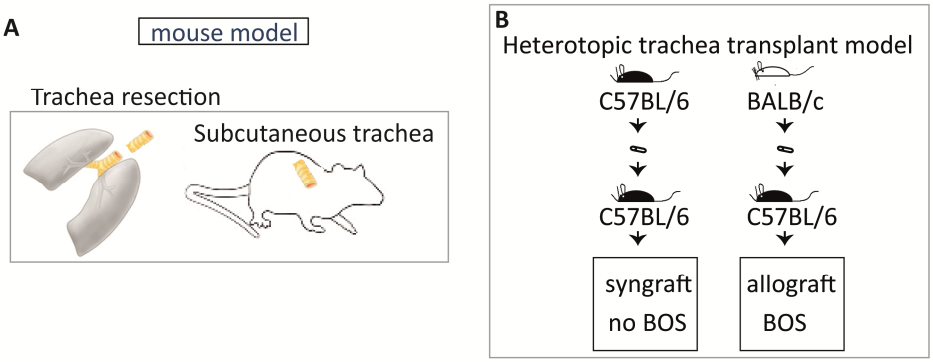

Figure 3.24: The heterotopic trachea transplant model.
Trachea of either C57BL/6 or Balb/c mice were transplanted in a pouch on the back of C57BL/6 mice to induce the phenotype of BOS. Syngeneic transplanted animals should reveal no BOS phenotype whereas allogeneic transplanted mice should develop the typical BOS phenotype in the transplanted trachea. (A) Schematically display of the operation procedure (Figure adapted and modified from Jungraithmayr *et al*[241]). (B) Overview of syngeneic vs. allogeneic transplanted animals.

3.2.1.1 Characterization of the HTT model by H&E and Masson's Trichrome staining

To validate the model and to judge effects of the specific treatment in the following experiments, syngrafts and allografts were characterized for differences. First, the histopathological changes were determined. According to the literature, Day 14 and 21 after transplantation were chosen as experimental end point for the analysis. Figure 3.25 shows H&E staining (Figure 3.25A) to visualize the architecture of the trachea and Masson's Trichrome (Figure 3.25B) staining to highlight general collagen deposition of syn- and allografts on day 14 and 21 post transplantation. The syngeneic transplanted tracheas revealed no evidence of BOS whereas the heterotopic transplanted tracheas demonstrated luminal occlusion and epithelial loss. This BOS phenotype worsened until day 21. After quantification of five animals per group with three different trachea slices per animal, significant differences were determined in epithelial loss and luminal occlusion (Figure 3.25C).

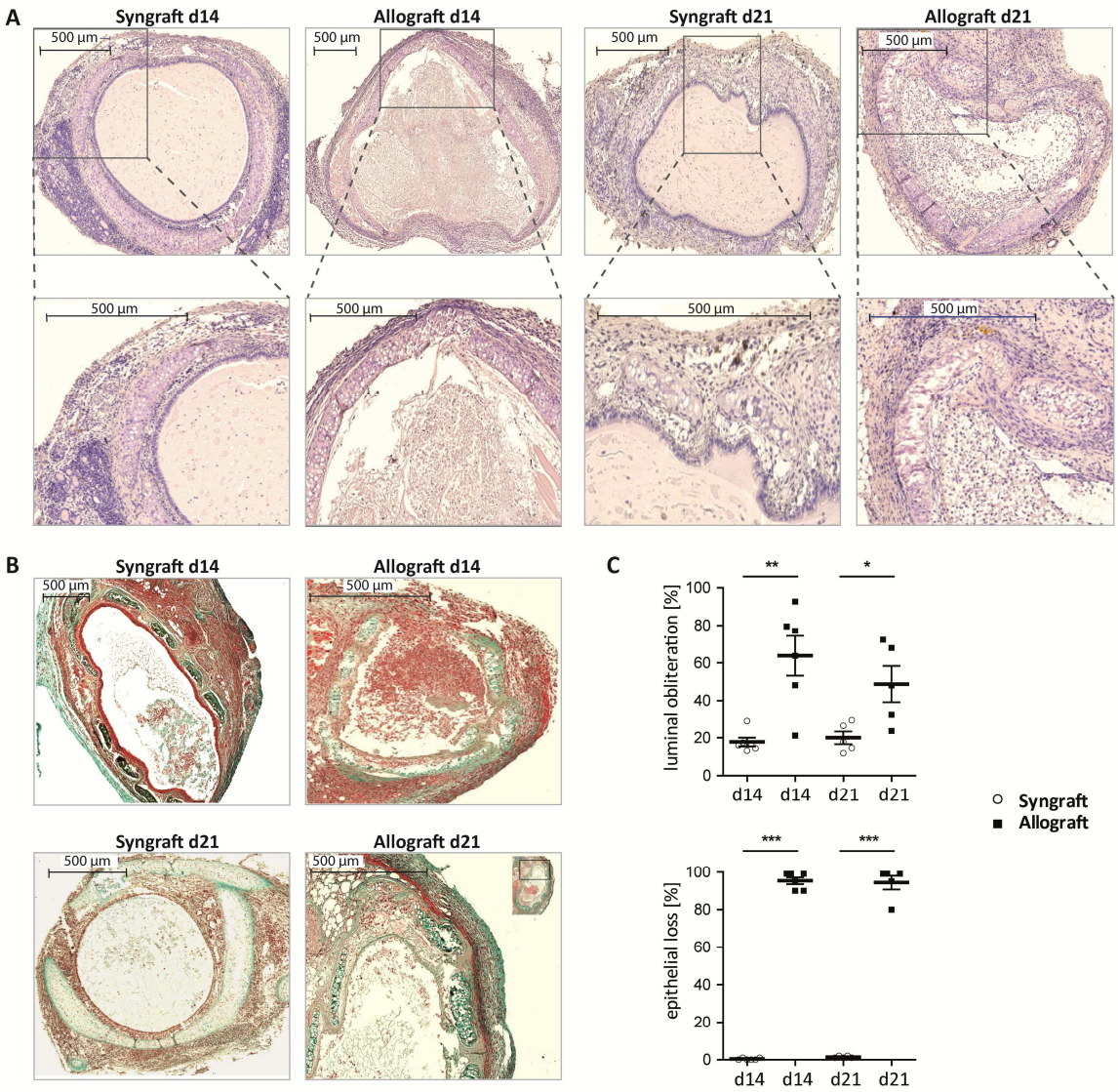

Figure 3.25: Lumina occlusion and epithelial damage can be detected in the allografts on day 14 and 21.
Tracheas were explanted on day 14 and 21, embedded in paraffin, and (A) H&E and (B) Masson's Trichrome stainings were performed. Figure A and B show explanted tracheas on day 14 and 21, exemplarily. (C) Quantification of luminal obliteration and epithelial damage. Statistical analysis: Anova with Dunnett's Multiple Comparison Test (mean ± SD). * $p<0.05$, ** $p<0.01$, and *** $p<0.001$.

3.2.1.2 Analysis of collagen deposition and epithelial damage

To validate that the alterations in the grafts, visualized in Figure 3.25, were caused by epithelial damage and collagen deposition, specific immunofluorescence staining was performed. As demonstrated in Figure 3.26, an intact epithelial layer with intact cilia (anti E-cadherin in green) was visualized in the control group whereas no epithelium was detected in the allografts, neither on day 14 nor on day 21. In addition, collagen deposition (red), narrowing the tracheas` lumen like a net structure, was highlighted by the immunofluorescence (IF) staining for collagen I. DAPI staining (blue) was used to visualize the nuclei (Figure 3.26). Isotype antibodies instead of specific antibodies were used as specificity control, revealing no staining beside DAPI (data not shown).

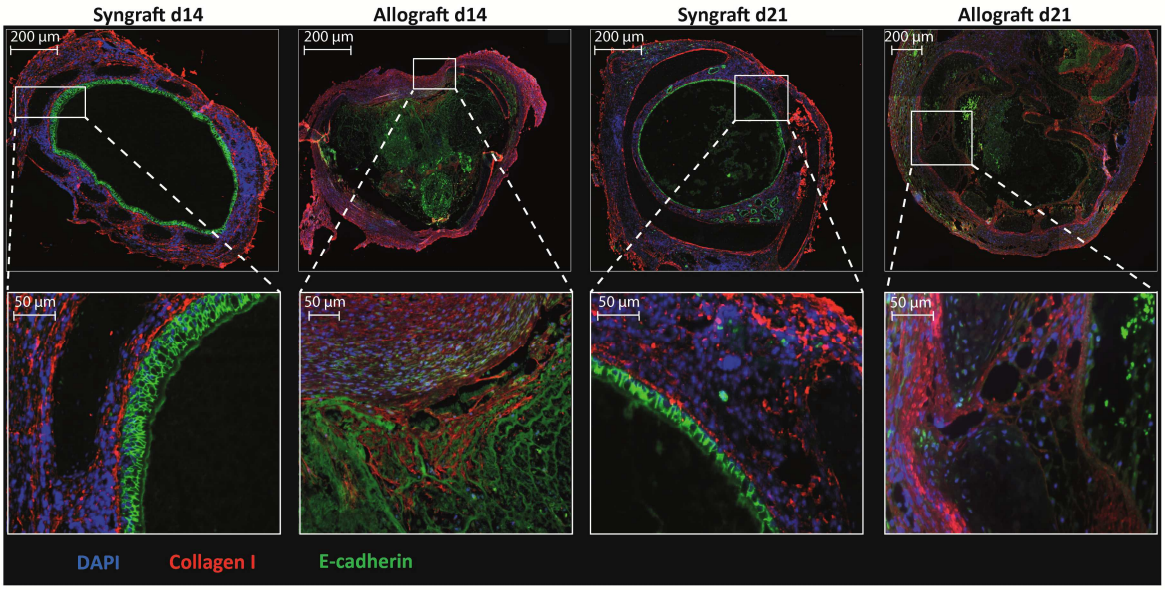

Figure 3.26: Epithelial loss and collagen deposition in explanted tracheas on day 14 and 21.
Experiments were performed as described in Figure 3.25 with specific IF stainings. Nuclei are highlighted with DAPI staining (blue), collagen with ab against collagen I (red), and the epithelium with ab against E-cadherin (green). Images were recorded on Axio imager.

3.2.1.3 Analysis of activated fibroblasts and vascularization

Increased appearance of activated fibroblasts, which are the main producer of collagen deposition, is a typical characteristic of BOS. As no specific marker for murine fibroblasts exists, α-smooth muscle actin (SMA), together with the prominent shape of fibroblasts is generally used as a marker to visualize this cell type. In addition, CD31, a marker for endothelial cells was also used in this study to detect neovascularization of transplanted tracheas. Whereas syngrafts did not show signs of intraluminal cell infiltration, allografts demonstrated an intraluminal accumulation of fibroblasts with their characteristic shape, stained in red (Figure 3.27). The fibroblast influx was very dominant 21 days post transplantation. Accumulation of endothelial cells (CD31: green) was detected especially on the sides of the trachea that were connected to the dermis of the recipient. That area is easier accessible for neovascularization. In generally, allografts had a tendency to show more endothelial cells but this could not be quantified (Figure 3.27).

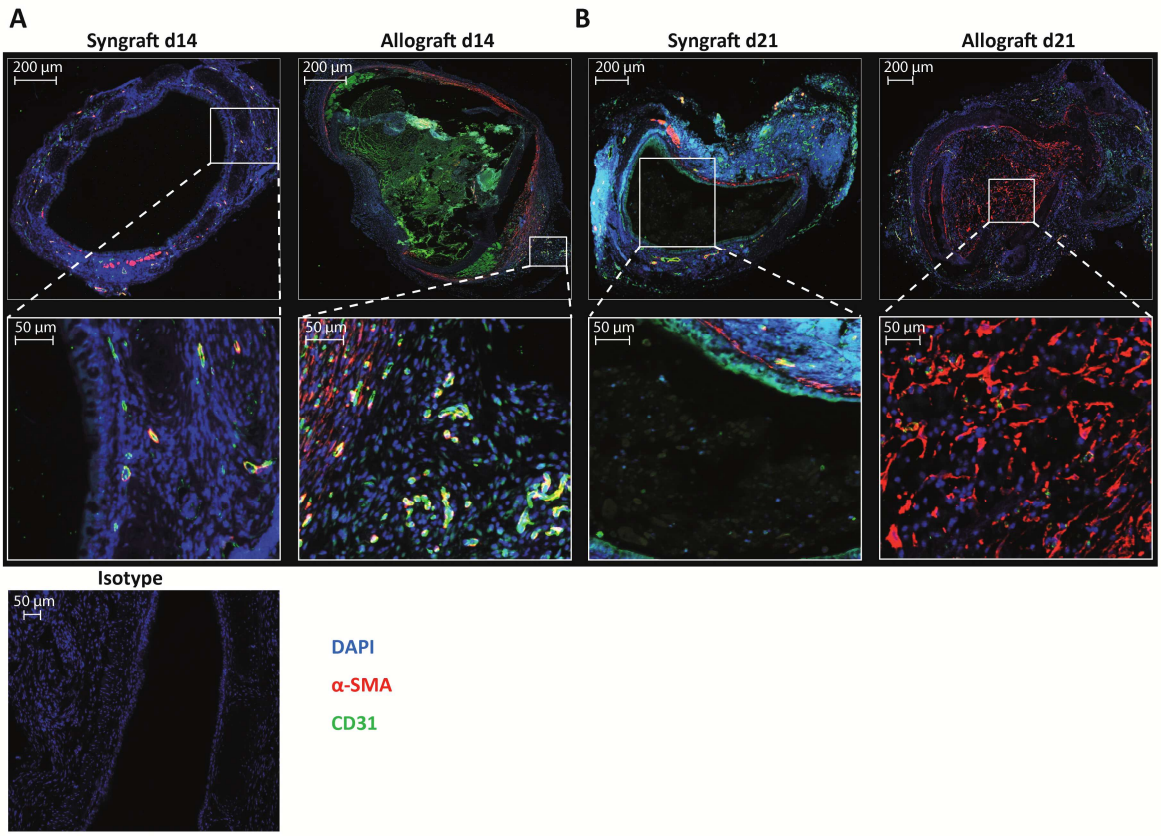

Figure 3.27: Fibroblast invasion and neovascularization in allografts on day 14 and 21.
Experiments were performed as described in Figure 3.25 with specific IF stainings 14 days (A) and 21 days (B) after transplantation. Nuclei are highlighted with DAPI staining (blue), fibroblasts with ab against α-SMA (red), and endothelium with ab against CD31 (green). Isotype staining visualizes the specificity of the used abs. Images were recorded on Axio imager.

3.2.1.4 Analysis of infiltrating lymphocytes

Another characteristic of BOS is the infiltration of inflammatory cells. At day 14 and 21, syngrafts showed no intraluminal $CD45^+$ leukocytes whereas allografts demonstrated an accumulation of leukocytes in the lumen that promoted the luminal occlusion. Leukocytes were detected in syngrafts, but exclusively in the lamina propria and in the epithelium, and not in the lumen of the tracheas (Figure 3.28).

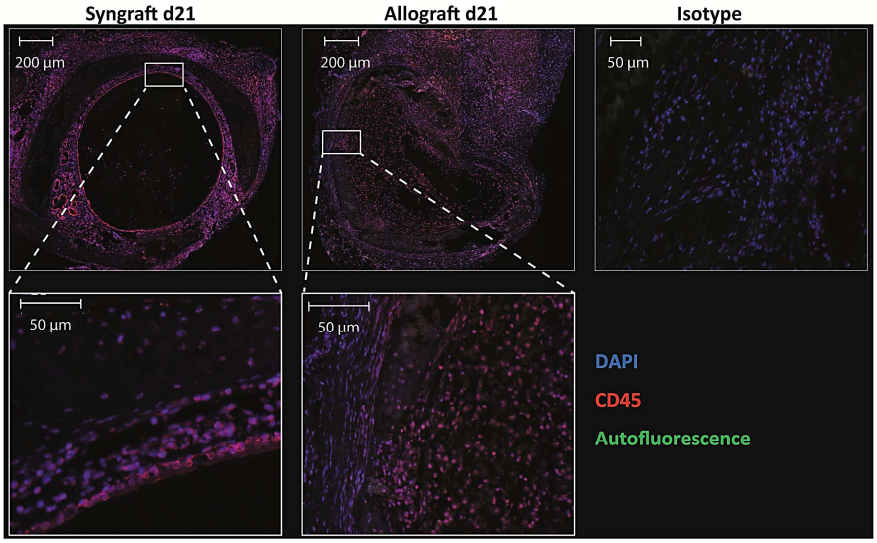

Figure 3.28: Inflammatory character of BOS by intraluminal leukocyte influx in allografts on day 21.
Experiments were performed as described in Figure 3.25 with specific IF staining against leukocytes. Tracheas of day 21 after transplantation are shown, exemplarily. Nuclei are highlighted with DAPI staining (blue) and leukocytes with ab against CD45 (red). Isotype staining visualizes the specificity of the used abs (right). Images were recorded on Axio imager.

To further analyze the composition of the $CD45^+$ leukocytes, staining against $CD3^+$ and galectin3 were performed. With these markers, T lymphocytes (CD3) and macrophages (galectin3) can be distinguished.

As shown in Figure 3.29, T lymphocytes were detected in syngrafts as well as in allografts. In line with the results of the entire leukocyte distribution, no lymphocytes were detected in the lumen of syngrafts whereas extensive intraluminal lymphocyte influx was determined in allografts.

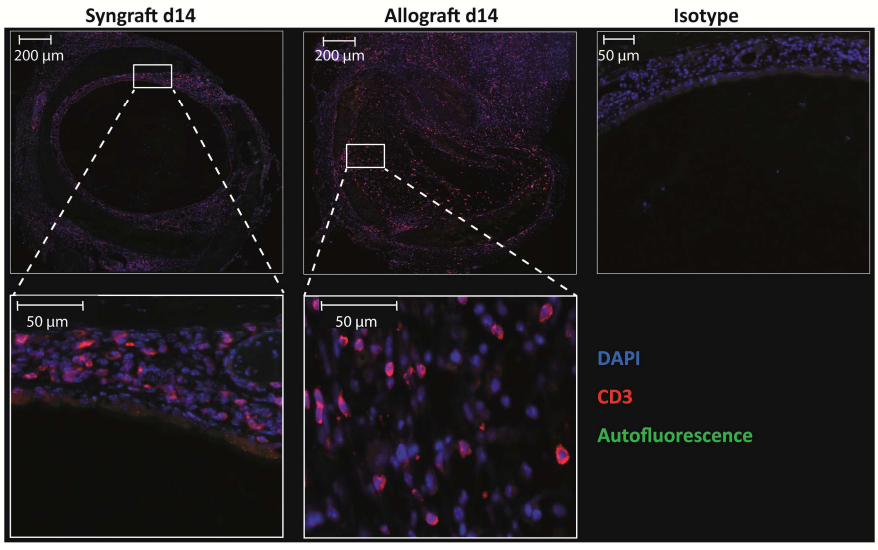

Figure 3.29: Invasion of intraluminal T lymphocytes in allografts on day 21.
Experiments were performed as described in Figure 3.25 with specific IF staining against T lymphocytes. Nuclei are highlighted with DAPI staining (blue) and T lymphocytes with ab against CD3 (red). Isotype staining visualizes the specificity of the used abs. Images were recorded on Axio imager.

Macrophages (galectin3 positive) were observed in the syngrafts and allografts. Allografts revealed a clear intraluminal localization of macrophages (Figure 3.30).

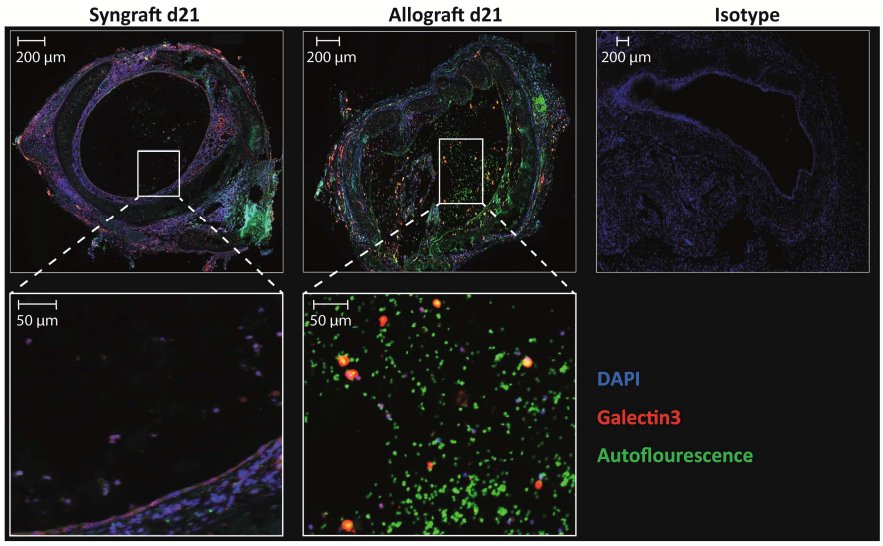

Figure 3.30: Invasion of macrophages in allografts on day 21.
Experiments were performed as described in Figure 3.25 with specific IF staining against macrophages. Nucleus is highlighted with DAPI staining (blue), macrophages with ab against galectin3 (red), and autofluorescence visualize in green. Isotype staining visualizes the specificity of used abs. Images were recorded on Axio imager.

3.2.2 Analysis of the HTT model by flow cytometry

To further characterize the HTT model, lymph nodes and whole blood from the aorta of syngeneic and allogeneic transplanted mice were collected on day 14 and 21 and analyzed for the distribution of leukocytes and myeloid cells.

3.2.2.1 Analysis of lymphocytes in blood and lymph nodes

Figure 3.31 details the gating strategy to distinguish whole blood lymphocyte subsets by flow cytometry, exemplary on day 14. First, lymphocytes were gated according to forward and side scatter followed by exclusion of dead and doublet cells, as detailed in the gating strategy in Figure 3.2ii-iii. Afterwards, $CD45^+$ cells were analyzed for percentage of NK cells (NK.1.1.), T lymphocytes (CD3), and B cells (CD19). Furthermore, $CD3^+$ T lymphocytes were further divided in their two main subpopulations and percentage of $CD4^+$ and $CD8^+$ T cells were quantified in each animal.

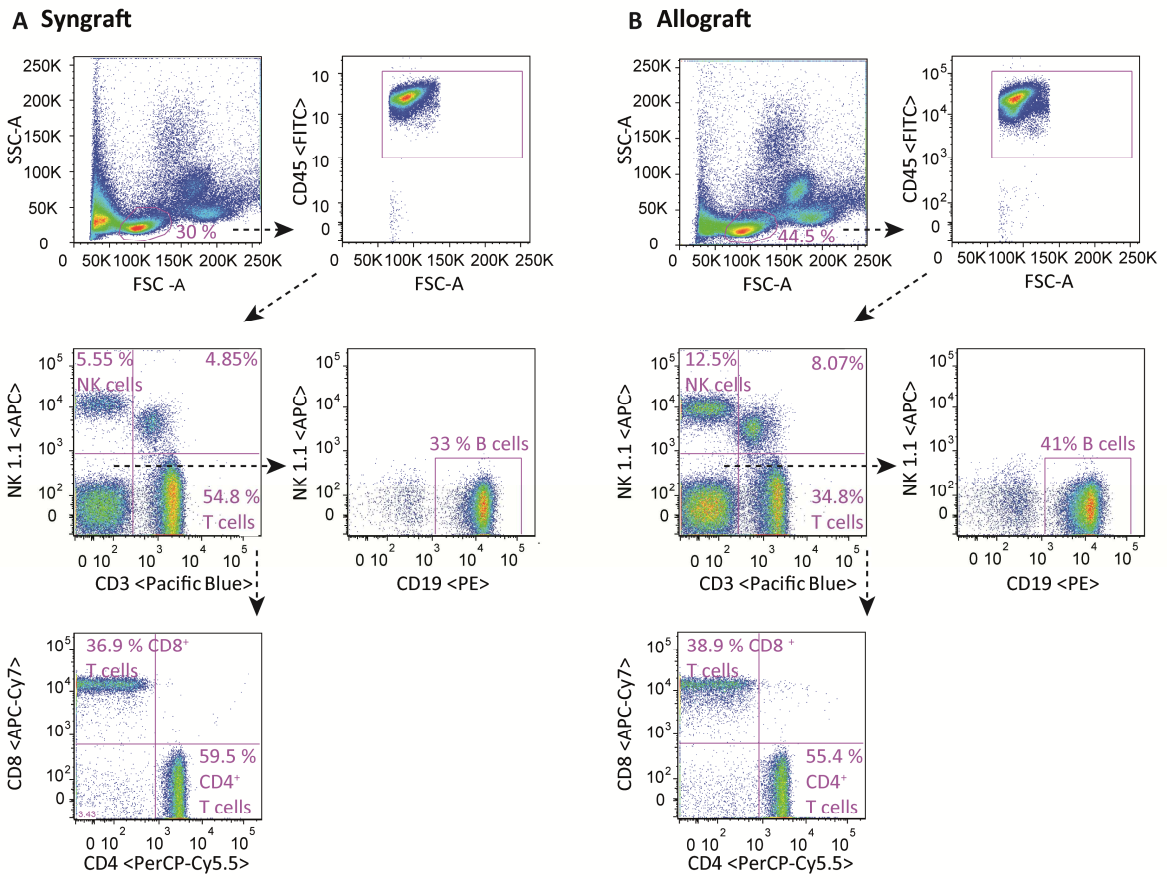

Figure 3.31: Gating strategy to analyze lymphocyte subsets in blood.
Blood of allogeneic and syngeneic transplanted animals was collected on day 14 and analyzed for the distribution of lymphocyte subsets in whole blood. After separating lymphocytes by forward and side scatter, followed by exclusion of dead and doublet cells, all $CD45^+$ cells were chosen. To further distinguish subpopulations, the following abs were used: NK1.1 (NK cells), CD3 (T cells), and CD19 (B cells). $CD3^+$ T lymphocytes were further distinguished in $CD4^+$ and $CD8^+$ T lymphocytes. Amount of NK, T, and B cells are visualized in relation to all lymphocytes. B cells are shown as subgate of pre-gated $CD3^-$ and $NK1.1^-$ cells. $CD4^+$ and $CD8^+$ T lymphocytes are shown in percentage in relation to pre-gated $CD3^+$ T lymphocytes. (A) syngeneic and (B) allogeneic transplanted animals on day 14.

To determine the distribution of lymphocyte subsets in lymph nodes (axillary and branchial) of syngeneic and allogeneic transplanted animals, the same gating strategy was used as described before for whole blood. Figure 3.32 summarizes the gating strategy that was used for lymph nodes of transplanted animals, exemplary on day 14.

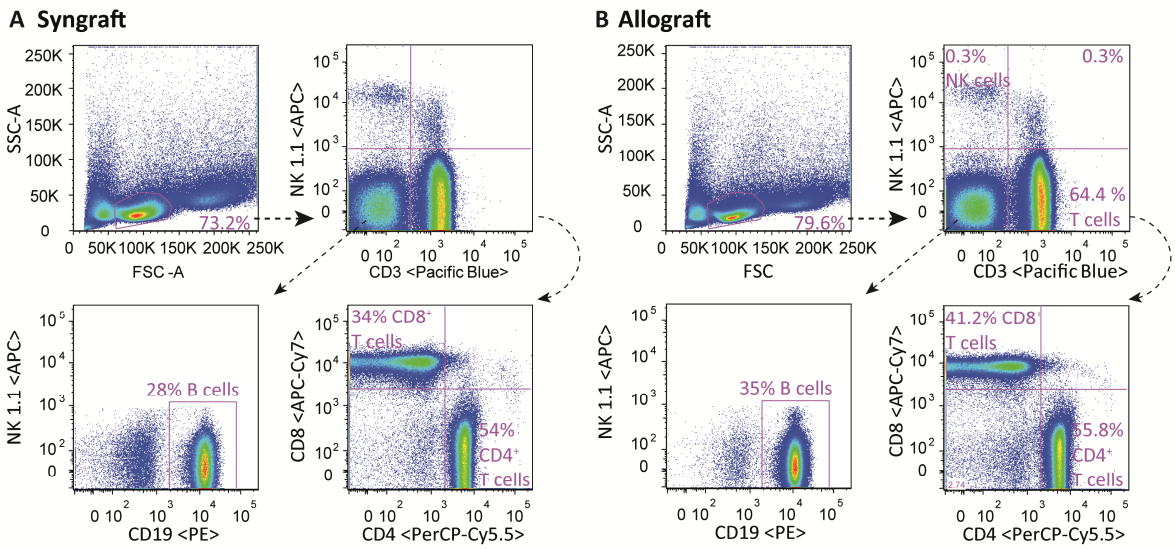

Figure 3.32: Gating strategy to analyze lymphocyte subsets in lymph nodes.
Lymph nodes of allogeneic and syngeneic transplanted animals were collected on day 14 and analyzed for the distribution of lymphocytes by flow cytometry. After separating lymphocytes by forward and side scatter, followed by exclusion of dead and doublet cells, all $CD45^+$ cells were chosen. To further distinguish the different lymphocyte subpopulations, the following abs were used: NK1.1 (NK cells), CD3 (T cells), and CD19 (B cells). $CD3^+$ T cells were further distinguished in $CD4^+$ and $CD8^+$ T cells. Amount of NK, T and B cells are visualize in percentages in relation to all lymphocytes. B cells are shown as subgate of pre-gated $CD3^-$ and $NK1.1^-$ cells. $CD4^+$ and $CD8^+$ T cells are shown in percentage in relation to pre-gated $CD3^+$ T cells. (A) syngeneic and (B) allogeneic transplanted animals on day 14.

The quantification of leukocyte subsets in blood and lymph nodes of syngeneic and allogeneic transplanted animals revealed no significant differences (Figure 3.33). In case of B cells, a tendency of increased cell numbers in allografts compared to syngrafts was detected on day 21 (lymph nodes). Furthermore, in comparison to non-transplanted animals, transplanted ones revealed lower percentages of NK cells (lymph nodes) and $CD8^+$ T lymphocytes (lymph nodes) as well as higher percentages of $CD4^+$ T cells (blood and lymph nodes), as depicted in Figure 3.33.

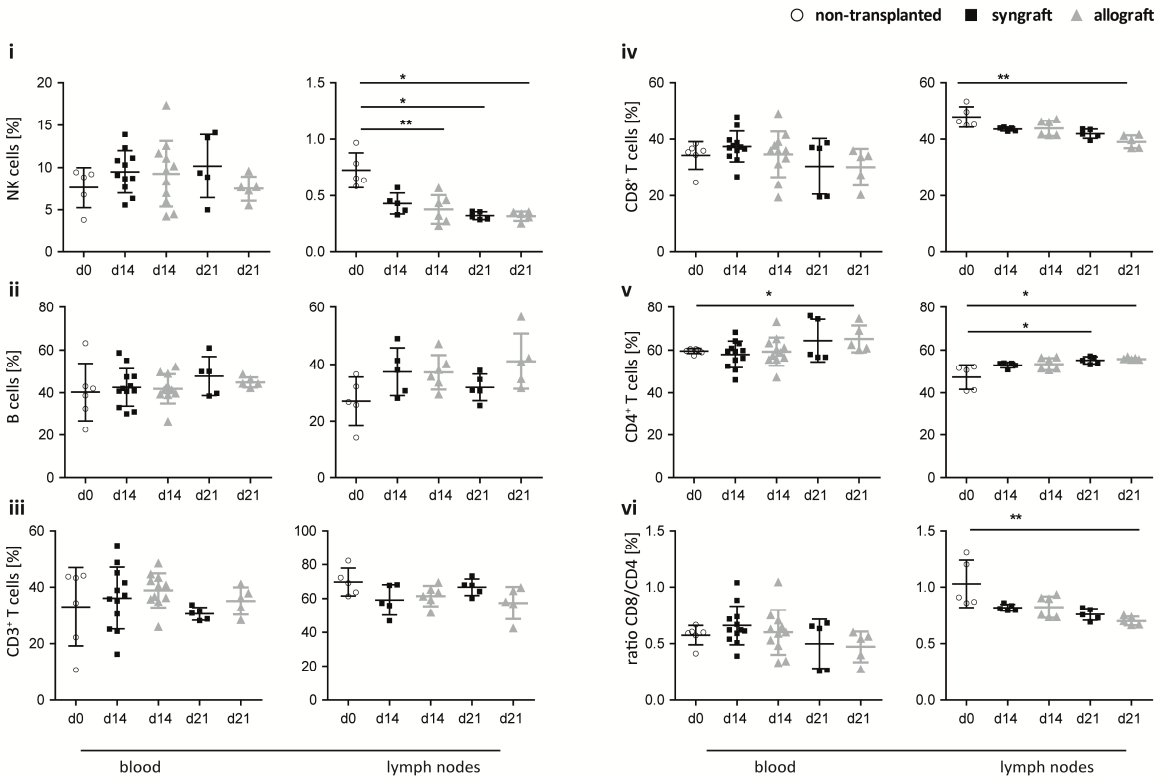

Figure 3.33: Quantification of lymphocyte subsets in blood and lymph nodes of transplanted mice. Blood and lymph nodes were collected of non-transplanted (do), syngeneic, and allogeneic transplanted (d14 and d21) mice. Flow cytometry analysis was performed to analyze the contribution of NK cells, B cells, and $CD3^+$ T lymphocytes which were further subdivided in $CD4^+$ and $CD8^+$ T lymphocytes. (i-iii) Percentage of specific cell types in relation to whole lymphocytes. (iv-v) Percentage of $CD4^+$ or $CD8^+$ T cells in relation to whole $CD3^+$ T lymphocytes. (vi) Ratio of $CD8^+$ and $CD4^+$ T lymphocytes. Data are shown as percentage of specific cell types in blood as well as in lymph nodes. Statistical analysis: Anova with Dunnett's Multiple Comparison Test (mean ± SD). *p<0.05 and **p<0.01.

3.2.2.2 Analysis of myeloid cells in blood and lymph nodes

After analyzing the distribution of lymphocytes, further analysis was performed to detect myeloid cells. Figure 3.34 detailed the gating strategy to distinguish myeloid cells in whole blood by flow cytometry, exemplary on day 14. First, all leukocytes were gated according to forward and side scatter, followed by exclusion of dead and doublet cells. Afterwards, CD45 positive cells were gated and subdivided in either cell granularity rich (SSC^{high}) or cell granularity poor (SSC^{low}) $CD11b^+$ myeloid cells. SSC^{high} and $CD11b^+$ cells were further divided in $GR1^+$ neutrophils or $GR1^-$ eosinophils. SSC^{low} and $CD11b^+$ cells were further subdivided in $CD11c^+$ and $GR1^-$ inflammatory or $CD11c^-$ and $GR1^{dim}$ resident monocytes.

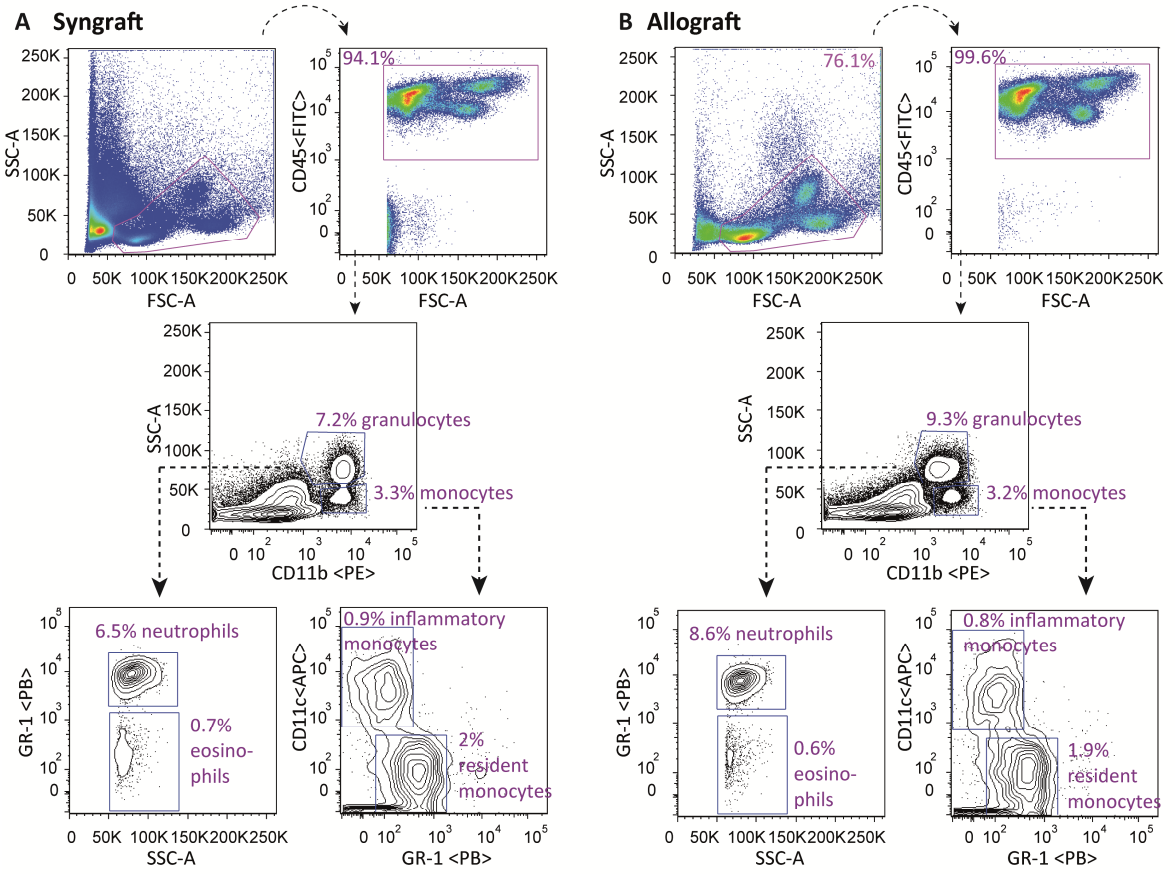

Figure 3.34: Gating strategy to analyze granulocytes and monocytes in blood.
Blood of allogeneic and syngeneic transplanted animals was collected on day 14 and analyzed for the distribution of granulocytes and monocytes in whole blood. Leukocytes were selected based on forward and side scatter and $CD45^+$ cells were chosen for further separation in their different subpopulations. $CD11b^+$ cells with high granulation were separated in neutrophilic granulocytes by high granulation (SSC^{high}) and high GR-1, whereas eosinophils were separated by high granulation and missing GR-1 expression. $CD11b^+$ cells with low granulation (SSC^{low}) were further distinguished in inflammatory ($CD11c^+$ and $GR1^-$) and resident ($CD11c^-$ and $GR1^{dim}$) monocytes. Amounts of monocytes, granulocytes, neutrophils, eosinophils, and inflammatory and resident monocytes are visualized in percentages in relation to all leukocytes. (A) syngeneic and (B) allogeneic transplanted animals on day 14.

Regarding myeloid cells in the draining lymph nodes, the focus was set on DCs. To obtain the distribution of $CD11c^+$ DCs in lymph nodes of syngeneic and allogeneic transplanted animals, CD45 and CD11c expressing cells that had MHC-II on their surface were defined as DCs. Figure 3.35 shows the percentage of DCs in relation to all leukocytes in lymph nodes of transplanted animals, exemplary on day 14.

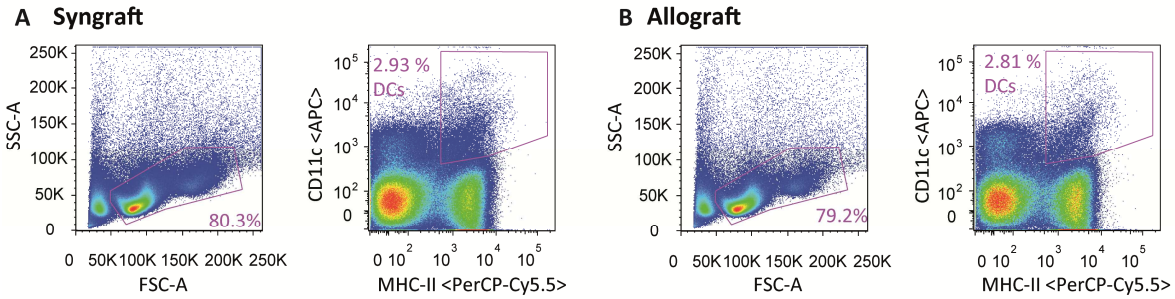

Figure 3.35: Gating strategy to analyze DCs in lymph nodes.
Lymph nodes of allogeneic and syngeneic transplanted animals were collected on day 14 and analyzed for the percentage of DCs in relation to whole leukocytes. Cells were pre-gated on leukocytes by forward and side scatter. To exclude dead and doublet cells, the same gating strategy was performed as described in Figure 3.2. To visualize DCs in lymph nodes, cells were stained for CD45, CD11c, and MHC-II. Cells which were positive for all three markers were counted as DCs. (A) syngeneic and (B) allogeneic transplanted animals on day 14.

The quantification of myeloid cells in blood and lymph nodes of syngeneic and allogeneic transplanted animals revealed no significant differences. In comparison to non-transplanted animals, transplanted ones revealed a slight but not significant decrease in resident monocytes.

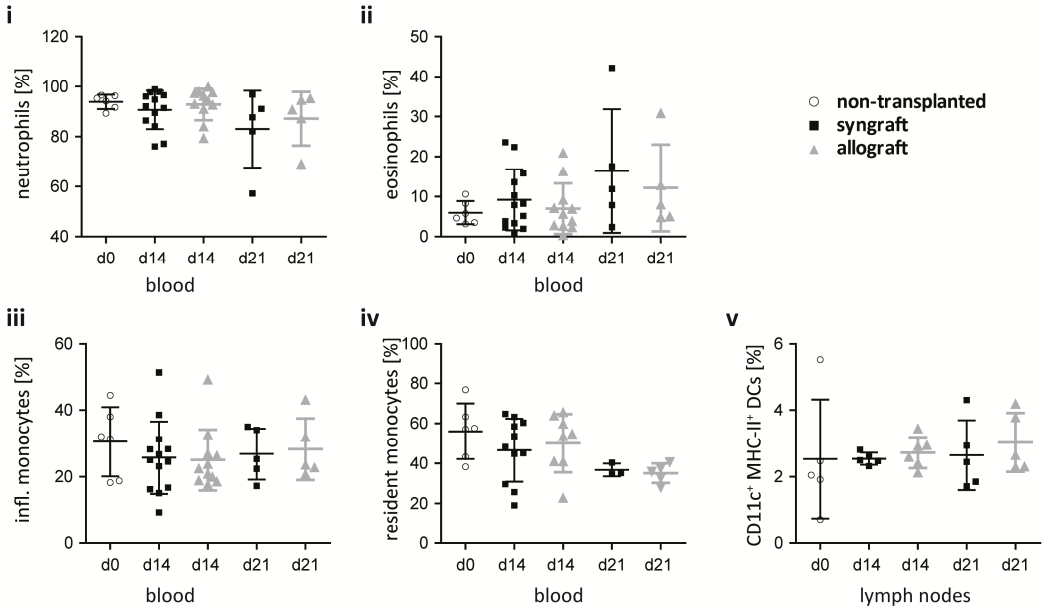

Figure 3.36: Quantification of myeloid cells.
Blood and lymph nodes were collected from non-transplanted (do), syngeneic, and allogeneic transplanted (d14 and d21) mice. Flow cytometry analysis was performed to analyze the contribution of myeloid cells. In blood, neutrophilic and eosinophilic granulocytes as well as inflammatory and resident monocytes were analyzed. Subgroups in the blood of mice are shown as percentage in relation to all pre-gated granulocytes or monocytes. To analyze myeloid cells in lymph nodes, DCs were quantified by CD11c and MHC-II surface expression. Numbers of DCs are shown in percentage in relation to all leukocytes. Statistical analysis: Anova with Dunnett's Multiple Comparison Test (mean ± SD).

In summary, the HTT model was established with allografts revealing the typical BOS phenotype, showing epithelial damage, subepithelial and luminal occlusion, and leukocyte influx. Leukocytes

and myeloid cells in blood and lymph nodes showed no significant differences between syngeneic and allogeneic transplanted animals.

3.2.3 Analysis of MMP expression in grafts

To gain insights into the role of MMP-12 and -13 for the development of the BOS phenotype, transcript levels of the different MMPs was analyzed in explanted tracheas on day 14. As control, data were normalized to tracheas of non-transplanted animals. As shown in Figure 3.37, a clear increase in the transcripts of all MMPs between transplanted and non-transplanted animals was detected. In contrast, changes in the transcript levels of TIMPs were either increased (TIMP-1) or decreased (TIMP-2 and -3) in the transplanted groups. With regards to changes between syngrafts and allografts, only MMP-13 expression showed a strong tendency to increase in the allografts compared to syngrafts. The other MMPs revealed no clear difference between syngrafts and allografts. Slight alterations were also detected in the expression profile of TIMPs. Whereas TIMP-1 showed a tendency to increase in allografts, TIMP-2 and -3 revealed a tendency to decrease. In summary, all MMPs and TIMPs demonstrated changes in the transcript levels in the transplant setting, yet independent of syngeneic or allogeneic except for MMP-13, which was increased in the allografts compared to syngrafts. This result indicates that alteration in MMP-13 expression might not only result from the general transplantation process but rather from the rejection process of the allograft.

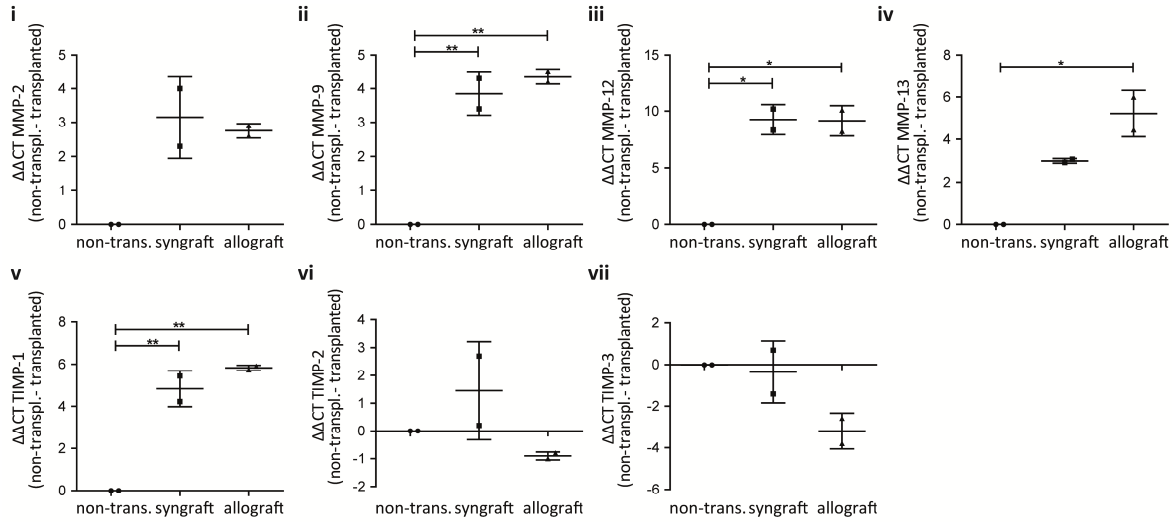

Figure 3.37: Increased MMP-13 expression in allografts.
Tracheas of either C57BL/6 (syngraft) or Balb/c (allograft) mice were transplanted in a pouch on the back of C57BL/6 mice to mimic the phenotype of BOS. On day 14, tracheas were explanted and the expression of MMPs and TIMPs in whole tracheas was analyzed by qRT-PCR. Tracheas of non-transplanted animals were used as control. Data are shown as ΔΔCT values of transplanted normalized to non-transplanted tracheas for two independent experiments (n = 2). Statistical analysis: Anova with Dunnett's Multiple Comparison Test. *p<0.05 and **p<0.01.

3.2.4 IHC analysis of MMPs in transplanted tracheas

After verifying mRNA expression of the selected MMPs in transplanted tracheas, the next aim was to localize MMP-12 and -13 proteins in these tracheas. Therefore, IF stainings of paraffin embedded tracheas with specific antibodies against MMP-12 and-13 were performed. As shown in Figure 3.38 and Figure 3.39, MMP-12 and -13 were detected in non-transplanted as well as in transplanted tracheas, consistent with the detection of respective mRNAs.

MMP-12 expression is shown in red (Figure 3.38). Although MMP-12 could be detected in all tracheas, the invading cells in the allografts (right) showed particularly strong MMP-12 staining.

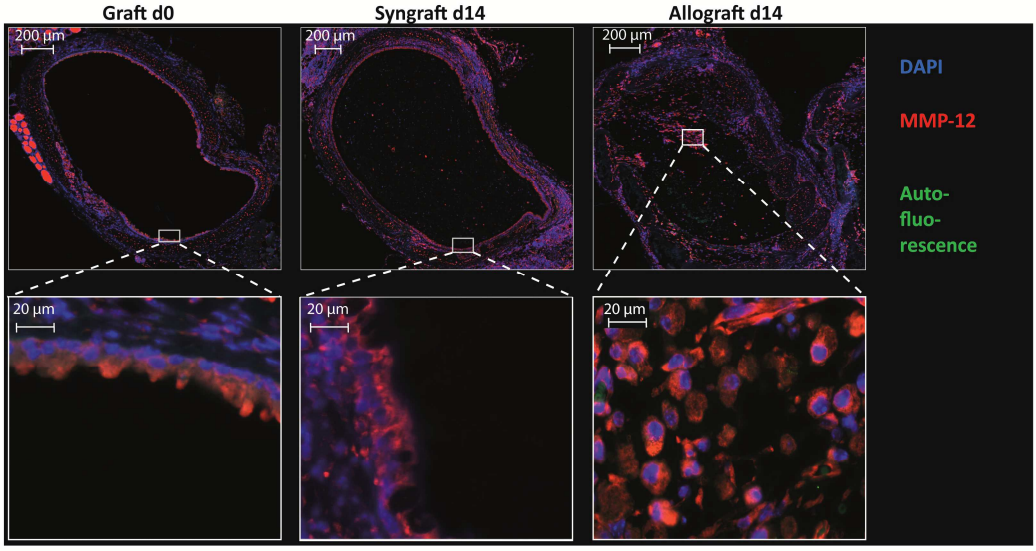

Figure 3.38: MMP-12 protein localization in tracheas before and after transplantation.
Tracheas were transplanted as described in section 2.2.10 and explanted on day 14. Specific IF staining against MMP-12 on paraffin embedded tracheas was performed. Nuclei are highlighted with DAPI staining (blue), MMP-12 is shown in red and autofluorescence visualized in green. Images were recorded on Axio imager.

Figure 3.39 shows the MMP-13 staining in red in non-transplanted tracheas, syngrafts, and allografts. In comparison to non-transplanted tracheas, a stronger MMP-13 staining was determined in syngrafts and allografts. As shown before for MMP-12, the invading cells detected in the lumen of the trachea were positive for MMP-13.

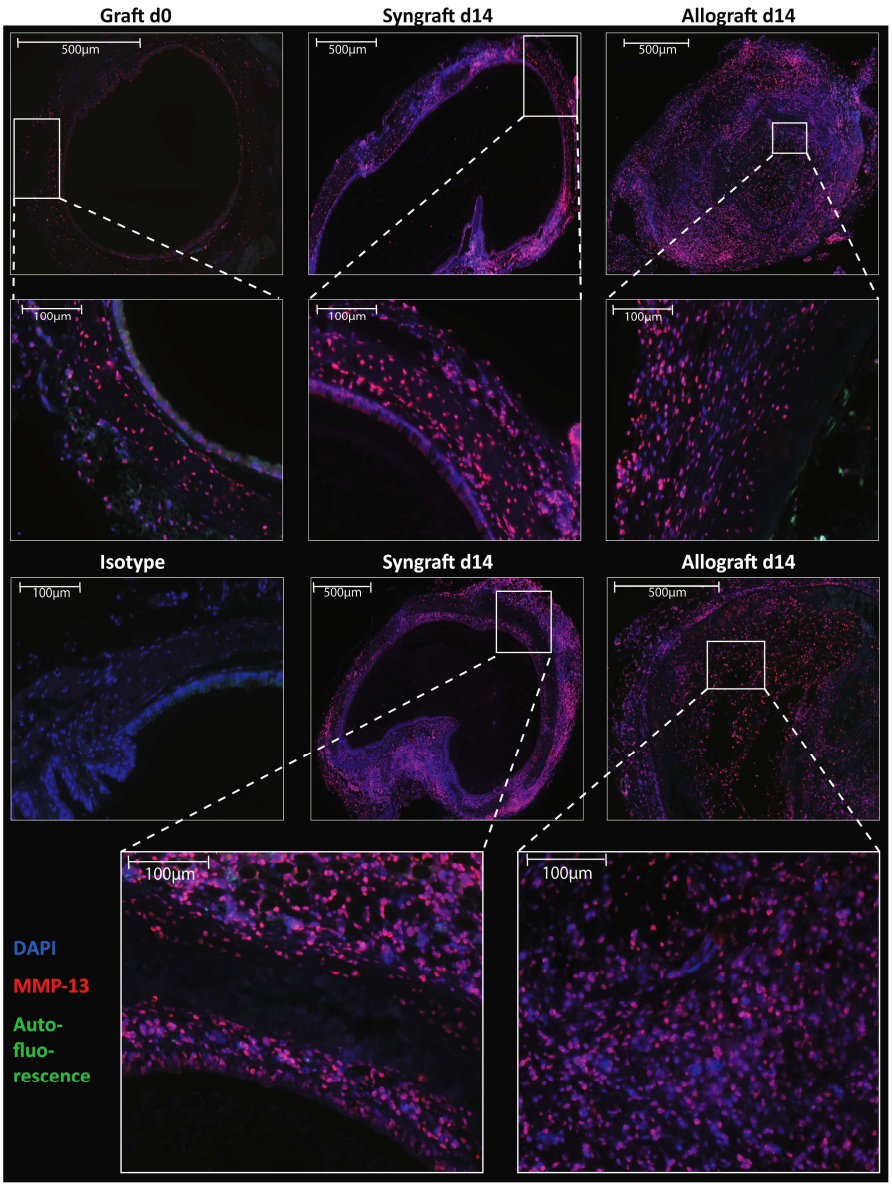

Figure 3.39: MMP-13 protein localization in tracheas before and after transplantation.
Tracheas were transplanted as described in section 2.2.10 and explanted on day 14. Specific IF staining against MMP-13 on paraffin embedded tracheas was implemented. Nuclei are highlighted with DAPI staining (blue), MMP-13 is shown in red, and autofluorescence visualized in green. Isotype staining proofed the specificity of the used antibodies. Images were recorded on Axio imager.

In summary, MMP-12 and -13 expression was verified in tracheas on mRNA level and protein level in syn- and allografts. IF staining visualized MMP-12 and -13 proteins in the invading cells in the lumen of the allografts. Co-staining with DC markers like CD11c could not be performed as the available antibodies did not work on paraffin embedded sections.

3.3 Treatment of BOS phenotype with MMP-13 inhibitor *in vivo*

3.3.1 Analysis of lymphocytes and myeloid cells in blood and lymph nodes of MMP-13 inhibitor-treated allografts

In a pilot study, the effect of MMP-13 inhibitor treatment for the development of experimental BOS was analyzed *in vivo*. Animals were syn- and allo-transplanted as described in section 2.2.10 and the MMP-13 inhibitor was administered i.p. every second day until day 14 and 21. Two concentrations, 74 µM (25 µg) (2 animals per group) and 296 µM (100 µg) (4 animals per group) of MMP-13 inhibitor per animal were tested. NaCl instead of the inhibitor was used as vehicle control. For both inhibitor concentrations no weight loss or other side effects were observed.

To analyze whether the inhibitor had any effect on the leukocyte composition, blood and lymph nodes were collected and differences between allogeneic transplanted mice treated with inhibitor or NaCl were analyzed as described in section 3.2.2. As shown in Figure 3.40, percentages of NK cells in blood but not in lymph nodes of inhibitor-treated mice increased 21 days post-transplantation. Furthermore, $CD4^+$ T cells increased after inhibitor treatment whereas $CD8^+$ T cells decreased on day 14 and 21 in blood of inhibitor-treated mice. In lymph nodes, both $CD4^+$ and $CD8^+$ T lymphocytes showed a tendency to decrease after inhibitor treatment.

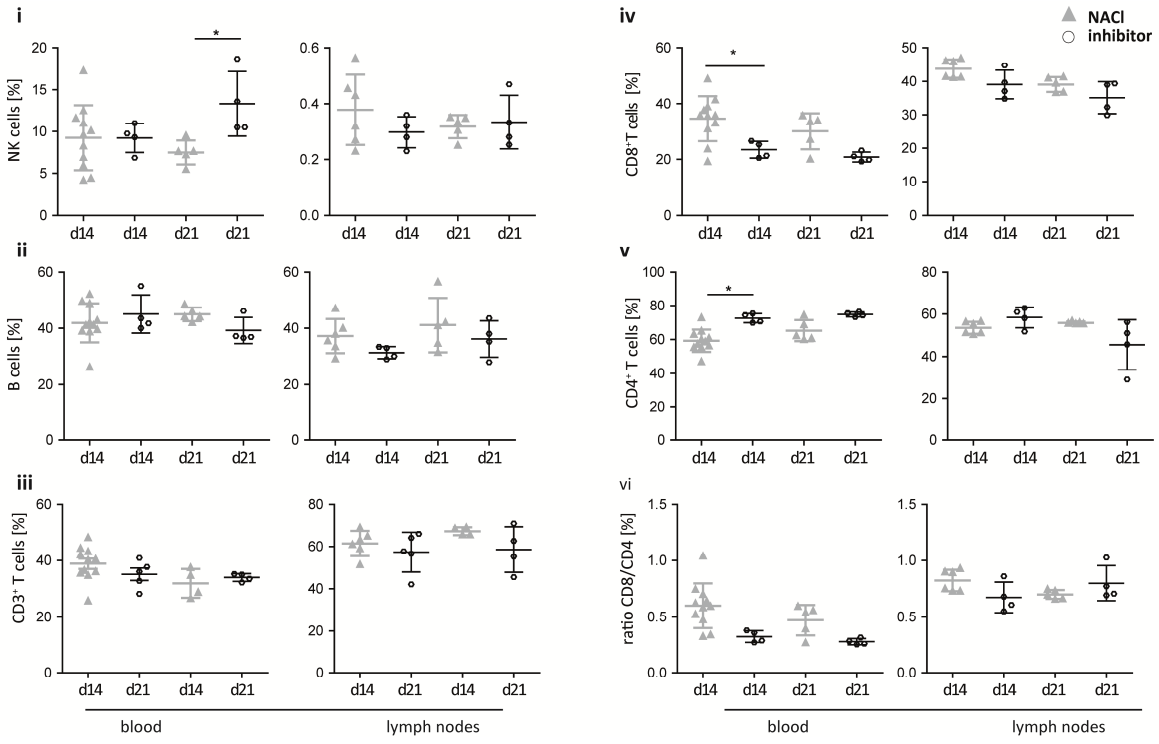

Figure 3.40: Quantification of lymphocytes in blood and lymph nodes of transplanted mice treated with MMP-13 inhibitor.
Blood and lymph nodes were collected from allogeneic transplanted (d14 and d21) mice treated with 296 µM MMP-13 inhibitor or NaCl. Flow cytometry analysis was performed to analyze the frequency of NK cells, B cells, and $CD3^+$ T lymphocytes, which were further subdivided in $CD4^+$ and $CD8^+$ T lymphocytes. (i-iii) Percentages of specific cells in relation to whole lymphocytes. (iv-v) Percentages of $CD4^+$ or $CD8^+$ T cells in relation to whole $CD3^+$ T lymphocytes. (vi) Ratio of $CD8^+$ to $CD4^+$ T lymphocytes. Data are shown as percentages of specific cell types in blood (left column) as well as in lymph nodes (right column). Statistical analysis: Anova with Dunnett's Multiple Comparison Test (mean ± SD). *$p<0.05$.

With regard to myeloid cells, no significant differences could be detected in the groups which were treated with inhibitor compared to controls.

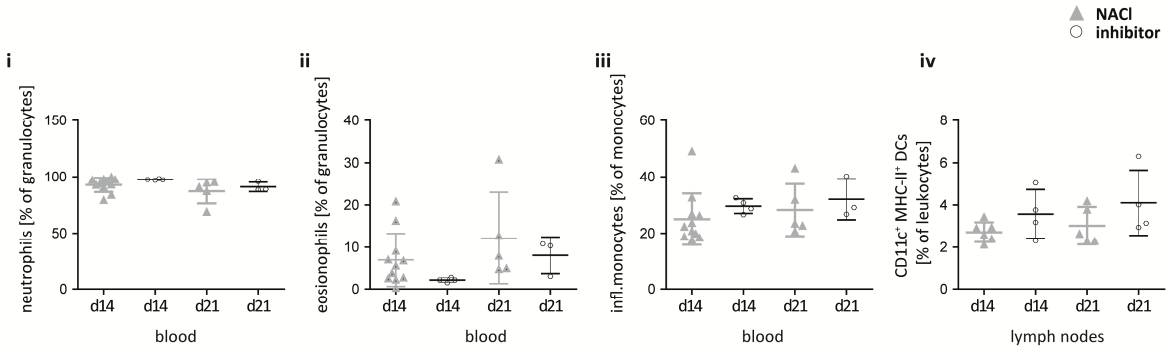

Figure 3.41: Quantification of myeloid cells after MMP-13 inhibitor treatment.
Blood and lymph nodes were collected from allogeneic transplanted (d14 and d21) mice treated with 296 µM MMP-13 inhibitor or with NaCl. Flow cytometry analysis was performed to analyze the frequency of myeloid cells. In blood, neutrophils and eosinophils were analyzed as well as inflammatory monocytes. Myeloid subgroups are shown as percentage in relation to all leukocytes. In lymph nodes, DCs were analyzed by CD11c and MHC-II surface expression. Data of DCs are shown in percentage in relation to all leukocytes. Statistical analysis: Anova with Dunnett's Multiple Comparison Test (mean ± SD). *p<0.05.

In summary, treatment with MMP-13 inhibitor showed a tendency to alter the lymphocyte distribution whereas frequencies of myeloid cells remained unchanged. Especially $CD8^+$ T cells showed a tendency to decrease in blood and lymph nodes of treated animals.

3.3.2 IHC analysis of transplanted animals treated with MMP-13 inhibitor

After collecting blood and lymph nodes from transplanted animals, syngrafts and allografts were explanted. H&E staining of the paraffin embedded tracheas revealed, like seen before, a clear difference between syngrafts and allografts treated with NaCl (Figure 3.25). Allografts from animals that had received NaCl showed the typical destruction of the epithelial layer and the luminal occlusion. In contrast, allografts treated with inhibitor revealed a milder luminal occlusion and moderate reepithelialization, especially with the higher inhibitor concentration of 296 µM.

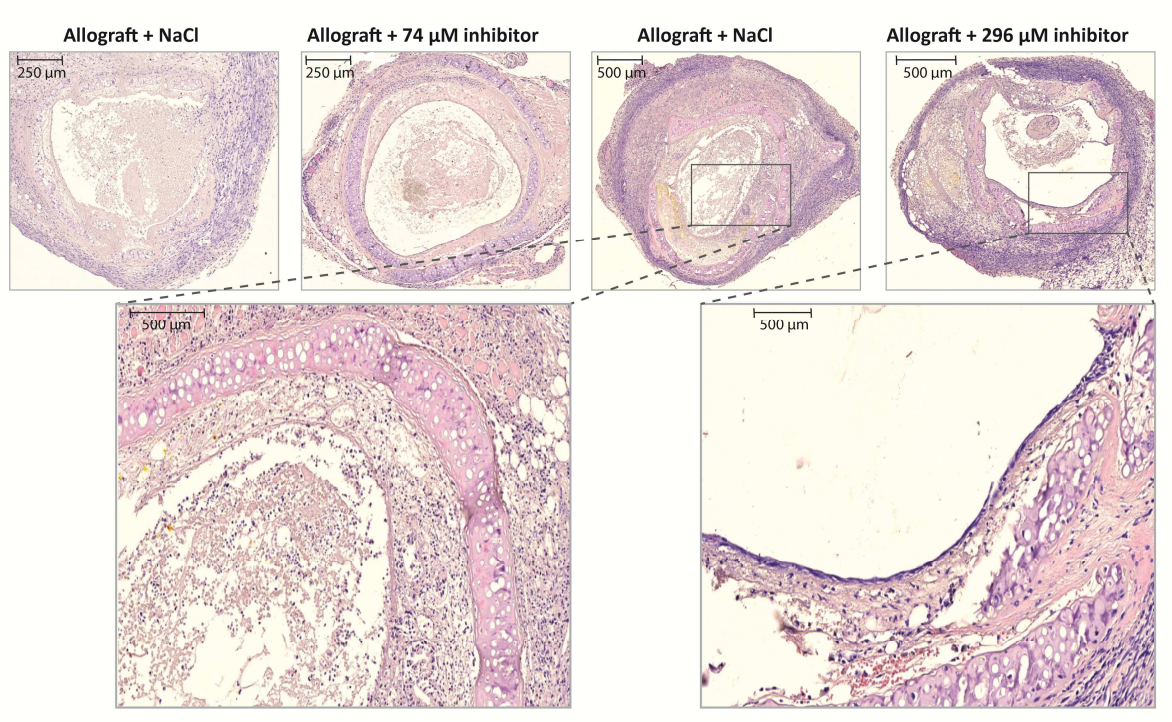

Figure 3.42: MMP-13 inhibitor treatment *in vivo* diminishes the development of the BOS phenotype moderately.
Allogeneic transplanted mice were treated with 74 µM (left) or 296 µM (right) MMP-13 inhibitor or with equivalent amount of NaCl as control i.p. every second day. Tracheas were explanted on day 14, embedded in paraffin, and H&E staining was performed.

As only few animals were treated, quantification was not possible. Whether inhibition of MMP-13 significantly attenuates the development of experimental BOS must be clarified in the future in larger animal studies.

In summary, this study confirmed the expression of MMP-12 and -13 in BMDCs *in vitro* and, furthermore, clearly demonstrated increased MMP-13 expression in response to the inflammatory stimulus LPS on mRNA as well as on activity level. Functional assays with a specific low molecular inhibitor of MMP-13 revealed a new role of MMP-13 in MHC-I presentation, endocytosis, and cytokine/chemokine release of BMDCs. Inhibition of MMP-13 in BMDCs reduced their capacity to activate $CD8^+$ T cells which is likely due to reduced peptide/MHC-I presentation by the BMDCs. Treatment of experimental BOS with the specific inhibitor of MMP-13 *in vivo* caused alterations in the lymphocyte distribution in blood and lymph nodes of inhibitor-treated animals, concerning NK cells, $CD4^+$, and $CD8^+$ T cells. Moreover, in a pilot study, treating allogenic transplanted animals with the inhibitor revealed a milder BOS phenotype with regard to epithelial loss and luminal occlusion. These preliminary *in vivo* experiments require validation in a larger animal cohort in the future.

4 DISCUSSION

BOS is currently still an incurable condition after lung transplantation, based on a long-term graft dysfunction in which both, DCs[113,114,229,231,233] and MMPs[202-208] are reported to be involved. DCs are professional APCs that link the innate and the adaptive immune system and drive the activation of the immune response. MMPs are proteases responsible for matrix degradation and involved in inflammatory processes, tissue repair[121,197], and immunity[121] by regulating cytokine/chemokine degradation[122,156,177,178] and migratory processes[175,176].

In order to identify the connection between DCs and MMPs in the development of BOS, first the immunological role of specific MMPs in DCs had to be identified. In the present study the focus was set on MMP-12 and -13 as they have already been shown to be expressed in murine pulmonary DCs under steady-state conditions[171].

In vitro analysis of BMDCs revealed that MMP-13 transcript level and activity increased in response to the inflammatory stimulus LPS, whereas MMP-12 transcript level did not change. The induction of MMP-13 suggests that, under inflammatory conditions, BMDCs may need MMP-13 for specific immunobiological functions to fully act as APCs. To substantiate this hypothesis, various functional assays were performed using a specific inhibitor of MMP-13. The results suggest an involvement of MMP-13 in endocytosis, peptide presentation via the MHC-I pathway, and modulation of the cytokine/chemokine profile of murine BMDCs. Furthermore, the reduced capacity of MHC-I presentation after MMP-13 inhibition led to downstream effects, reducing $CD8^+$ T lymphocyte activation. In contrast, MMP-13 apparently did not regulated migration or maturation of BMDCs.

To provide further evidence for a potential relevance of MMP-13 in the pathogenesis of BOS, an *in vivo* mouse model (the heterotopic trachea transplant model) was established. Using the murine HTT model, an increase in MMP-13 mRNA expression was observed in allografts compared to syngrafts. Furthermore, MMP-13 could be localized in explanted tracheas by immunofluorescence staining. Based on these promising *in vitro* results, an *in vivo* pilot study was initiated whereby mice with trachea allografts were treated with the low molecular MMP-13 inhibitor. The results from this study provide initial evidence that the treatment with the low molecular MMP-13 inhibitor alleviates the BOS phenotype compared to vehicle-treated control. Follow-up studies are required to substantiate the evidence.

In summary, this is the first time to the best of my knowledge that a role of MMP-13 in OVA endocytosis, MHC-I presentation, and cytokine release of BMDCs was demonstrated. Moreover, MMP-13 seems to be important for the communication between DC and the adaptive immune cells in that the inhibition of MMP-13 reduced the capacity of BMDCs to activate T lymphocytes. The DC-T lymphocyte interplay has important consequences for the regulation of inflammatory

conditions and preliminary evidence could be provided that MMP-13 inhibition might help to attenuate the development or severity of the BOS phenotype.

4.1 MMP-13 expression by BMDCs in response to inflammatory stimulus

DCs have various assets that allow them to act as professional APCs. In response to inflammatory stimuli, DCs change their phenotype and behavior to act optimal as guardian against invading pathogens[17-19]. Specific MMPs have been reported to be expressed in DCs. Especially MMP-12 and -13 were described to be higher expressed in murine pulmonary DCs than in macrophages and monocytes under homeostatic conditions[171].

Generation of DCs from bone marrow cells, as used here for the *in vitro* analysis, is a standard method to gain high numbers of murine myeloid DCs[97-100]. These BMDCs were used in this thesis to elucidate potential functions of MMP-12 and -13 in the DC immunobiology. As this was a complete new area of MMP biology, it was intended to cover a broad spectrum of assays. Thus, the required high cell number and cells with a stable phenotype could be achieved with BMDCs. Based on the results obtained here with these *in vitro* generated BMDCs, selected key processes may be studied in primary cells, such as in DCs isolated from the spleen[242] or even better from the lung[13] in the future. This is an important next step, as primary cells, instructed by the surrounding environment, likely display somewhat different behavior as the *in vitro* generated cells.

The first aim was to analyze alterations in the expression profile of MMP-12 and -13 in BMDCs in response to the inflammatory stimulus LPS (section 3.1.2). In line with the literature, MMP-13 mRNA expression increased significantly due to LPS treatment in BMDCs[170]. In contrast, no significant change was detected in case of murine MMP-12 expression. The lack of difference in the MMP-12 gene expression between immature and LPS stimulated mature BMDCs is in line with observations of an RNA array study[170]. As MMPs are expressed as inactive pro-enzymes, the activity state of MMPs is even more important than the expression level. Using specific MMP activity assays, a significant increase of active MMP-12 and -13 after LPS stimulation was detected in BMDCs. In case of MMP-12 measurements, the observed increase might be due to an increase in MMP-3 instead of MMP-12, since the assay does not discriminate between these closely related MMPs. In case of MMP-13 activity measurements, specificity is assured, as here a pre-separation step with a MMP-13 specific antibody is included.

In summary, LPS stimulation increased MMP-13 mRNA expression as well as activity, supporting the hypothesis of an involvement of MMP-13 in DC function. Concerning MMP-12, no alteration in mRNA expression was detected and MMP-12 activity could not be measured as no specific assay is available. The increase in MMP activity suggests that, under inflammatory conditions, BMDCs need MMP-13 for specific functions to fully act as APCs.

4.2 Participation of MMP-12 and -13 in the process of cell migration

MMPs are known to participate in cell migration. Cell migration in general and, specifically, in the connection with MMPs, makes an important contribution to various diseases such as cancer, myocardial infarction, and hypertension[243-249]. The importance of MMP-12 for cell migration has already been reported for macrophages by MMP-12 knock-out studies[172]. Shipley and co-workers demonstrated that macrophages generated from MMP-12 ko mice have a markedly diminished capacity to degrade extracellular matrix components and are unable to penetrate reconstituted basement membranes *in vitro* and *in vivo*, using elastin and matrigel as target substrates[172]. Furthermore, a higher activity of MMP-12 was reported to correlate with increased fibroblast migration. This was demonstrated by the group of Haq *et al.* who showed, in the fibroblast cell line COS7, an increase in MMP-12 activity and migration through collagen IV after transfection with MMP-12 variants[250]. In addition, Sato and colleagues substantiated the importance of MMP-12 for fibroblast migration in experimental BOS, using broad-spectrum MMP-inhibitors in two mouse models, the orthotopic lung transplantation and the intrapulmonary tracheal transplantation model, as well as by wound healing assays *in vitro*[251]. As this group used broad-spectrum inhibitors, the results cannot allude to a specific contribution of MMP-12 to the migration of fibroblasts *in vivo*. However, this study underlines the general importance of MMPs in the development of BOS.

Concerning MMP-13, a participation in migration is mainly reported for keratinocytes[158] and fibroblasts[252,253]. The role of MMP-13 in keratinocyte migration was shown by Hattori *et al.* who demonstrated a reduced migration in MMP-13 ko cells, using a wound healing assay[158]. In addition, Lecomte and co-workers reported a contribution of MMP-13 in fibroblast migration by showing tumor-infiltrating myofibroblasts as main producers of MMP-13 and a diminished cell migration in MMP-13 ko cells[253].

Regarding DC biology little is known about the contribution of MMP-12 and -13 for DC migration. Most of the studies analyzing the importance of MMPs for DCs reported MMP-9 as crucial for migration, studied in murine Langerhans cells[254] and BMDCs[245], as well as in human DCs[246]. A recent study demonstrated a reduced number of migrating Langerhans cells by using a specific MMP-9 blocking antibody[254]. Furthermore, impaired migration of MMP-9 ko BMDCs through tracheal epithelial tight junctions, reported by the group of Ichiyasu *et al.*, substantiates the evidence that MMP-9 might participate in DC migration. These results could further be validated in human DCs by Chabot and colleagues, who demonstrated a reduced migration of monocyte-derived DCs after blocking with a specific MMP-9 antibody. Kis-Toth and co-workers reported the importance of MMP-9 in human monocyte-derived $CD1a^-$ DCs, using a broad spectrum inhibitor[255]. Conclusively, while MMP-9 was intensively studied in different DC subgroups, the role of MMP-12 and -13 for DC migration remains elusive. Therefore, in the present study, the impact of MMP-12 and -13 for migration of BMDCs was analyzed (section 3.1.3.2). The previously mentioned group of Kis-Toth demonstrated beside MMP-9, a participation of MMP-12

in the migration of human $CD1a^+$ monocyte-derived DCs. This subgroup of DCs showed an increase in MMP-12 expression in response to LPS treatment and demonstrated a decline in the migration capacity by using a broad-spectrum inhibitor[255]. Using murine BMDCs in the current study, no increase in MMP-12 mRNA expression and no alteration in the number of migrated cells was detected neither after specific inhibition of MMP-12 nor in MMP-12 ko cells. The differences observed, regarding the participation of MMP-12 in DC migration, might be explained by the analysis of different DC subgroups and/or the different species in both studies. In addition, the group of Kis-Toth used a broad spectrum inhibitor, precluding the assessment of a specific role of MMP-12. The observed effects might be attributed to other MMPs, such as MMP-1, -2, -3, -7, -8, -9, -12, -14, and -26, which are targeted by this inhibitor.

In the current study, dependent on their target substrate, the influence of MMP-12 inhibition on migration was studied using collagen I and IV, whereas the influence of MMP-13 blockade was studied using collagen I. As expected, in the absence of the chemoattractant CCL19, no migration was detected through collagen I, validating direct migration of BMDCs in this assay. In case of collagen IV, 17% ± 8.5% (mean ± SD) of cells migrated in the absent of CCL19. The reason for this might be that the very thin collagen IV layer allowed migration without chemoattractant in a non-directed way. When comparing LPS-stimulated and non-stimulated cells, LPS-stimulated BMDCs showed an increase of migrated cells through collagen I compared to non-stimulated cells. This observation is likely due to the induction of the C-C chemokine receptor type 7 (CCR7) which is induced during DC maturation and enables the recognition of the ligand CCL19[256]. In contrast, in case of collagen IV, fewer cells migrated after LPS stimulus. The reason for this might be the stronger cell adherence after LPS stimulation which leads to a measurable effect only in case of the thin collagen IV layer as here the migration time was only four hours instead of 24 hours in collagen I. Within the longer time frame the adherence effect might lose its impact on the migration outcome.

As mentioned in section 1.2.4, MMP-12 and -13 have various target substrates. To substantiate the observation that MMP-12 or MMP-13 has no major role in the migration of BMDCs, other target substrates, such as fibronectin or laminin should be tested in future studies. In addition, to mimic tissue conditions more closely, matrigel, a reconstituted basement membrane consisting of a combination of different target substrates, could be used. Beside this, one might also envisage that MMP-12 or -13 has a subordinated role in the process of migration and MMP-9 being the major player. In this scenario, any effect that might emerge by MMP-12 or -13 inhibition would be obscured by the still active MMP-9. Pre-treatment with MMP-9 inhibitor might help to reveal such presumptive effects of MMP-12 or -13. In the settings used here, neither MMP-12, nor MMP-13 seems to play a role in the migration of BMDCs.

4.3 Participation of MMP-13 in OVA endocytosis

To the best of my knowledge, to date nothing has been reported about the participation of MMPs in the process of endocytosis. Using soluble OVA, inhibition of MMP-13 decreased the capability of BMDCs to capture this specific antigen (section 3.1.3.3). As in case of MMP-12 inhibitor the vehicle control (DMSO) showed an unexpected effect, MMP-12 inhibitor might be dissolved in another dissolvent, e.g. ethanol, for future studies. Here, to sidestep the vehicle effect, MMP-12 ko cells were used. These cells showed a reduced uptake of soluble OVA in comparison to wt cells. Yet, a phenotypic comparison of the MMP-12 ko and wt cells revealed a clear difference in the MHC-II surface expression profile. High MHC-II surface expression is generally associated with a mature DC type which takes up less soluble OVA compared to immature DCs with a low MHC-II surface expression[257]. The BMDCs of MMP-12 ko mice showed reduced uptake of soluble OVA and simultaneously higher MHC-II surface expression than BMDCs from wt mice. Therefore, the reduced endocytosis might be due to the different maturation profile of wt and ko cells after one week of cultivation. The different maturation states of wt and ko DCs preclude drawing any conclusion regarding an involvement of MMPs in the process of endocytosis.

In case of the MMP-13 inhibitor, no side effect was detected as the dissolvent was water. Here, MMP-13 inhibition significantly reduced the capability of BMDCs to take up soluble OVA. The uptake of large amounts of soluble OVA (MFI^{high}) in DCs is mainly executed by the mannose receptor which mediates cross-presentation of OVA peptides via MHC-I, whereas uptake of small amounts of OVA (MFI^{low}) via micropinocytosis drives OVA into the classical MHC-II pathway[14,36,258-261]. Although mature DCs are reported to poorly take up antigens, recent studies demonstrated that mature DCs still perform receptor-mediated endocytosis and phagocytosis[262]. Here, MHC-II^{high} BMDCs took up both, large and low amounts of OVA and both processes were decreased by inhibition of MMP-13. These results lead to further interesting research questions regarding the precise mechanisms how MMP-13 is involved in antigen uptake. In the future, blocking the mannose receptor or pinocytosis can help to discriminate between these two pathways and provide insight into the question which pathway of antigen uptake is regulated by MMP-13. Mannose receptor independent pathways may be studied using mannose receptor deficient mice[263].

The hypothesis that MMP-13 may regulate the pathway of mannose receptor mediated endocytosis is of interest, as some MMPs have already been reported to become activated after mannose receptor-ligand interaction. MMP-9 for instance is induced by receptor-mediated signaling mechanisms involving the binding of mannosylated ligands to mannose receptors[264]. Furthermore, increased MMP-2 production was reported following human mannose receptor-mediated HIV-1 entry, published by López-Herrera and colleagues[264]. In addition, the urokinase plasminogen activator receptor–associated protein/endo180, a member of the mannose receptor family, has already been reported to serve as a specific cell surface receptor for MMP-13 which, after binding, becomes activated by uPA-mediated plasminogen activation[265]. Based on these research studies,

one can assume that the treatment with soluble OVA might increase MMP-13 activity via the mannose receptor pathway. The subsequent OVA-mannose receptor complex internalization via clathrin-coated pits might further be regulated by the former activated MMP-13 enzymes. This might explain the reduced OVA endocytosis upon blocking of MMP-13, but this hypothesis remains to be studied in the future.

Besides this, it will be of importance to study the relevance of MMP-13 for the uptake of other antigens, including those with low expression levels or particulate antigens, such as latex beads. Studies of phagocytosis by fluorescent bacteria would be another angle to pursue.

In this study, downstream effects of the reduced endocytosis on T cells were not detected, as no cumulative effect was seen when DCs were treated with MMP-13 inhibitor before plus after the OVA-uptake. Obviously, despite reduced uptake due to MMP-13 inhibition enough OVA can still be captured by BMDCs to provide sufficient antigen presentation to OVA specific T cells. Effects on other antigens might be stronger and might result in downstream consequences. This remains to be studied in the future.

4.4 Role of MMP-13 for the phenotype of BMDCs

While the precise mechanism how MMP-13 regulates the endocytosis of OVA system remains to be determined, further analysis clearly demonstrated that $CD8^+$ T cell activation is reduced when BMDCs are treated with MMP-13 inhibitor by a mechanism apparently independent of endocytosis (section 3.1.3.4). The independency from endocytosis can be assumed as a similar reduction in T cell activation was detected when the MMP-13 inhibitor was applied after the endocytosis phase was completed. An alteration in the MHC-I surface expression could be one reason for the reduced $CD8^+$ T cell activation as MHC–I, but not MHC-II surface expression was found to be reduced after MMP-13 inhibition (section 3.1.3.5). Successful T cell activation requires the formation of an intact immunological synapse between DCs and T lymphocytes, which is dependent on the recognition of the peptide-MHC complex by the specific T cell receptor[61]. The diminished MHC-I surface expression, measured by flow cytometry, might be sufficient to impair formation of a fully functional immunological synapse which may explain the decreased $CD8^+$ T cell activation. One reason for the reduced MHC-I surface presentation could be an alteration in the MHC-I recycling process. Alternatively, MMP-13 might promote BMDCs to efficiently load exogenous peptide onto MHC-I via the cross-presentation pathway, and thereby, leading to reduced MHC-I surface expression and $CD8^+$ T cell activation after MMP-13 inhibition. The $CD8^+$ T cell line (B3Z) used in this study, neither needs cytokine stimulation nor co-stimulatory molecules by DCs. Therefore, it is likely that the reduced T cell activation in this system is caused by the reduced MHC-I presentation. To further study the mechanism leading to the reduced MHC-I presentation, total amount of MHC-I in MMP-13 inhibitor-treated or untreated permeabilized cells might shed light on the issue of altered MHC-I recycling as a way to modulate surface MHC-I levels.

Co-stimulatory molecules such as CD80, CD86, and CD40 are required for efficient T cell activation by DCs under physiological conditions[20,239]. No influence of MMP-13 on these maturation markers was detected (section 3.1.3.6). Therefore, the maturation process of BMDCs seems to be independent of MMP-13. In contrast, a clear decline in the surface expression of CD11c was observed. CD11c binds to complement fragment (iC3b), adhesion molecules and matrix proteins. Hence, the group of Sadhu suggested an involvement of CD11c in antigen presentation and inflammation[266]. As a strong CD11c reduction was detected only with high inhibitor concentrations it is unlikely to affect antigen presentation in this system.

To study T cell activation under more physiological conditions, the utilization of OT-I/-II cells instead of the T cell lines B3Z and DOBW would be of interest in the future. OT-I/-II cells are specific T cells which recognize specific OVA-peptides on either MHC-I or MHC-II like B3Z/DOBW cells. The advantage of these primary cells is that they are not immortalized and need co-stimulatory and cytokine signals from APCs to get activated, representing more physiological conditions.

4.5 Regulation of BMDC cytokine/chemokine profile by MMP-13

Several MMPs have been reported to process specific cytokines and modulate chemokine gradients. MMP-mediated proteolysis is reported to inactivate chemokines and to generate antagonistic or synergistic derivatives[267]. MMP-13 is reported to process CXCL5, CXCL8, CXCL12, and CCL7. While the chemotactic potency of CXCL5 and CXCL8 is increased by MMP-13 proteolysis, CXCL12 and CCL7 become inactivated or transformed into an antagonist[267]. Beside these reports, to the best of my knowledge, no other chemokines/cytokines have been reported to be regulated by MMP-13. In this study, 18 different cytokines/chemokines were analyzed using a Luminex screening assay (section 3.1.3.7). It was observed that cytokines that regulate Th1/Th17 cell polarization, such as IL-12p70, IL-23p19, and IL-6 were decreased by inhibition of MMP-13, whereas cytokines that affect mainly neutrophils remained unaffected. IL-12, which was strongly decreased by inhibition of MMP-13, is known to serve as a critical mediator of $CD8^+$ T cell activation[69-72] and reduces apoptosis in $CD8^+$ T cells by increasing survival and expansion of effector/memory T cell populations[76]. IL-23, another potent pro-inflammatory cytokine, which plays a dominant role in memory T cell response and in autoimmune diseases by stimulating a unique T cell subset to produce IL-17[77,268], was similarly reduced by inhibition of MMP-13. Interestingly, IL-12 and IL-23 share the same p40 subunit which they require for secretion[69]. Along this line, IL-6, which belongs to the same family like IL-12 and IL-23 and shows homology to their subunits, was also significantly reduced due to inhibition of MMP-13. The homology of the three cytokines and the fact that IL-6 is a downstream factor of IL-12 might explain their concerted reduction upon inhibition of MMP-13 as they might exhibit a joint processing site. As the Luminex assay does not distinguish between the activation status of enzymes, changes in the proteolytic activity of MMP-13 by its inhibition that might further result in

modified cytokine activity, as reported before for CXCL5, CXCL8, CXCL12, and CCL7, could not be the explanation for the reduced amount of cytokines detected in the current study. Currently, it is unknown whether the observed moderations in the secreted amounts of cytokines/chemokines are caused on the transcriptional or translational level. Various possibilities might lead to the reduction in detected cytokines. MMP-13 might process the cytokines in a way that reduces the binding affinity to the capture or detection antibodies. An involvement of MMP-13 in the secretion process of IL-12 and IL-23 might be another explanation whereby the reduced MMP-13 activity leads to an accumulation inside the cell. Furthermore, it was reported that cross-linking of complement receptors results in a potent inhibition of the production of human and mouse IL-12[73]. Therefore, an indirect way of MMP-13 regulating IL-12 or IL-23 secretion via changes in the complement system might also be assumed. Of note, previous reports have already linked IL-12 and IL-23 to specific MMPs. Godefroy *et al*. demonstrated an indirect effect of MMP-2 on IL-12p70 via degradation of the type-I IFN receptor that inhibited signal transducers and activators of transcription (STAT)1 phosphorylation and thereby reduced IL-12p35 production[269]. In line with this, Oriss *et al.* reported MMP-9 as indirect regulator of IL-23 via membrane stem cell factor and receptor tyrosine kinase c-kit ligation[270]. Participation of MMP-13 in similar pathways via alterations of transcription factors required for IL-12/-23 production or inhibition might be conceivable. Furthermore, an indirect involvement of MMP-13 via activation of other MMPs might be taken into consideration. In summary, the inhibition of MMP-13 apparently participates in the process of polarizing the T cell response by modulating the cytokine and chemokine profile of DCs. The underlying mechanism remains to be determined in the future.

Although the screening assay covered a wide range of cytokine/chemokines, cytokines that promote Th2 polarization, such as IL-4, were not included in the multiplex assay. It would be of great interest in the future to determine whether cytokines that promote Th2 polarization are also altered by inhibition of MMP-13.

While pro-inflammatory cytokines decreased after MMP-13 inhibition, CXCL10, an inhibitor of neovascularization and hematopoietic progenitor cells increased. Considering future pharmaceutical application of MMP-13 inhibitors, the increase of CXCL10 concomitant to the decrease in inflammatory cytokines might be advantageous as the inflammatory immune response is dampened by reducing vascularization and immune cell supply *in vivo*[271].

In summary, our data revealed that MMP-13 regulates BMDC cytokine/chemokine profile of mainly pro-inflammatory T cell targeting cytokines. Potential consequences of the altered cytokine profile on T cells were not studied here, as the used immortalized T cell lines are resilient to cytokine changes. However, the strong decrease of specific cytokines gives rise to interesting upcoming research questions. The previous mentioned OT-I/-II T cells could be used for these analyses.

4.6 The relevance of the murine heterotopic trachea transplant model

The *in vitro* results using murine BMDC suggested that inhibition of MMP-13 might be a promising therapeutic strategy to ameliorate inflammatory processes that are dependent on MHC-I antigen presentation and polarization by pro-inflammatory cytokines. These could be autoinflammatory disease or graft dysfunction after transplantation, such as in BOS where the immune system must be attenuated.

To provide evidence for a potential relevance of MMP-13 in the pathogenesis of BOS, a mouse model of experimental BOS was established (section 3.2.1). The heterotopic trachea transplant model is a model described in the literature that allows mimicking the phenotype of BOS in a reasonable time frame with acceptable surgical effort. Other models used in the literature to study experimental BOS *in vivo* are the orthotopic tracheal transplantation in mice (introduced by Ikonen and colleagues in 2000[272]), the intrapulmonary tracheal implantation, and the orthotopic lung transplantation. In the orthotopic tracheal transplantation model, implanting a segment of a donor trachea into the recipient trachea allows studying allotransplant perfusion and a strong role for microvasculature in the development of BOS was detected[273-275]. In the intrapulmonary tracheal implantation model a long tracheal segment is placed into the recipient`s lung by pleural incision to the intrapulmonary milieu[276]. Perfusion of the transplanted graft and the possibility to study neovascularization from pulmonary circulation are the advantages of this model. Using the intrapulmonary tracheal implantation model an importance of MMPs in the pathogenesis of BOS was demonstrated in the past[277]. The fourth model to study BOS in rodents is the orthotopic lung transplantation. In this model the whole left or right lung is transplanted and recipient`s artery, vein, and main bronchus are connected to the respective vessels and bronchus of the graft. This model reproduces the surgical procedure in human lung transplantations with high accuracy. The disadvantages are the requirement of high surgical skills and long observation time. In the course of the current study, the heterotopic trachea transplant model was established. Although the other models introduced above mimic the physiological scenario of BOS more closely, the heterotopic trachea transplant model could confirm and reproduce results that were obtained with the intrapulmonary and the orthotopic models and support, thereby, the usage of this model. Furthermore, the model has been shown to share many of the characteristics of BOS in the clinic in that heterotopic tracheal allografts exhibit epithelial damage, leukocyte influx, matrix deposition, fibroblast invasion, and luminal occlusion. So far, the greatest gain in knowledge was achieved with the help of the heterotopic trachea transplant model, as it provides reliable and reproducible results. In summary, the optimal model to study BOS and allograft rejection does not exist. Which model suffices rather depends on the research question. For this thesis it was decided to use the heterotopic trachea transplant model as has proven to provide reliable and reproducible results while being much less invasive and having low infection risk.

4.7 MMP-13 in the murine heterotopic trachea transplant (HTT) model

Previous studies have already provided evidence for an involvement of MMPs, other than MMP-12 and -13 in the development of BOS in rodent models as well as in patients[206-208,233,278]. Fernandez and co-worker were able to demonstrate the importance of MMP-9 by MMP-9 ko mice studies, showing an involvement of MMP-9 in mononuclear cell infiltration, T cell alloreactivity, and cytokine/chemokine regulation[206]. The group of Khatwa reported a relation between MMP-8 (neutrophil collagenase) and the severity of experimental BOS by showing that MMP-8 is important for polymorphonuclear leukocytes migration[207]. Others reported an increase in MMP-2 and membrane type 1 MMP activity in experimental BOS[208]. However, all of these MMPs are expressed by a broad spectrum of cells and, as such, these MMPs are not ideal targets for pharmaceutical inhibitor therapies.

Here, using the murine HTT model, an increase in MMP-13 mRNA expression in allografts compared to syngrafts was demonstrated (section 3.2.3). Regarding MMP-13, only little has been reported about its role in BOS. Using the HTT model, Sato and colleagues demonstrated peaks in MMP-3, -9, and -13 mRNA expression in the micro-dissected intraluminal tissue of the allografts at day seven, which decreased again over time[278]. In the current study, the increase in MMP-13 mRNA expression in allografts compared to syngrafts was verified supporting the idea that MMP-13 might participate in the development of experimental BOS. The other MMPs measured in the present study, MMP-2, -9, and -12 showed an increase in mRNA expression in both, syngrafts and allografts. Therefore, it seems more likely that the induction of these MMPs is due to the surgical procedure. Furthermore, MMP-13 could be localized in transplanted tracheas by IF staining on paraffin embedded tissue sections, on day 14 and 21. Sato and co-workers also detected MMP-13 in the graft lumen in immunofluorescence images[278]. In contrast to this previous study where MMP-13 was no longer detected after day 14, the present study revealed MMP-13 in infiltrating cells in the graft lumen still on day 21 using immunofluorescence staining. All the previously reported studies[206-208] were merely descriptive and did not investigate the possible functions of MMP-13.

The importance of DCs in the development of experimental BOS has already been reported by the group of Lambrecht and Kleinjan who showed a denser DC network in allografts compared to syngrafts using CD11c, MHC-II, and the specific DC shape as markers of DCs. They further used flow cytometry analysis to show a higher accumulation of DC subtypes ($CD11c^+/MHC\text{-}II^+/CD11b^+/CD103^-$ or $CD11c^{+/}MHC\text{-}II^+/CD11b^-CD103^+$ subtype) in whole tracheas of allografts compared to syngrafts[233]. Due to the possibility of generating very thin tissue slices (2 µm), paraffin embedded tissue sections were used to generate high quality histological stainings. This advantage outweighed the disadvantage that the paraffin embedding procedure may cover or alter some antibody binding sites which cannot be restored by the boiling procedure. Hence, due to these technical limitations, the DC marker (CD11c) could not be used in paraffin embedded tissue. To

detect a co-localization of MMP-13 with DCs, new frozen tracheas must be generated and stained in the future. However, assuming future validation, the research results of Lambrecht and co-workers support the idea of an involvement of DCs in the pathogenesis.

In a pilot study performed in this thesis, where the MMP-13 inhibitor was applied every second day into transplanted mice, an attenuation of the BOS phenotype was observed (section 3.3). Other studies already provided hints that experimental BOS is ameliorated in specific MMP ko[206] mice or after the treatment with broad spectrum inhibitors[251,277], exemplifying the importance of MMPs for the BOS pathogenesis. Regarding MMP-8 and -9, specific ko mice seem to be protected from experimental BOS[207]. However, the disadvantage of MMP-9 is its broad expression in a variety of cell types posing a potential risk of side effects in humans after blocking. Regarding MMP-8, also known as neutrophil collagenase, inhibitor treatment mainly blocks the migration of polymorphonuclear leukocytes. Thus, even if MMP-8 plays an important role in BOS, it may not be sufficient to block only polymorphonuclear leukocyte migration to moderate disease progression, as other leukocytes are also involved.

Concerning human therapies, broad spectrum inhibitors cannot be used due to expected strong side effects. Therefore, the MMP-13 specific small molecule inhibitor seems promising. The MMP-13 inhibitor was used in this thesis instead of ko mice to provide results with translational relevance concerning a role of MMP-13 in the development of BOS. Indeed, the *in vivo* MMP-13 inhibitor treatment study revealed promising results with an attenuated BOS phenotype. Following this pilot study, a more extent of an animal study must be performed to confirm the *in vivo* results and to find the most effective dose.

4.8 Conclusion and future direction

The aim of this thesis was to elucidate the role of MMP-12 and -13 in murine BMDCs and the contribution of DCs to the development of experimental BOS.

Increased mRNA expression and activity of MMP-13 in response to the inflammatory stimulus LPS was detected in BMDCs. Functional assays revealed a participation of MMP-13 in OVA endocytosis, MHC-I presentation, and cytokine profile of BMDCs whereas an involvement of MMP-13 in the migration and maturation was not evident. Observed alterations in the MHC-I presentation capability of DCs seemed to have downstream effects concluded from the observation of reduced $CD8^+$ T cell activation. In the second part of the thesis, an attempt was undertaken to define the relevance of the *in vitro* findings for the pathogenesis of BOS *in vivo*. Using the murine heterotopic trachea transplant model, an increase of MMP-13 mRNA expression in allografts compared to syngrafts was detected, supporting the idea of a role of MMP-13 for BOS development. In a pilot treatment study, using the MMP-13 inhibitor, an attenuated BOS phenotype was observed in the heterotopic trachea transplant model. The *in vitro* results together with the preliminary findings in experimental BOS provide new insight into the role of MMP-13 in DC biology and its potential contribution to the pathogenesis of BOS.

Collectively, the findings of the current study identified for the first time an involvement of MMP-13 in the immunobiological functions of BMDCs. How exactly MMP-13 regulates endocytosis, MHC-I presentation, and the cytokine profile remains to be determined in the future.

Having established the optimal settings for BMDCs in the different *in vitro* assays allows transferring these assays to sparse primary cell types. This enables future studies on primary DCs, which can only be isolated in very low numbers from the lungs. Similarly, using primary T cells in the T cell activation assay will allow evaluating the effect of the altered cytokine profile of MMP-13 inhibited DCs on T cell polarization. In the current study, this could not be assessed as B3Z and DOBW T cells are immortalized and need neither co-stimulatory signals nor cytokines.

In future *in vivo* analyses, higher animal numbers will allow reliable quantification of the effects of the MMP-13 inhibitor treatment, the quantification of the amount of DCs, and the co-localization of DCs with MMP-13 in the allografts.

Last but not least, it remains an intriguing open question whether a role of MMP-13 can be substantiated in human DC biology and in human BOS patients. Due to the lack of a unique DC marker, only a limited number of investigations has addressed this issue, showing contradictory results. Efforts must be increased to quantify DCs in the lung and bronchoalveolar lavage fluid of patients. Regarding a potential role of MMP-13 in DC biology, *in vitro* experiments, like those presented here, should be performed with human DCs. With regards to human biology, a functional analog of murine MMP13 may show a similar impact on DC immunobiology. Therefore, additional MMPs should be analyzed in parallel to MMP-13 for their contribution to DC biology.

5 LITERATURE

1. Fearon DT, Locksley RM. The instructive role of innate immunity in the acquired immune response. *Science.* Apr 5 1996;272(5258):50-53.
2. Hoffmann JA, Kafatos FC, Janeway CA, Ezekowitz RA. Phylogenetic perspectives in innate immunity. *Science.* May 21 1999;284(5418):1313-1318.
3. Medzhitov R, Janeway CA, Jr. Innate immunity: the virtues of a nonclonal system of recognition. *Cell.* Oct 31 1997;91(3):295-298.
4. Matzinger P. Tolerance, danger, and the extended family. *Annu. Rev. Immunol.* 1994;12:991-1045.
5. Rescigno M. Functional specialization of antigen presenting cells in the gastrointestinal tract. *Curr. Opin. Immunol.* Feb 2010;22(1):131-136.
6. Banchereau J, Steinman RM. Dendritic cells and the control of immunity. *Nature.* Mar 19 1998;392(6673):245-252.
7. Bell D, Young JW, Banchereau J. Dendritic cells. *Adv. Immunol.* 1999;72:255-324.
8. Hart DN. Dendritic cells: unique leukocyte populations which control the primary immune response. *Blood.* Nov 1 1997;90(9):3245-3287.
9. Steinman RM. The dendritic cell system and its role in immunogenicity. *Annu. Rev. Immunol.* 1991;9:271-296.
10. McWilliam AS, Napoli S, Marsh AM, et al. Dendritic cells are recruited into the airway epithelium during the inflammatory response to a broad spectrum of stimuli. *J. Exp. Med.* Dec 1 1996;184(6):2429-2432.
11. McWilliam AS, Nelson D, Thomas JA, Holt PG. Rapid dendritic cell recruitment is a hallmark of the acute inflammatory response at mucosal surfaces. *J. Exp. Med.* Apr 1 1994;179(4):1331-1336.
12. Austyn JM, Kupiec-Weglinski JW, Hankins DF, Morris PJ. Migration patterns of dendritic cells in the mouse. Homing to T cell-dependent areas of spleen, and binding within marginal zone. *J. Exp. Med.* Feb 1 1988;167(2):646-651.
13. Vermaelen K, Pauwels R. Pulmonary dendritic cells. *Am. J. Respir. Crit. Care Med.* Sep 1 2005;172(5):530-551.
14. Sallusto F, Cella M, Danieli C, Lanzavecchia A. Dendritic cells use macropinocytosis and the mannose receptor to concentrate macromolecules in the major histocompatibility complex class II compartment: downregulation by cytokines and bacterial products. *J. Exp. Med.* Aug 1 1995;182(2):389-400.
15. Inaba K, Inaba M, Naito M, Steinman RM. Dendritic cell progenitors phagocytose particulates, including bacillus Calmette-Guerin organisms, and sensitize mice to mycobacterial antigens in vivo. *J. Exp. Med.* Aug 1 1993;178(2):479-488.
16. Reis e Sousa C, Stahl PD, Austyn JM. Phagocytosis of antigens by Langerhans cells in vitro. *J. Exp. Med.* Aug 1 1993;178(2):509-519.
17. Mellman I, Steinman RM. Dendritic cells: specialized and regulated antigen processing machines. *Cell.* Aug 10 2001;106(3):255-258.
18. Trombetta ES, Mellman I. Cell biology of antigen processing in vitro and in vivo. *Annu. Rev. Immunol.* 2005;23:975-1028.
19. Winzler C, Rovere P, Rescigno M, et al. Maturation stages of mouse dendritic cells in growth factor-dependent long-term cultures. *J. Exp. Med.* Jan 20 1997;185(2):317-328.
20. Sallusto F, Lanzavecchia A. Efficient presentation of soluble antigen by cultured human dendritic cells is maintained by granulocyte/macrophage colony-stimulating factor plus interleukin 4 and downregulated by tumor necrosis factor alpha. *J. Exp. Med.* Apr 1 1994;179(4):1109-1118.
21. Pierre P, Turley SJ, Gatti E, et al. Developmental regulation of MHC class II transport in mouse dendritic cells. *Nature.* Aug 21 1997;388(6644):787-792.
22. Cella M, Engering A, Pinet V, Pieters J, Lanzavecchia A. Inflammatory stimuli induce accumulation of MHC class II complexes on dendritic cells. *Nature.* Aug 21 1997;388(6644):782-787.

23. Banchereau J, Briere F, Caux C, et al. Immunobiology of dendritic cells. *Annu. Rev. Immunol.* 2000;18:767-811.
24. Rescigno M, Granucci F, Citterio S, Foti M, Ricciardi-Castagnoli P. Coordinated events during bacteria-induced DC maturation. *Immunol. Today.* May 1999;20(5):200-203.
25. Akbari O, Panjwani N, Garcia S, Tascon R, Lowrie D, Stockinger B. DNA vaccination: transfection and activation of dendritic cells as key events for immunity. *J. Exp. Med.* Jan 4 1999;189(1):169-178.
26. Hacker H, Mischak H, Miethke T, et al. CpG-DNA-specific activation of antigen-presenting cells requires stress kinase activity and is preceded by non-specific endocytosis and endosomal maturation. *EMBO J.* Nov 2 1998;17(21):6230-6240.
27. Hartmann G, Krieg AM. CpG DNA and LPS induce distinct patterns of activation in human monocytes. *Gene Ther.* May 1999;6(5):893-903.
28. Hartmann G, Weiner GJ, Krieg AM. CpG DNA: a potent signal for growth, activation, and maturation of human dendritic cells. *Proc. Natl. Acad. Sci. U. S. A.* Aug 3 1999;96(16):9305-9310.
29. Cella M, Salio M, Sakakibara Y, Langen H, Julkunen I, Lanzavecchia A. Maturation, activation, and protection of dendritic cells induced by double-stranded RNA. *J. Exp. Med.* Mar 1 1999;189(5):821-829.
30. Bates EE, Ravel O, Dieu MC, et al. Identification and analysis of a novel member of the ubiquitin family expressed in dendritic cells and mature B cells. *Eur. J. Immunol.* Oct 1997;27(10):2471-2477.
31. Rock KL, Goldberg AL. Degradation of cell proteins and the generation of MHC class I-presented peptides. *Annu. Rev. Immunol.* 1999;17:739-779.
32. Pamer E, Cresswell P. Mechanisms of MHC class I--restricted antigen processing. *Annu. Rev. Immunol.* 1998;16:323-358.
33. Inaba K, Pack M, Inaba M, Sakuta H, Isdell F, Steinman RM. High levels of a major histocompatibility complex II-self peptide complex on dendritic cells from the T cell areas of lymph nodes. *J. Exp. Med.* Aug 29 1997;186(5):665-672.
34. Inaba K, Turley S, Yamaide F, et al. Efficient presentation of phagocytosed cellular fragments on the major histocompatibility complex class II products of dendritic cells. *J. Exp. Med.* Dec 7 1998;188(11):2163-2173.
35. Tan MC, Mommaas AM, Drijfhout JW, et al. Mannose receptor-mediated uptake of antigens strongly enhances HLA class II-restricted antigen presentation by cultured dendritic cells. *Eur. J. Immunol.* Sep 1997;27(9):2426-2435.
36. Engering AJ, Cella M, Fluitsma D, et al. The mannose receptor functions as a high capacity and broad specificity antigen receptor in human dendritic cells. *Eur. J. Immunol.* Sep 1997;27(9):2417-2425.
37. Cresswell P. Invariant chain structure and MHC class II function. *Cell.* Feb 23 1996;84(4):505-507.
38. Lehner PJ, Cresswell P. Processing and delivery of peptides presented by MHC class I molecules. *Curr. Opin. Immunol.* Feb 1996;8(1):59-67.
39. Castellino F, Zhong G, Germain RN. Antigen presentation by MHC class II molecules: invariant chain function, protein trafficking, and the molecular basis of diverse determinant capture. *Hum. Immunol.* May 1997;54(2):159-169.
40. Nijman HW, Kleijmeer MJ, Ossevoort MA, et al. Antigen capture and major histocompatibility class II compartments of freshly isolated and cultured human blood dendritic cells. *J. Exp. Med.* Jul 1 1995;182(1):163-174.
41. Villadangos JA, Schnorrer P. Intrinsic and cooperative antigen-presenting functions of dendritic-cell subsets in vivo. *Nat. Rev. Immunol.* Jul 2007;7(7):543-555.
42. Joffre OP, Segura E, Savina A, Amigorena S. Cross-presentation by dendritic cells. *Nat. Rev. Immunol.* Aug 2012;12(8):557-569.
43. Kovacsovics-Bankowski M, Rock KL. A phagosome-to-cytosol pathway for exogenous antigens presented on MHC class I molecules. *Science.* Jan 13 1995;267(5195):243-246.
44. Houde M, Bertholet S, Gagnon E, et al. Phagosomes are competent organelles for antigen cross-presentation. *Nature.* Sep 25 2003;425(6956):402-406.

45. Guermonprez P, Saveanu L, Kleijmeer M, Davoust J, Van Endert P, Amigorena S. ER-phagosome fusion defines an MHC class I cross-presentation compartment in dendritic cells. *Nature.* Sep 25 2003;425(6956):397-402.
46. Burgdorf S, Scholz C, Kautz A, Tampe R, Kurts C. Spatial and mechanistic separation of cross-presentation and endogenous antigen presentation. *Nat. Immunol.* May 2008;9(5):558-566.
47. Firat E, Saveanu L, Aichele P, et al. The role of endoplasmic reticulum-associated aminopeptidase 1 in immunity to infection and in cross-presentation. *J. Immunol.* Feb 15 2007;178(4):2241-2248.
48. Saveanu L, Carroll O, Weimershaus M, et al. IRAP identifies an endosomal compartment required for MHC class I cross-presentation. *Science.* Jul 10 2009;325(5937):213-217.
49. Shen L, Sigal LJ, Boes M, Rock KL. Important role of cathepsin S in generating peptides for TAP-independent MHC class I crosspresentation in vivo. *Immunity.* Aug 2004;21(2):155-165.
50. Bertholet S, Goldszmid R, Morrot A, et al. Leishmania antigens are presented to CD8+ T cells by a transporter associated with antigen processing-independent pathway in vitro and in vivo. *J. Immunol.* Sep 15 2006;177(6):3525-3533.
51. Nair-Gupta P, Blander JM. An updated view of the intracellular mechanisms regulating cross-presentation. *Front. Immunol.* 2013;4:401.
52. Sigal LJ, Crotty S, Andino R, Rock KL. Cytotoxic T-cell immunity to virus-infected non-haematopoietic cells requires presentation of exogenous antigen. *Nature.* Mar 4 1999;398(6722):77-80.
53. Ingulli E, Mondino A, Khoruts A, Jenkins MK. In vivo detection of dendritic cell antigen presentation to CD4(+) T cells. *J. Exp. Med.* Jun 16 1997;185(12):2133-2141.
54. Luther SA, Gulbranson-Judge A, Acha-Orbea H, MacLennan IC. Viral superantigen drives extrafollicular and follicular B cell differentiation leading to virus-specific antibody production. *J. Exp. Med.* Feb 3 1997;185(3):551-562.
55. Caux C, Vanbervliet B, Massacrier C, et al. B70/B7-2 is identical to CD86 and is the major functional ligand for CD28 expressed on human dendritic cells. *J. Exp. Med.* Nov 1 1994;180(5):1841-1847.
56. Inaba K, Witmer-Pack M, Inaba M, et al. The tissue distribution of the B7-2 costimulator in mice: abundant expression on dendritic cells in situ and during maturation in vitro. *J. Exp. Med.* Nov 1 1994;180(5):1849-1860.
57. Ridge JP, Di Rosa F, Matzinger P. A conditioned dendritic cell can be a temporal bridge between a CD4+ T-helper and a T-killer cell. *Nature.* Jun 4 1998;393(6684):474-478.
58. Bennett SR, Carbone FR, Karamalis F, Flavell RA, Miller JF, Heath WR. Help for cytotoxic-T-cell responses is mediated by CD40 signalling. *Nature.* Jun 4 1998;393(6684):478-480.
59. Schoenberger SP, Toes RE, van der Voort EI, Offringa R, Melief CJ. T-cell help for cytotoxic T lymphocytes is mediated by CD40-CD40L interactions. *Nature.* Jun 4 1998;393(6684):480-483.
60. Caux C, Massacrier C, Vanbervliet B, et al. Activation of human dendritic cells through CD40 cross-linking. *J. Exp. Med.* Oct 1 1994;180(4):1263-1272.
61. Bromley SK, Burack WR, Johnson KG, et al. The immunological synapse. *Annu. Rev. Immunol.* 2001;19:375-396.
62. Dubois B, Massacrier C, Vanbervliet B, et al. Critical role of IL-12 in dendritic cell-induced differentiation of naive B lymphocytes. *J. Immunol.* Sep 1 1998;161(5):2223-2231.
63. Dubois B, Vanbervliet B, Fayette J, et al. Dendritic cells enhance growth and differentiation of CD40-activated B lymphocytes. *J. Exp. Med.* Mar 3 1997;185(5):941-951.
64. Geldhof AB, Moser M, De Baetselier P. IL-12-activated NK cells recognize B7 costimulatory molecules on tumor cells and autologous dendritic cells. *Adv. Exp. Med. Biol.* 1998;451:203-210.
65. Shah PD. Dendritic cells but not macrophages are targets for immune regulation by natural killer cells. *Cell. Immunol.* Feb 1987;104(2):440-445.

66. Lewis KL, Reizis B. Dendritic cells: arbiters of immunity and immunological tolerance. *Cold Spring Harb. Perspect. Biol.* Aug 2012;4(8):a007401.
67. Sela U, Olds P, Park A, Schlesinger SJ, Steinman RM. Dendritic cells induce antigen-specific regulatory T cells that prevent graft versus host disease and persist in mice. *J. Exp. Med.* Nov 21 2011;208(12):2489-2496.
68. Trinchieri G. Interleukin-12: a proinflammatory cytokine with immunoregulatory functions that bridge innate resistance and antigen-specific adaptive immunity. *Annu. Rev. Immunol.* 1995;13:251-276.
69. Trinchieri G. Interleukin-12 and the regulation of innate resistance and adaptive immunity. *Nat. Rev. Immunol.* Feb 2003;3(2):133-146.
70. Trinchieri G, Pflanz S, Kastelein RA. The IL-12 family of heterodimeric cytokines: new players in the regulation of T cell responses. *Immunity.* Nov 2003;19(5):641-644.
71. Del Vecchio M, Bajetta E, Canova S, et al. Interleukin-12: biological properties and clinical application. *Clin. Cancer Res.* Aug 15 2007;13(16):4677-4685.
72. Lee JB, Lee KA, Chang J. Phenotypic changes induced by IL-12 priming regulate effector and memory CD8 T cell differentiation. *Int. Immunol.* Sep 2007;19(9):1039-1048.
73. Kang BY, Kim E, Kim TS. Regulatory mechanisms and their therapeutic implications of interleukin-12 production in immune cells. *Cell. Signal.* Jun 2005;17(6):665-673.
74. Cella M, Scheidegger D, Palmer-Lehmann K, Lane P, Lanzavecchia A, Alber G. Ligation of CD40 on dendritic cells triggers production of high levels of interleukin-12 and enhances T cell stimulatory capacity: T-T help via APC activation. *J. Exp. Med.* Aug 1 1996;184(2):747-752.
75. Koch F, Stanzl U, Jennewein P, et al. High level IL-12 production by murine dendritic cells: upregulation via MHC class II and CD40 molecules and downregulation by IL-4 and IL-10. *J. Exp. Med.* Aug 1 1996;184(2):741-746.
76. Chang J, Cho JH, Lee SW, Choi SY, Ha SJ, Sung YC. IL-12 priming during in vitro antigenic stimulation changes properties of CD8 T cells and increases generation of effector and memory cells. *J. Immunol.* Mar 1 2004;172(5):2818-2826.
77. Parham C, Chirica M, Timans J, et al. A receptor for the heterodimeric cytokine IL-23 is composed of IL-12Rbeta1 and a novel cytokine receptor subunit, IL-23R. *J. Immunol.* Jun 1 2002;168(11):5699-5708.
78. Oppmann B, Lesley R, Blom B, et al. Novel p19 protein engages IL-12p40 to form a cytokine, IL-23, with biological activities similar as well as distinct from IL-12. *Immunity.* Nov 2000;13(5):715-725.
79. Schuijs MJ, Willart MA, Hammad H, Lambrecht BN. Cytokine targets in airway inflammation. *Curr. Opin. Pharmacol.* Jun 2013;13(3):351-361.
80. Eberlein J, Nguyen TT, Victorino F, Golden-Mason L, Rosen HR, Homann D. Comprehensive assessment of chemokine expression profiles by flow cytometry. *J. Clin. Invest.* Mar 2010;120(3):907-923.
81. Morelli AE, Zahorchak AF, Larregina AT, et al. Cytokine production by mouse myeloid dendritic cells in relation to differentiation and terminal maturation induced by lipopolysaccharide or CD40 ligation. *Blood.* Sep 1 2001;98(5):1512-1523.
82. Shortman K, Liu YJ. Mouse and human dendritic cell subtypes. *Nat. Rev. Immunol.* Mar 2002;2(3):151-161.
83. Liu YJ. IPC: professional type 1 interferon-producing cells and plasmacytoid dendritic cell precursors. *Annu. Rev. Immunol.* 2005;23:275-306.
84. Dzionek A, Fuchs A, Schmidt P, et al. BDCA-2, BDCA-3, and BDCA-4: three markers for distinct subsets of dendritic cells in human peripheral blood. *J. Immunol.* Dec 1 2000;165(11):6037-6046.
85. Jongbloed SL, Kassianos AJ, McDonald KJ, et al. Human CD141+ (BDCA-3)+ dendritic cells (DCs) represent a unique myeloid DC subset that cross-presents necrotic cell antigens. *J. Exp. Med.* Jun 7 2010;207(6):1247-1260.
86. Zhou T, Chen Y, Hao L, Zhang Y. DC-SIGN and immunoregulation. *Cell. Mol. Immunol.* Aug 2006;3(4):279-283.
87. Condon TV, Sawyer RT, Fenton MJ, Riches DW. Lung dendritic cells at the innate-adaptive immune interface. *J. Leukoc. Biol.* Nov 2011;90(5):883-895.

88. Manh TP, Alexandre Y, Baranek T, Crozat K, Dalod M. Plasmacytoid, conventional, and monocyte-derived dendritic cells undergo a profound and convergent genetic reprogramming during their maturation. *Eur. J. Immunol.* Jul 2013;43(7):1706-1715.
89. Nestle FO, Zheng XG, Thompson CB, Turka LA, Nickoloff BJ. Characterization of dermal dendritic cells obtained from normal human skin reveals phenotypic and functionally distinctive subsets. *J. Immunol.* Dec 1 1993;151(11):6535-6545.
90. Schuler G, Steinman RM. Murine epidermal Langerhans cells mature into potent immunostimulatory dendritic cells in vitro. *J. Exp. Med.* Mar 1 1985;161(3):526-546.
91. Wu L, Li CL, Shortman K. Thymic dendritic cell precursors: relationship to the T lymphocyte lineage and phenotype of the dendritic cell progeny. *J. Exp. Med.* Sep 1 1996;184(3):903-911.
92. Vremec D, Shortman K. Dendritic cell subtypes in mouse lymphoid organs: cross-correlation of surface markers, changes with incubation, and differences among thymus, spleen, and lymph nodes. *J. Immunol.* Jul 15 1997;159(2):565-573.
93. Maraskovsky E, Brasel K, Teepe M, et al. Dramatic increase in the numbers of functionally mature dendritic cells in Flt3 ligand-treated mice: multiple dendritic cell subpopulations identified. *J. Exp. Med.* Nov 1 1996;184(5):1953-1962.
94. Pulendran B, Lingappa J, Kennedy MK, et al. Developmental pathways of dendritic cells in vivo: distinct function, phenotype, and localization of dendritic cell subsets in FLT3 ligand-treated mice. *J. Immunol.* Sep 1 1997;159(5):2222-2231.
95. den Haan JM, Lehar SM, Bevan MJ. CD8(+) but not CD8(-) dendritic cells cross-prime cytotoxic T cells in vivo. *J. Exp. Med.* Dec 18 2000;192(12):1685-1696.
96. Ohteki T, Fukao T, Suzue K, et al. Interleukin 12-dependent interferon gamma production by CD8alpha+ lymphoid dendritic cells. *J. Exp. Med.* Jun 21 1999;189(12):1981-1986.
97. Inaba K, Inaba M, Romani N, et al. Generation of large numbers of dendritic cells from mouse bone marrow cultures supplemented with granulocyte/macrophage colony-stimulating factor. *J. Exp. Med.* Dec 1 1992;176(6):1693-1702.
98. Scheicher C, Mehlig M, Zecher R, Reske K. Dendritic cells from mouse bone marrow: in vitro differentiation using low doses of recombinant granulocyte-macrophage colony-stimulating factor. *J. Immunol. Methods.* Oct 2 1992;154(2):253-264.
99. Caux C, Dezutter-Dambuyant C, Schmitt D, Banchereau J. GM-CSF and TNF-alpha cooperate in the generation of dendritic Langerhans cells. *Nature.* Nov 19 1992;360(6401):258-261.
100. Szabolcs P, Moore MA, Young JW. Expansion of immunostimulatory dendritic cells among the myeloid progeny of human CD34+ bone marrow precursors cultured with c-kit ligand, granulocyte-macrophage colony-stimulating factor, and TNF-alpha. *J. Immunol.* Jun 1 1995;154(11):5851-5861.
101. Romani N, Reider D, Heuer M, et al. Generation of mature dendritic cells from human blood. An improved method with special regard to clinical applicability. *J. Immunol. Methods.* Sep 27 1996;196(2):137-151.
102. Reddy A, Sapp M, Feldman M, Subklewe M, Bhardwaj N. A monocyte conditioned medium is more effective than defined cytokines in mediating the terminal maturation of human dendritic cells. *Blood.* Nov 1 1997;90(9):3640-3646.
103. Kim SJ, Diamond B. Modulation of tolerogenic dendritic cells and autoimmunity. *Semin. Cell Dev. Biol.* Apr 18 2014.
104. Mackern-Oberti JP, Vega F, Llanos C, Bueno SM, Kalergis AM. Targeting Dendritic Cell Function during Systemic Autoimmunity to Restore Tolerance. *Int J Mol Sci.* 2014;15(9):16381-16417.
105. Specht JM, Wang G, Do MT, et al. Dendritic cells retrovirally transduced with a model antigen gene are therapeutically effective against established pulmonary metastases. *J. Exp. Med.* Oct 20 1997;186(8):1213-1221.
106. Schuler G, Steinman RM. Dendritic cells as adjuvants for immune-mediated resistance to tumors. *J. Exp. Med.* Oct 20 1997;186(8):1183-1187.
107. Rogers NM, Ferenbach DA, Isenberg JS, Thomson AW, Hughes J. Dendritic cells and macrophages in the kidney: a spectrum of good and evil. *Nat Rev Nephrol.* Sep 30 2014.

108. Soderberg-Naucler C, Fish KN, Nelson JA. Reactivation of latent human cytomegalovirus by allogeneic stimulation of blood cells from healthy donors. *Cell.* Oct 3 1997;91(1):119-126.
109. Salazar F, Ghaemmaghami AM. Allergen recognition by innate immune cells: critical role of dendritic and epithelial cells. *Front. Immunol.* 2013;4:356.
110. D'Hulst A I, Vermaelen KY, Brusselle GG, Joos GF, Pauwels RA. Time course of cigarette smoke-induced pulmonary inflammation in mice. *Eur. Respir. J.* Aug 2005;26(2):204-213.
111. Lambrecht BN, De Veerman M, Coyle AJ, Gutierrez-Ramos JC, Thielemans K, Pauwels RA. Myeloid dendritic cells induce Th2 responses to inhaled antigen, leading to eosinophilic airway inflammation. *J. Clin. Invest.* Aug 2000;106(4):551-559.
112. Lynch JP, Mazzone SB, Rogers MJ, et al. The plasmacytoid dendritic cell: at the cross-roads in asthma. *Eur. Respir. J.* Jan 2014;43(1):264-275.
113. Leonard CT, Soccal PM, Singer L, et al. Dendritic cells and macrophages in lung allografts: A role in chronic rejection? *Am. J. Respir. Crit. Care Med.* Apr 2000;161(4 Pt 1):1349-1354.
114. Yousem SA, Ray L, Paradis IL, Dauber JA, Griffith BP. Potential role of dendritic cells in bronchiolitis obliterans in heart-lung transplantation. *Ann. Thorac. Surg.* Mar 1990;49(3):424-428.
115. Steinman RM, Banchereau J. Taking dendritic cells into medicine. *Nature.* Sep 27 2007;449(7161):419-426.
116. Gross J, Lapiere CM. Collagenolytic activity in amphibian tissues: a tissue culture assay. *Proc. Natl. Acad. Sci. U. S. A.* Jun 15 1962;48:1014-1022.
117. Parks WC, Shapiro SD. Matrix metalloproteinases in lung biology. *Respir. Res.* 2001;2(1):10-19.
118. Nelson AR, Fingleton B, Rothenberg ML, Matrisian LM. Matrix metalloproteinases: biologic activity and clinical implications. *J. Clin. Oncol.* Mar 2000;18(5):1135-1149.
119. Sternlicht MD, Werb Z. How matrix metalloproteinases regulate cell behavior. *Annu. Rev. Cell Dev. Biol.* 2001;17:463-516.
120. Birkedal-Hansen H, Moore WG, Bodden MK, et al. Matrix metalloproteinases: a review. *Crit. Rev. Oral Biol. Med.* 1993;4(2):197-250.
121. Parks WC, Wilson CL, Lopez-Boado YS. Matrix metalloproteinases as modulators of inflammation and innate immunity. *Nat. Rev. Immunol.* Aug 2004;4(8):617-629.
122. Nagase H, Visse R, Murphy G. Structure and function of matrix metalloproteinases and TIMPs. *Cardiovasc. Res.* Feb 15 2006;69(3):562-573.
123. Bode W, Maskos K. Structural basis of the matrix metalloproteinases and their physiological inhibitors, the tissue inhibitors of metalloproteinases. *Biol. Chem.* Jun 2003;384(6):863-872.
124. Song F, Wisithphrom K, Zhou J, Windsor LJ. Matrix metalloproteinase dependent and independent collagen degradation. *Front. Biosci.* 2006;11:3100-3120.
125. Springman EB, Angleton EL, Birkedal-Hansen H, Van Wart HE. Multiple modes of activation of latent human fibroblast collagenase: evidence for the role of a Cys73 active-site zinc complex in latency and a "cysteine switch" mechanism for activation. *Proc. Natl. Acad. Sci. U. S. A.* Jan 1990;87(1):364-368.
126. Van Wart HE, Birkedal-Hansen H. The cysteine switch: a principle of regulation of metalloproteinase activity with potential applicability to the entire matrix metalloproteinase gene family. *Proc. Natl. Acad. Sci. U. S. A.* Jul 1990;87(14):5578-5582.
127. Mignatti P, Rifkin DB. Biology and biochemistry of proteinases in tumor invasion. *Physiol. Rev.* Jan 1993;73(1):161-195.
128. Peppin GJ, Weiss SJ. Activation of the endogenous metalloproteinase, gelatinase, by triggered human neutrophils. *Proc. Natl. Acad. Sci. U. S. A.* Jun 1986;83(12):4322-4326.
129. Gu Z, Kaul M, Yan B, et al. S-nitrosylation of matrix metalloproteinases: signaling pathway to neuronal cell death. *Science.* Aug 16 2002;297(5584):1186-1190.
130. Knauper V, Murphy G. Methods for studying activation of matrix metalloproteinases. *Methods Mol. Biol.* 2010;622:233-243.
131. Clark IM, Cawston TE. Fragments of human fibroblast collagenase. Purification and characterization. *Biochem. J.* Oct 1 1989;263(1):201-206.

132. Kleiner DE, Jr., Tuuttila A, Tryggvason K, Stetler-Stevenson WG. Stability analysis of latent and active 72-kDa type IV collagenase: the role of tissue inhibitor of metalloproteinases-2 (TIMP-2). *Biochemistry.* Feb 16 1993;32(6):1583-1592.
133. Willenbrock F, Crabbe T, Slocombe PM, et al. The activity of the tissue inhibitors of metalloproteinases is regulated by C-terminal domain interactions: a kinetic analysis of the inhibition of gelatinase A. *Biochemistry.* Apr 27 1993;32(16):4330-4337.
134. Heath JK, Reynolds JJ, Meikle MC. Osteopetrotic (grey-lethal) bone produces collagenase and TIMP in organ culture: regulation by vitamin A. *Biochem. Biophys. Res. Commun.* May 16 1990;168(3):1171-1176.
135. Zucker S, Cao J. Selective matrix metalloproteinase (MMP) inhibitors in cancer therapy: ready for prime time? *Cancer Biol. Ther.* Dec 2009;8(24):2371-2373.
136. Shapiro SD, Kobayashi DK, Ley TJ. Cloning and characterization of a unique elastolytic metalloproteinase produced by human alveolar macrophages. *J. Biol. Chem.* Nov 15 1993;268(32):23824-23829.
137. Belaaouaj A, Shipley JM, Kobayashi DK, et al. Human macrophage metalloelastase. Genomic organization, chromosomal location, gene linkage, and tissue-specific expression. *J. Biol. Chem.* Jun 16 1995;270(24):14568-14575.
138. Chandler S, Cossins J, Lury J, Wells G. Macrophage metalloelastase degrades matrix and myelin proteins and processes a tumour necrosis factor-alpha fusion protein. *Biochem. Biophys. Res. Commun.* Nov 12 1996;228(2):421-429.
139. Gronski TJ, Jr., Martin RL, Kobayashi DK, et al. Hydrolysis of a broad spectrum of extracellular matrix proteins by human macrophage elastase. *J. Biol. Chem.* May 2 1997;272(18):12189-12194.
140. Banda MJ, Rice AG, Griffin GL, Senior RM. Alpha 1-proteinase inhibitor is a neutrophil chemoattractant after proteolytic inactivation by macrophage elastase. *J. Biol. Chem.* Mar 25 1988;263(9):4481-4484.
141. Banda MJ, Werb Z. Mouse macrophage elastase. Purification and characterization as a metalloproteinase. *Biochem. J.* Feb 1 1981;193(2):589-605.
142. Hiller O, Lichte A, Oberpichler A, Kocourek A, Tschesche H. Matrix metalloproteinases collagenase-2, macrophage elastase, collagenase-3, and membrane type 1-matrix metalloproteinase impair clotting by degradation of fibrinogen and factor XII. *J. Biol. Chem.* Oct 20 2000;275(42):33008-33013.
143. Koolwijk P, Sidenius N, Peters E, et al. Proteolysis of the urokinase-type plasminogen activator receptor by metalloproteinase-12: implication for angiogenesis in fibrin matrices. *Blood.* May 15 2001;97(10):3123-3131.
144. Knauper V, Lopez-Otin C, Smith B, Knight G, Murphy G. Biochemical characterization of human collagenase-3. *J. Biol. Chem.* Jan 19 1996;271(3):1544-1550.
145. Freije JM, Diez-Itza I, Balbin M, et al. Molecular cloning and expression of collagenase-3, a novel human matrix metalloproteinase produced by breast carcinomas. *J. Biol. Chem.* Jun 17 1994;269(24):16766-16773.
146. Lovejoy B, Welch AR, Carr S, et al. Crystal structures of MMP-1 and -13 reveal the structural basis for selectivity of collagenase inhibitors. *Nat. Struct. Biol.* Mar 1999;6(3):217-221.
147. Gomis-Ruth FX, Gohlke U, Betz M, et al. The helping hand of collagenase-3 (MMP-13): 2.7 A crystal structure of its C-terminal haemopexin-like domain. *J. Mol. Biol.* Dec 6 1996;264(3):556-566.
148. Welgus HG, Kobayashi DK, Jeffrey JJ. The collagen substrate specificity of rat uterus collagenase. *J. Biol. Chem.* Dec 10 1983;258(23):14162-14165.
149. Knauper V, Cowell S, Smith B, et al. The role of the C-terminal domain of human collagenase-3 (MMP-13) in the activation of procollagenase-3, substrate specificity, and tissue inhibitor of metalloproteinase interaction. *J. Biol. Chem.* Mar 21 1997;272(12):7608-7616.
150. Welgus HG, Grant GA, Sacchettini JC, Roswit WT, Jeffrey JJ. The gelatinolytic activity of rat uterus collagenase. *J. Biol. Chem.* Nov 5 1985;260(25):13601-13606.

151. Lemaitre V, Jungbluth A, Eeckhout Y. The recombinant catalytic domain of mouse collagenase-3 depolymerizes type I collagen by cleaving its aminotelopeptides. *Biochem. Biophys. Res. Commun.* Jan 3 1997;230(1):202-205.
152. Fosang AJ, Last K, Knauper V, Murphy G, Neame PJ. Degradation of cartilage aggrecan by collagenase-3 (MMP-13). *FEBS Lett.* Feb 12 1996;380(1-2):17-20.
153. Nethery A, O'Grady RL. Interstitial collagenase from rat mammary carcinoma cells: interaction with substrates and inhibitors. *Invasion Metastasis.* 1991;11(5):241-248.
154. Eeckhout Y, Riccomi H, Cambiaso C, Vaes G, Masson P. Studies on properties common to collagen and Clq. *Arch. Int. Physiol. Biochim.* 1976;84(3):611-612.
155. Leeman MF, Curran S, Murray GI. The structure, regulation, and function of human matrix metalloproteinase-13. *Crit. Rev. Biochem. Mol. Biol.* 2002;37(3):149-166.
156. Nissinen L, Kahari VM. Matrix metalloproteinases in inflammation. *Biochim. Biophys. Acta.* Aug 2014;1840(8):2571-2580.
157. Schmidt-Hansen B, Ornas D, Grigorian M, et al. Extracellular S100A4(mts1) stimulates invasive growth of mouse endothelial cells and modulates MMP-13 matrix metalloproteinase activity. *Oncogene.* Jul 15 2004;23(32):5487-5495.
158. Hattori N, Mochizuki S, Kishi K, et al. MMP-13 plays a role in keratinocyte migration, angiogenesis, and contraction in mouse skin wound healing. *Am. J. Pathol.* Aug 2009;175(2):533-546.
159. Yamagiwa H, Tokunaga K, Hayami T, et al. Expression of metalloproteinase-13 (Collagenase-3) is induced during fracture healing in mice. *Bone.* Aug 1999;25(2):197-203.
160. Inada M, Wang Y, Byrne MH, et al. Critical roles for collagenase-3 (Mmp13) in development of growth plate cartilage and in endochondral ossification. *Proc. Natl. Acad. Sci. U. S. A.* Dec 7 2004;101(49):17192-17197.
161. Wahlgren J, Maisi P, Sorsa T, et al. Expression and induction of collagenases (MMP-8 and -13) in plasma cells associated with bone-destructive lesions. *J. Pathol.* Jun 2001;194(2):217-224.
162. Westhoff CS, Freudiger D, Petrow P, et al. Characterization of collagenase 3 (matrix metalloproteinase 13) messenger RNA expression in the synovial membrane and synovial fibroblasts of patients with rheumatoid arthritis. *Arthritis Rheum.* Jul 1999;42(7):1517-1527.
163. Ravanti L, Heino J, Lopez-Otin C, Kahari VM. Induction of collagenase-3 (MMP-13) expression in human skin fibroblasts by three-dimensional collagen is mediated by p38 mitogen-activated protein kinase. *J. Biol. Chem.* Jan 22 1999;274(4):2446-2455.
164. Blavier L, Delaisse JM. Matrix metalloproteinases are obligatory for the migration of preosteoclasts to the developing marrow cavity of primitive long bones. *J. Cell Sci.* Dec 1995;108 (Pt 12):3649-3659.
165. Mitchell PG, Magna HA, Reeves LM, et al. Cloning, expression, and type II collagenolytic activity of matrix metalloproteinase-13 from human osteoarthritic cartilage. *J. Clin. Invest.* Feb 1 1996;97(3):761-768.
166. Reboul P, Pelletier JP, Tardif G, Cloutier JM, Martel-Pelletier J. The new collagenase, collagenase-3, is expressed and synthesized by human chondrocytes but not by synoviocytes. A role in osteoarthritis. *J. Clin. Invest.* May 1 1996;97(9):2011-2019.
167. Mao D, Lee JK, VanVickle SJ, Thompson RW. Expression of collagenase-3 (MMP-13) in human abdominal aortic aneurysms and vascular smooth muscle cells in culture. *Biochem. Biophys. Res. Commun.* Aug 11 1999;261(3):904-910.
168. Nagel S, Sandy JD, Meyding-Lamade U, Schwark C, Bartsch JW, Wagner S. Focal cerebral ischemia induces changes in both MMP-13 and aggrecan around individual neurons. *Brain Res.* Sep 14 2005;1056(1):43-50.
169. Botos I, Meyer E, Swanson SM, Lemaitre V, Eeckhout Y, Meyer EF. Structure of recombinant mouse collagenase-3 (MMP-13). *J. Mol. Biol.* Oct 1 1999;292(4):837-844.
170. Chen Z, Gordon JR, Zhang X, Xiang J. Analysis of the gene expression profiles of immature versus mature bone marrow-derived dendritic cells using DNA arrays. *Biochem. Biophys. Res. Commun.* Jan 11 2002;290(1):66-72.

171. Zaslona Z, Wilhelm J, Cakarova L, et al. Transcriptome profiling of primary murine monocytes, lung macrophages and lung dendritic cells reveals a distinct expression of genes involved in cell trafficking. *Respir. Res.* 2009;10:2.
172. Shipley JM, Wesselschmidt RL, Kobayashi DK, Ley TJ, Shapiro SD. Metalloelastase is required for macrophage-mediated proteolysis and matrix invasion in mice. *Proc. Natl. Acad. Sci. U. S. A.* Apr 30 1996;93(9):3942-3946.
173. Takaishi H, Kimura T, Dalal S, Okada Y, D'Armiento J. Joint diseases and matrix metalloproteinases: a role for MMP-13. *Curr. Pharm. Biotechnol.* Feb 2008;9(1):47-54.
174. Stickens D, Behonick DJ, Ortega N, et al. Altered endochondral bone development in matrix metalloproteinase 13-deficient mice. *Development.* Dec 2004;131(23):5883-5895.
175. Leppert D, Waubant E, Galardy R, Bunnett NW, Hauser SL. T cell gelatinases mediate basement membrane transmigration in vitro. *J. Immunol.* May 1 1995;154(9):4379-4389.
176. Baratelli FE, Heuze-Vourc'h N, Krysan K, et al. Prostaglandin E2-dependent enhancement of tissue inhibitors of metalloproteinases-1 production limits dendritic cell migration through extracellular matrix. *J. Immunol.* Nov 1 2004;173(9):5458-5466.
177. Schonbeck U, Mach F, Libby P. Generation of biologically active IL-1 beta by matrix metalloproteinases: a novel caspase-1-independent pathway of IL-1 beta processing. *J. Immunol.* Oct 1 1998;161(7):3340-3346.
178. Ito A, Mukaiyama A, Itoh Y, et al. Degradation of interleukin 1beta by matrix metalloproteinases. *J. Biol. Chem.* Jun 21 1996;271(25):14657-14660.
179. Wilson CL, Ouellette AJ, Satchell DP, et al. Regulation of intestinal alpha-defensin activation by the metalloproteinase matrilysin in innate host defense. *Science.* Oct 1 1999;286(5437):113-117.
180. Saarialho-Kere U, Kerkela E, Jeskanen L, et al. Accumulation of matrilysin (MMP-7) and macrophage metalloelastase (MMP-12) in actinic damage. *J. Invest. Dermatol.* Oct 1999;113(4):664-672.
181. Suomela S, Kariniemi AL, Snellman E, Saarialho-Kere U. Metalloelastase (MMP-12) and 92-kDa gelatinase (MMP-9) as well as their inhibitors, TIMP-1 and -3, are expressed in psoriatic lesions. *Exp. Dermatol.* Jun 2001;10(3):175-183.
182. Matsumoto S, Kobayashi T, Katoh M, et al. Expression and localization of matrix metalloproteinase-12 in the aorta of cholesterol-fed rabbits: relationship to lesion development. *Am. J. Pathol.* Jul 1998;153(1):109-119.
183. Curci JA, Liao S, Huffman MD, Shapiro SD, Thompson RW. Expression and localization of macrophage elastase (matrix metalloproteinase-12) in abdominal aortic aneurysms. *J. Clin. Invest.* Dec 1 1998;102(11):1900-1910.
184. Cornelius LA, Nehring LC, Harding E, et al. Matrix metalloproteinases generate angiostatin: effects on neovascularization. *J. Immunol.* Dec 15 1998;161(12):6845-6852.
185. Kerkela E, Bohling T, Herva R, Uria JA, Saarialho-Kere U. Human macrophage metalloelastase (MMP-12) expression is induced in chondrocytes during fetal development and malignant transformation. *Bone.* Nov 2001;29(5):487-493.
186. Belvisi MG, Bottomley KM. The role of matrix metalloproteinases (MMPs) in the pathophysiology of chronic obstructive pulmonary disease (COPD): a therapeutic role for inhibitors of MMPs? *Inflamm. Res.* Mar 2003;52(3):95-100.
187. Nenan S, Boichot E, Lagente V, Bertrand CP. Macrophage elastase (MMP-12): a pro-inflammatory mediator? *Mem. Inst. Oswaldo Cruz.* Mar 2005;100 Suppl 1:167-172.
188. Hautamaki RD, Kobayashi DK, Senior RM, Shapiro SD. Requirement for macrophage elastase for cigarette smoke-induced emphysema in mice. *Science.* Sep 26 1997;277(5334):2002-2004.
189. Vincenti MP, Brinckerhoff CE. Transcriptional regulation of collagenase (MMP-1, MMP-13) genes in arthritis: integration of complex signaling pathways for the recruitment of gene-specific transcription factors. *Arthritis Res.* 2002;4(3):157-164.
190. Uitto VJ, Airola K, Vaalamo M, et al. Collagenase-3 (matrix metalloproteinase-13) expression is induced in oral mucosal epithelium during chronic inflammation. *Am. J. Pathol.* Jun 1998;152(6):1489-1499.

191. Heppner KJ, Matrisian LM, Jensen RA, Rodgers WH. Expression of most matrix metalloproteinase family members in breast cancer represents a tumor-induced host response. *Am. J. Pathol.* Jul 1996;149(1):273-282.
192. Uria JA, Stahle-Backdahl M, Seiki M, Fueyo A, Lopez-Otin C. Regulation of collagenase-3 expression in human breast carcinomas is mediated by stromal-epithelial cell interactions. *Cancer Res.* Nov 1 1997;57(21):4882-4888.
193. Johansson N, Airola K, Grenman R, Kariniemi AL, Saarialho-Kere U, Kahari VM. Expression of collagenase-3 (matrix metalloproteinase-13) in squamous cell carcinomas of the head and neck. *Am. J. Pathol.* Aug 1997;151(2):499-508.
194. Airola K, Johansson N, Kariniemi AL, Kahari VM, Saarialho-Kere UK. Human collagenase-3 is expressed in malignant squamous epithelium of the skin. *J. Invest. Dermatol.* Aug 1997;109(2):225-231.
195. Johansson N, Vaalamo M, Grenman S, et al. Collagenase-3 (MMP-13) is expressed by tumor cells in invasive vulvar squamous cell carcinomas. *Am. J. Pathol.* Feb 1999;154(2):469-480.
196. Uria JA, Balbin M, Lopez JM, et al. Collagenase-3 (MMP-13) expression in chondrosarcoma cells and its regulation by basic fibroblast growth factor. *Am. J. Pathol.* Jul 1998;153(1):91-101.
197. Greenlee KJ, Werb Z, Kheradmand F. Matrix metalloproteinases in lung: multiple, multifarious, and multifaceted. *Physiol. Rev.* Jan 2007;87(1):69-98.
198. Nishijima C, Hayakawa I, Matsushita T, et al. Autoantibody against matrix metalloproteinase-3 in patients with systemic sclerosis. *Clin. Exp. Immunol.* Nov 2004;138(2):357-363.
199. Demedts IK, Brusselle GG, Bracke KR, Vermaelen KY, Pauwels RA. Matrix metalloproteinases in asthma and COPD. *Curr. Opin. Pharmacol.* Jun 2005;5(3):257-263.
200. Molet S, Belleguic C, Lena H, et al. Increase in macrophage elastase (MMP-12) in lungs from patients with chronic obstructive pulmonary disease. *Inflamm. Res.* Jan 2005;54(1):31-36.
201. Sagel SD, Kapsner RK, Osberg I. Induced sputum matrix metalloproteinase-9 correlates with lung function and airway inflammation in children with cystic fibrosis. *Pediatr. Pulmonol.* Mar 2005;39(3):224-232.
202. Taghavi S, Krenn K, Jaksch P, Klepetko W, Aharinejad S. Broncho-alveolar lavage matrix metalloproteases as a sensitive measure of bronchiolitis obliterans. *Am. J. Transplant.* Jun 2005;5(6):1548-1552.
203. Hubner RH, Meffert S, Mundt U, et al. Matrix metalloproteinase-9 in bronchiolitis obliterans syndrome after lung transplantation. *Eur. Respir. J.* Mar 2005;25(3):494-501.
204. Chen P, Farivar AS, Mulligan MS, Madtes DK. Tissue inhibitor of metalloproteinase-1 deficiency abrogates obliterative airway disease after heterotopic tracheal transplantation. *Am. J. Respir. Cell Mol. Biol.* Apr 2006;34(4):464-472.
205. Beeh KM, Beier J, Kornmann O, Micke P, Buhl R. Sputum levels of metalloproteinase-9 and tissue inhibitor of metalloproteinase-1, and their ratio correlate with airway obstruction in lung transplant recipients: relation to tumor necrosis factor-alpha and interleukin-10. *J. Heart Lung Transplant.* Nov 2001;20(11):1144-1151.
206. Fernandez FG, Campbell LG, Liu W, et al. Inhibition of obliterative airway disease development in murine tracheal allografts by matrix metalloproteinase-9 deficiency. *Am. J. Transplant.* Apr 2005;5(4 Pt 1):671-683.
207. Khatwa UA, Kleibrink BE, Shapiro SD, Subramaniam M. MMP-8 promotes polymorphonuclear cell migration through collagen barriers in obliterative bronchiolitis. *J. Leukoc. Biol.* Jan 2010;87(1):69-77.
208. Inaki N, Tsunezuka Y, Kawakami K, et al. Increased matrix metalloproteinase-2 and membrane type 1 matrix metalloproteinase activity and expression in heterotopically transplanted murine tracheas. *J. Heart Lung Transplant.* Feb 2004;23(2):218-227.
209. Aurora P, Edwards LB, Kucheryavaya AY, et al. The Registry of the International Society for Heart and Lung Transplantation: thirteenth official pediatric lung and heart-lung transplantation report--2010. *J. Heart Lung Transplant.* Oct 2010;29(10):1129-1141.

210. Verleden GM. Chronic allograft rejection (obliterative bronchiolitis). *Semin. Respir. Crit. Care Med.* Oct 2001;22(5):551-558.
211. Sato M. Chronic lung allograft dysfunction after lung transplantation: the moving target. *Gen. Thorac. Cardiovasc. Surg.* Feb 2013;61(2):67-78.
212. U.S. Department of Health and Human Services HRaSA, Healthcare Systems Bureau, Division of Transplantation, Rockville, MD. *Annual Report of the U.S. Organ Procurement and Transplantation Network and the Scientific Registry of Transplant Recipients: Transplant Data 1999-2008.* 2009.
213. Vanaudenaerde BM, Meyts I, Vos R, et al. A dichotomy in bronchiolitis obliterans syndrome after lung transplantation revealed by azithromycin therapy. *Eur. Respir. J.* Oct 2008;32(4):832-843.
214. Estenne M, Hertz MI. Bronchiolitis obliterans after human lung transplantation. *Am. J. Respir. Crit. Care Med.* Aug 15 2002;166(4):440-444.
215. Estenne M, Maurer JR, Boehler A, et al. Bronchiolitis obliterans syndrome 2001: an update of the diagnostic criteria. *J. Heart Lung Transplant.* Mar 2002;21(3):297-310.
216. Nicod LP. Mechanisms of airway obliteration after lung transplantation. *Proc Am Thorac Soc.* Jul 2006;3(5):444-449.
217. Hertz MI, Jessurun J, King MB, Savik SK, Murray JJ. Reproduction of the obliterative bronchiolitis lesion after heterotopic transplantation of mouse airways. *Am. J. Pathol.* Jun 1993;142(6):1945-1951.
218. Snyder LD, Palmer SM. Immune mechanisms of lung allograft rejection. *Semin. Respir. Crit. Care Med.* Oct 2006;27(5):534-543.
219. Neuringer IP, Chalermskulrat W, Aris R. Obliterative bronchiolitis or chronic lung allograft rejection: a basic science review. *J. Heart Lung Transplant.* Jan 2005;24(1):3-19.
220. Neuringer IP, Mannon RB, Coffman TM, et al. Immune cells in a mouse airway model of obliterative bronchiolitis. *Am. J. Respir. Cell Mol. Biol.* Sep 1998;19(3):379-386.
221. Yousem SA, Berry GJ, Cagle PT, et al. Revision of the 1990 working formulation for the classification of pulmonary allograft rejection: Lung Rejection Study Group. *J. Heart Lung Transplant.* Jan 1996;15(1 Pt 1):1-15.
222. Glanville AR, Aboyoun CL, Havryk A, Plit M, Rainer S, Malouf MA. Severity of lymphocytic bronchiolitis predicts long-term outcome after lung transplantation. *Am. J. Respir. Crit. Care Med.* May 1 2008;177(9):1033-1040.
223. Hachem RR, Khalifah AP, Chakinala MM, et al. The significance of a single episode of minimal acute rejection after lung transplantation. *Transplantation.* Nov 27 2005;80(10):1406-1413.
224. Husain AN, Siddiqui MT, Holmes EW, et al. Analysis of risk factors for the development of bronchiolitis obliterans syndrome. *Am. J. Respir. Crit. Care Med.* Mar 1999;159(3):829-833.
225. Tullius SG, Tilney NL. Both alloantigen-dependent and -independent factors influence chronic allograft rejection. *Transplantation.* Feb 15 1995;59(3):313-318.
226. Kelly K, Hertz MI. Obliterative bronchiolitis. *Clin. Chest Med.* Jun 1997;18(2):319-338.
227. Trulock EP. Lung transplantation. *Am. J. Respir. Crit. Care Med.* Mar 1997;155(3):789-818.
228. Grossman EJ, Shilling RA. Bronchiolitis obliterans in lung transplantation: the good, the bad, and the future. *Transl. Res.* Apr 2009;153(4):153-165.
229. Benichou G. Direct and indirect antigen recognition: the pathways to allograft immune rejection. *Front. Biosci.* May 15 1999;4:D476-480.
230. Solari MG, Thomson AW. Human dendritic cells and transplant outcome. *Transplantation.* Jun 15 2008;85(11):1513-1522.
231. Lechler RI, Batchelor JR. Restoration of immunogenicity to passenger cell-depleted kidney allografts by the addition of donor strain dendritic cells. *J. Exp. Med.* Jan 1 1982;155(1):31-41.
232. Milne DS, Gascoigne AD, Coaker J, et al. Mononuclear phagocyte populations in the transplanted human lung. *Transplantation.* Sep 15 1998;66(5):671-673.

233. KleinJan A, Willart MA, Kuipers H, Coyle AJ, Hoogsteden HC, Lambrecht BN. Inducible costimulator blockade prolongs airway luminal patency in a mouse model of obliterative bronchiolitis. *Transplantation.* Nov 27 2008;86(10):1436-1444.
234. Smith GN, Jr., Mickler EA, Payne KK, et al. Lung transplant metalloproteinase levels are elevated prior to bronchiolitis obliterans syndrome. *Am. J. Transplant.* Jul 2007;7(7):1856-1861.
235. Hele DJ, Yacoub MH, Belvisi MG. The heterotopic tracheal allograft as an animal model of obliterative bronchiolitis. *Respir. Res.* 2001;2(3):169-183.
236. Karttunen J, Sanderson S, Shastri N. Detection of rare antigen-presenting cells by the lacZ T-cell activation assay suggests an expression cloning strategy for T-cell antigens. *Proc. Natl. Acad. Sci. U. S. A.* Jul 1 1992;89(13):6020-6024.
237. Harding CV, Collins DS, Kanagawa O, Unanue ER. Liposome-encapsulated antigens engender lysosomal processing for class II MHC presentation and cytosolic processing for class I presentation. *J. Immunol.* Nov 1 1991;147(9):2860-2863.
238. Grove DA, Xu J, Joodi R, et al. Attenuation of early airway obstruction by mesenchymal stem cells in a murine model of heterotopic tracheal transplantation. *J. Heart Lung Transplant.* Mar 2011;30(3):341-350.
239. Steinman RM, Pack M, Inaba K. Dendritic cell development and maturation. *Adv. Exp. Med. Biol.* 1997;417:1-6.
240. Meunier L, Bohjanen K, Voorhees JJ, Cooper KD. Retinoic acid upregulates human Langerhans cell antigen presentation and surface expression of HLA-DR and CD11c, a beta 2 integrin critically involved in T-cell activation. *J. Invest. Dermatol.* Dec 1994;103(6):775-779.
241. Jungraithmayr W, Jang JH, Schrepfer S, Inci I, Weder W. Small animal models of experimental obliterative bronchiolitis. *Am. J. Respir. Cell Mol. Biol.* Jun 2013;48(6):675-684.
242. Inaba K, Swiggard WJ, Steinman RM, Romani N, Schuler G. Isolation of dendritic cells. *Curr. Protoc. Immunol.* May 2001;Chapter 3:Unit 3.7.
243. Giannelli G, Falk-Marzillier J, Schiraldi O, Stetler-Stevenson WG, Quaranta V. Induction of cell migration by matrix metalloprotease-2 cleavage of laminin-5. *Science.* Jul 11 1997;277(5323):225-228.
244. Westermarck J, Kahari VM. Regulation of matrix metalloproteinase expression in tumor invasion. *FASEB J.* May 1999;13(8):781-792.
245. Ichiyasu H, McCormack JM, McCarthy KM, Dombkowski D, Preffer FI, Schneeberger EE. Matrix metalloproteinase-9-deficient dendritic cells have impaired migration through tracheal epithelial tight junctions. *Am. J. Respir. Cell Mol. Biol.* Jun 2004;30(6):761-770.
246. Chabot V, Reverdiau P, Iochmann S, et al. CCL5-enhanced human immature dendritic cell migration through the basement membrane in vitro depends on matrix metalloproteinase-9. *J. Leukoc. Biol.* Apr 2006;79(4):767-778.
247. Creemers EE, Cleutjens JP, Smits JF, Daemen MJ. Matrix metalloproteinase inhibition after myocardial infarction: a new approach to prevent heart failure? *Circ. Res.* Aug 3 2001;89(3):201-210.
248. Zozulya AL, Reinke E, Baiu DC, Karman J, Sandor M, Fabry Z. Dendritic cell transmigration through brain microvessel endothelium is regulated by MIP-1alpha chemokine and matrix metalloproteinases. *J. Immunol.* Jan 1 2007;178(1):520-529.
249. Castro MM, Tanus-Santos JE. Inhibition of matrix metalloproteinases (MMPs) as a potential strategy to ameliorate hypertension-induced cardiovascular alterations. *Curr. Drug Targets.* Mar 2013;14(3):335-343.
250. Haq I, Lowrey GE, Kalsheker N, Johnson SR. Matrix metalloproteinase-12 (MMP-12) SNP affects MMP activity, lung macrophage infiltration and protects against emphysema in COPD. *Thorax.* Nov 2011;66(11):970-976.
251. Sato M, Hirayama S, Lara-Guerra H, et al. MMP-dependent migration of extrapulmonary myofibroblast progenitors contributing to posttransplant airway fibrosis in the lung. *Am. J. Transplant.* May 2009;9(5):1027-1036.
252. Burgstaller G, Oehrle B, Koch I, Lindner M, Eickelberg O. Multiplex profiling of cellular invasion in 3D cell culture models. *PLoS One.* 2013;8(5):e63121.

253. Lecomte J, Masset A, Blacher S, et al. Bone marrow-derived myofibroblasts are the providers of pro-invasive matrix metalloproteinase 13 in primary tumor. *Neoplasia.* Oct 2012;14(10):943-951.
254. Kobayashi Y, Matsumoto M, Kotani M, Makino T. Possible involvement of matrix metalloproteinase-9 in Langerhans cell migration and maturation. *J. Immunol.* Dec 1 1999;163(11):5989-5993.
255. Kis-Toth K, Bacskai I, Gogolak P, Mazlo A, Szatmari I, Rajnavolgyi E. Monocyte-derived dendritic cell subpopulations use different types of matrix metalloproteinases inhibited by GM6001. *Immunobiology.* Nov 2013;218(11):1361-1369.
256. Yanagihara S, Komura E, Nagafune J, Watarai H, Yamaguchi Y. EBI1/CCR7 is a new member of dendritic cell chemokine receptor that is up-regulated upon maturation. *J. Immunol.* Sep 15 1998;161(6):3096-3102.
257. Garrett WS, Chen LM, Kroschewski R, et al. Developmental control of endocytosis in dendritic cells by Cdc42. *Cell.* Aug 4 2000;102(3):325-334.
258. Watts C, Amigorena S. Antigen traffic pathways in dendritic cells. *Traffic.* Apr 2000;1(4):312-317.
259. Regnault A, Lankar D, Lacabanne V, et al. Fcgamma receptor-mediated induction of dendritic cell maturation and major histocompatibility complex class I-restricted antigen presentation after immune complex internalization. *J. Exp. Med.* Jan 18 1999;189(2):371-380.
260. Burgdorf S, Kautz A, Bohnert V, Knolle PA, Kurts C. Distinct pathways of antigen uptake and intracellular routing in CD4 and CD8 T cell activation. *Science.* Apr 27 2007;316(5824):612-616.
261. Burgdorf S, Lukacs-Kornek V, Kurts C. The mannose receptor mediates uptake of soluble but not of cell-associated antigen for cross-presentation. *J. Immunol.* Jun 1 2006;176(11):6770-6776.
262. Platt CD, Ma JK, Chalouni C, et al. Mature dendritic cells use endocytic receptors to capture and present antigens. *Proc. Natl. Acad. Sci. U. S. A.* Mar 2 2010;107(9):4287-4292.
263. Lee SJ, Evers S, Roeder D, et al. Mannose receptor-mediated regulation of serum glycoprotein homeostasis. *Science.* Mar 8 2002;295(5561):1898-1901.
264. Rivera-Marrero CA, Schuyler W, Roser S, Ritzenthaler JD, Newburn SA, Roman J. M. tuberculosis induction of matrix metalloproteinase-9: the role of mannose and receptor-mediated mechanisms. *Am. J. Physiol. Lung Cell Mol. Physiol.* Mar 2002;282(3):L546-555.
265. Engelholm LH, Nielsen BS, Netzel-Arnett S, et al. The urokinase plasminogen activator receptor-associated protein/endo180 is coexpressed with its interaction partners urokinase plasminogen activator receptor and matrix metalloprotease-13 during osteogenesis. *Lab. Invest.* Oct 2001;81(10):1403-1414.
266. Sadhu C, Ting HJ, Lipsky B, et al. CD11c/CD18: novel ligands and a role in delayed-type hypersensitivity. *J. Leukoc. Biol.* Jun 2007;81(6):1395-1403.
267. Van Lint P, Libert C. Chemokine and cytokine processing by matrix metalloproteinases and its effect on leukocyte migration and inflammation. *J. Leukoc. Biol.* Dec 2007;82(6):1375-1381.
268. Hunter CA. New IL-12-family members: IL-23 and IL-27, cytokines with divergent functions. *Nat. Rev. Immunol.* Jul 2005;5(7):521-531.
269. Godefroy E, Manches O, Dreno B, et al. Matrix metalloproteinase-2 conditions human dendritic cells to prime inflammatory T(H)2 cells via an IL-12- and OX40L-dependent pathway. *Cancer Cell.* Mar 8 2011;19(3):333-346.
270. Oriss TB, Krishnamoorthy N, Raundhal M, et al. Cutting Edge: MMP-9 inhibits IL-23p19 expression in dendritic cells by targeting membrane stem cell factor affecting lung IL-17 response. *J. Immunol.* Jun 15 2014;192(12):5471-5475.
271. Farber JM. Mig and IP-10: CXC chemokines that target lymphocytes. *J. Leukoc. Biol.* Mar 1997;61(3):246-257.
272. Ikonen TS, Brazelton TR, Berry GJ, Shorthouse RS, Morris RE. Epithelial re-growth is associated with inhibition of obliterative airway disease in orthotopic tracheal allografts in non-immunosuppressed rats. *Transplantation.* Sep 27 2000;70(6):857-863.

273. Jiang X, Khan MA, Tian W, et al. Adenovirus-mediated HIF-1alpha gene transfer promotes repair of mouse airway allograft microvasculature and attenuates chronic rejection. *J. Clin. Invest.* Jun 2011;121(6):2336-2349.
274. Babu AN, Murakawa T, Thurman JM, et al. Microvascular destruction identifies murine allografts that cannot be rescued from airway fibrosis. *J. Clin. Invest.* Dec 2007;117(12):3774-3785.
275. Khan MA, Nicolls MR. Complement-mediated microvascular injury leads to chronic rejection. *Adv. Exp. Med. Biol.* 2013;735:233-246.
276. Dutly AE, Andrade CF, Verkaik R, et al. A novel model for post-transplant obliterative airway disease reveals angiogenesis from the pulmonary circulation. *Am. J. Transplant.* Feb 2005;5(2):248-254.
277. Sato M, Hwang DM, Guan Z, et al. Regression of allograft airway fibrosis: the role of MMP-dependent tissue remodeling in obliterative bronchiolitis after lung transplantation. *Am. J. Pathol.* Sep 2011;179(3):1287-1300.
278. Sato M, Liu M, Anraku M, et al. Allograft airway fibrosis in the pulmonary milieu: a disorder of tissue remodeling. *Am. J. Transplant.* Mar 2008;8(3):517-528.

LIST OF TABLES

LIST OF FIGURES

LIST OF ABBREVIATIONS

A

Ag	Antigen
Anova	Analysis of variance
APC	Antigen-presenting cell
APMA	4-Aminophenylmercuric Acetate
APS	Ammonium peroxodisulfate
α-SMA	Alpha smooth muscle actin

B

BAL	Bronchoalveolar lavage
BMDC	Bone marrow-derived dendritic cell
BOS	Bronchiolitis obliterans syndrome
bp	Base pairs
BSA	Bovine serum albumin

C

c	Concentration
CCL	Chemokine (C-C motif) ligand
CD	Cluster of differentiation
cDCs	Classical dendritic cell
cDNA	Complementary DNA
CLAD	Chronic lung allograft dysfunction
COPD	Chronic obstructive pulmonary disease
CPRG	Chlorophenol red-β-D-galactopyranoside
CXCL	Chemokine (C-X-C motif) ligand
°C	Degrees Celsius

D

d	Day
Da	Dalton
DAPI	4',6-diamidino-2-phenylindole
DC-LAMP	DC lysosome-associated membrane protein
DCs	Dendritic cell
DC-SIGN	Dendritic Cell-Specific Intercellular adhesion molecule-3-Grabbing Non-integrin
Denat.	Denaturated
DMEM	Dulbecco's Modified Eagle's Medium
DMSO	Dimethyl sulfoxide
DNA	Deoxyribonucleic acid
dNTP	Desoxy-nucleotide-tri-phosphate
dsRNA	Double-stranded RNA
DTT	Dithiothreitol

E

ECM	Extracellular matrix

EDTA	Ethylenediaminetetraacetic acid
ELISA	Enzyme-linked immunosorbent assay
ER	Endoplasmatic reticulum

F

FBS	Fetal bovine serum
Fc	Fragment crystallizable
FD	Fold difference
FEV1	Forced expiratory volume 1
FRET	Fluorescence resonance energy transfer
FSC	Forward Scatter

G

g	Gram
G	Gravity
GAPDH	Glyceraldehyde 3-phosphate dehydrogenase
Gly	Glycin
GM-CSF	Granulocyte macrophage colony-stimulating factor

H

h	Hour(s)
H&E	Hematoxylin and eosin
HEPES	N-2-hydroxyethylpiperazine-N-2-ethane sulfonic acid
HRP	Horseradish peroxidase
HTT	Heterotopic trachea transplant

I

i.p.	Intraperitoneal
ICAM	Intercellular adhesion molecules
IF	Immunofluorescence
IFN	Interferon
IgG	Immunoglobulin protein G
IL	Interleukin
IMPs	Smaller inhibitor of metalloproteinase

K

k	Kilo
KO	Knock-out

L

l	Liter
L	Ligand
LFA	Lymphocyte function-associated antigen
LIMPs	Large inhibitor of metalloproteinase
LIX	LPS-induced CXC chemokine
LPS	Lipopolysaccharide

M

m	Milli
M	Molar
mA	Milli Ampere
max.	Maximum
mc	Monoclonal
M-CSF	Macrophage colony-stimulating factor
mDC	Myeloid dendritic cell
$MgCl_2$	Magnesiumchlorid
MHC-I/-II	Major histocompatibility complex class I/II
min	Minimum
min	Minute
ml	Milliliter
MMP	Matrix metalloproteinase
MR	Mannose receptor
mRNA	Messenger RNA
MT-MMP	Membrane-type MMP
µ	Micro

N

n	Nano
NaCl	Sodium chloride
NaOH	Natriumhydroxid
NK	Natural killer
No	Number
NP40	Nonidet P-40

O

ON	Over night
OVA	Ovalbumin

P

p	Pico
PAGE	Polyacrylamide gel electrophoresis
PBS	Phosphatate buffered saline
pc	Polyclonal
PC	Polycarbonate
PCR	Polymerase chain reaction
pDC	Plasmacytoid dendritic cell
PFA	Paraformaldehyde
PI	Propidium iodide
PS	Phospholipid phosphatidylserine

Q

qRT-PCR	Quantitative real-time polymerase chain reaction

R

RAS	Restrictive allograft syndrome
RIPA	Radio-immunoprecipitation assay
RNA	Ribonucleic acid
rpm	Revolutions per minute
RT	Room temperature

S

s	Second
SDS	Sodium dodecyl sulphate
SNP	Single nucleotide polymorphism
SSC	Side Scatter
STAT	Signal Transducers and Activators of Transcription

T

TAE	Tris-acetate-EDTA
TAP	Transporter associated with antigen processing
TBS	Tris-buffered saline
TBS-T	Tris-buffered saline with TWEEN®20
TCR	T cell receptor
TEMED	N,N,N',N'-Tetramethylenediamine
TERC	Telomerase RNA component
TERT	Telomerase reverse transcriptase
TGF	Transforming growth factor
Th1/Th2/Th17	T helper cells type 1/2/17
TIMP	Tissue inhibitor of metalloproteinase
TLR	Toll-like receptors
TNF	Tumor necrosis factor
tPA	Tissue-type plasminogen activator
Tregs	Regulatory T cell
TRIS	Tris(hydroxymethyl)-aminomethane

U

U	Unit
uPA	Urokinase type plasminogen activator
uPAR	Urokinase-type plasminogen activator receptor

V

V	Volt
V	Volume
vs	Versus

W

W	Weight
WST	Water soluble tetrazolium
WT	Wild-type

ACKNOWLEDGEMENT

Foremost, I would like to express my special thanks to **Prof. Dr. Elfriede Nößner**, for her kind and excellent supervision, extensive scientific discussions, and encouraging support during the past four years.

I am grateful to **Dr. Werner von Wulffen, Dr. Marion Frankenberger**, and **Prof. Oliver Eickelberg** for giving me the opportunity to write my thesis in the Comprehensive Pneumology Center and the chance to gain interesting experiences at diverse conferences.

I would also particularly like to thank **Heidi Villena-Hermoza** for her kind support and for her outstanding technical assistance.

I am grateful to all current and former members of the CPC who supported me during my thesis especially, **Bettina Oehrle, Ilona Keller, Andrea Schamberger, Dr. Barbara Berschneider, Dr. Katharina Heinzelmann, Elisabeth Hennen, Kyra Peters, Katharina Lippl, Ann-Christin Beitel, Daniela Dietel, Konstanze Heise, and Deniz Bölükbas** for their kind support and for technical assistance.

Furthermore, I want to highlight the friendship of my fellow PhD students. In particular I want to thank **Bettina Oehrle, Emma Gbandi, Sabine Bartel, Andrea Schamberger, Franziska Uhl, Nunja Habel-Ungewitter, Lilia Zvintzou, Ilona Keller,** and **Murali Sarguru** for the fun time in and outside the lab.

Special thanks to **Andrea Schamberger** for her fussy proofreading of abstracts and her musically support in the lab and to **Ilona Keller** that her office was always open for me.

Special thanks to **Bettina Oehrle** for her help during the last four years, for the fun on conferences, for carefully proofreading my thesis, more than once, and for simply being the best friend ever!

I dearly thank my **parents** for their help, their support and that they are always encouraging me. Special thanks to **my mother** who took care of Nero when I was in the lab and to **Amelia** and **Frank Schlott** who supported me with Nero in addition.

My deepest thanks to **Fabian** who always discussed with me scientific issues, even late at night or at the weekends and who always supported me, even he was busy with his own thesis.
– Thank you for always being there for me.

EIDESSTATTLICHE VERSICHERUNG

Ich, Juliane Bartmann, erkläre hiermit an Eides statt, dass ich die vorliegende Dissertation mit dem Thema

Immunobiological Functions of Matrix Metalloproteinase-13 in Bone Marrow-Derived Dendritic Cells and its Contribution to the Pathogenesis of Bronchiolitis Obliterans Syndrome

selbständig verfasst, mich außer der angegebenen keiner weiteren Hilfsmittel bedient und alle Erkenntnisse, die aus dem Schrifttum ganz oder annähernd übernommen sind, als solche kenntlich gemacht und nach ihrer Herkunft unter Bezeichnung der Fundstelle einzeln nachgewiesen habe. Ich erkläre des Weiteren, dass die hier vorgelegte Dissertation nicht in gleicher oder in ähnlicher Form bei einer anderen Stelle zur Erlangung eines akademischen Grades eingereicht wurde.

Ort, Datum

Unterschrift